Tonalitic Melt Formation from Amphibolite in Hanko Archipelago

Emil Andersson, 40402-404-2015

emil.andersson(a).abo.fi

Master's thesis in geology

Supervisors: Olav Eklund and Kaisa Nikkilä

Faculty of Science and Engineering

Åbo Akademi University, 2021

Andersson Emil, 2021. *Tonalitic Melt Formation from Amphibolite in Hanko Archipelago*. Master's thesis in geology and mineralogy. 49 pages, 24 figures, 3 tables and 8 appendixes. Faculty of Science and Engineering, Åbo Akademi University. Supervisors Prof. Olav Eklund and PhD Kaisa Nikkilä.

ABSTRACT

Water-fluxed and dehydration melting have critical roles in tonalitic melt production in orogenic belts. The melting of amphibolite at middle-lower crustal depths is usually caused by influx of externally derived hydrous fluids or dehydration of amphibole. Water-flux decreases the melting point of amphibolite, whereas dehydration melting requires high PT conditions. Water-fluxed melting of amphibolite produces peritectic hornblende, whereas dehydration melting produces anhydrous peritectic minerals such as pyroxene and garnet. Furthermore, water-fluxed and dehydration melting also have different geochemical characteristics. Hanko archipelago consists of migmatised metavolcanic and metasedimentary rocks. The age of regional metamorphosis and melt formation has been determined by Hopgood et al. (1983) and Bredenberg (2019) to be ca. 1.89 – 1.86 Ga. The earlier metamorphism is thought to have been completely erased from Southern Finland and the well-preserved metamorphic culmination took place ca. 1.83 Ga. Hopgood et al (1983) have argued that an earlier partial melting took place in Southern Finland. The Hanko archipelago is dominated by amphibolite and tonalite. The tonalitic leucosome that occurs in the area is thought to have been part of amphibolite partial melting during the early Svecofennian deformation ca 1.89 Ga. It has been suggested that tonalitic leucosome and tonalite are products of water-fluxed melting and derive from the same source.

In this thesis, field observations, petrographic description, SEM-EDX analysis, and WDXRF-analysis of paleosome, melanosome, leucosome and tonalite were conducted to investigate the melting process and the correlation between leucosome and tonalite. Both leucosome and tonalite contained peritectic hornblende, shared the same microstructures and textures as well as geochemical characteristics that are attributed to water-fluxed melting. However, mineral analysis of biotite, amphibole and plagioclase revealed that they derive from different sources. Furthermore, PT conditions were different for both rocks, indicating that they crystallised in different environments. Therefore, both leucosome and tonalite are products of water-fluxed melting but derive from different sources.

Keywords: water-fluxed melting, dehydration melting, tonalite, migmatite

Content

1. INTRODUCTION

The influx of externally derived hydrous fluids or the dehydration of amphibole is the common cause of partial melting of amphibolites at middle-lower crustal depths. It is thought that this type of anatexis is the main reason for the widespread occurrence of tonalitic and trondhjemitic melts in orogenic belts. Dehydration melting has been in the spotlight for many previous studies, but water-fluxed melting has not been as much in the focus, even though the latter is one of the major melt-forming processes in the middle-lower crust during orogenesis. Plate margin structures such as crustal-scale shear zones contribute to water-fluxed melting. To understand melt formation, migration to drainage, and crustal rheology during orogenesis, one must consider both water-fluxed melting and dehydration melting processes (Yuyoung & Moonsup, 2020).

In Southern Finland, two migmatite belts exist that formed during the Svecofennian orogeny: northern migmatite belt, that is located between Kimito and Fiskars, and southern migmatite belt, that is in Hanko-Ekenäs area (Fig. 1). In southernmost Finland, there is the granite-migmatite belt and north of it the tonalite-/granodiorite-migmatite belt (Mouri et al, 1999). The migmatite belts differ from each other in composition and age. The tonalite-/granodiorite-migmatite belt has a potassium-deficient leucosome, while the granite-migmatite belt has a more potassium-rich leucosome (Ehlers et al, 1993; Mouri et al, 1999).

The age of regional metamorphism and melt formation south of Southern Finland's granite-migmatite belt has been determined to be ca. 1.89–1.86 Ga (Hopgood et.al, 1983; Bredenberg, 2019). It has been suggested that the earlier metamorphism has been completely erased from Southern Finland and the well-preserved metamorphic culmination took place ca. 1.83 Ga. Furthermore, e.g., Hopgood et.al (1983) has argued that an earlier partial melting took place in Southern Finland. The MIGMA project, that is ongoing in the study area, has also found indications that an earlier partial melting has occurred.

The granite-migmatite belt is a part of the Uusimaa belt. The Uusimaa belt's south coast cuts through South Finland's major shear zone. The shear zone represents the southern border for the granite-migmatite belt (Ehlers et al, 1993). The archipelago south of the major shear zone is the study area for this thesis. The area is of a great interest due to

records of an early migmatisation found by Hopgood et al. (1983) and Bredenberg (2019). This may indicate that the area has been affected by an earlier metamorphic culmination before the late-Svecofennian (1.83 Ga) metamorphism as the rest of the Uusimaa belt (Kähkönen, 2005).

This thesis aims to study the tonalite melt formation in the Hanko archipelago and examine whether there is a correlation between the tonalitic leucosome and areas that consist of extensive tonalite area. To study this, I have focused on tonalitic leucosomes in areas consisting of amphibolite, tonalite, and granodiorite. Tonalitic leucosome has been observed in the area and thought to be part of amphibolite partial melting during the early Svecofennian deformation ca. 1.89 Ga. To study the relationships between tonalitic leucosome and tonalite that occur in the study area, I have used field observations, petrographical descriptions, major and trace element analysis, as well as mineral analysis. Furthermore, the nature of the partial melting is studied to learn whether external hydrous fluids have participated in the partial melting or whether it has been caused by dehydration melting. This is important because a small quantity of fluids could influence immensely the physical and chemical properties of a rock such as melting temperatures, melt chemistry, viscosity, and density. Therefore, influx of water affects fundamental magmatic processes such as anatexis, magma ascent, crystallisation, and eruption (Weinberg & Hasalová, 2015).

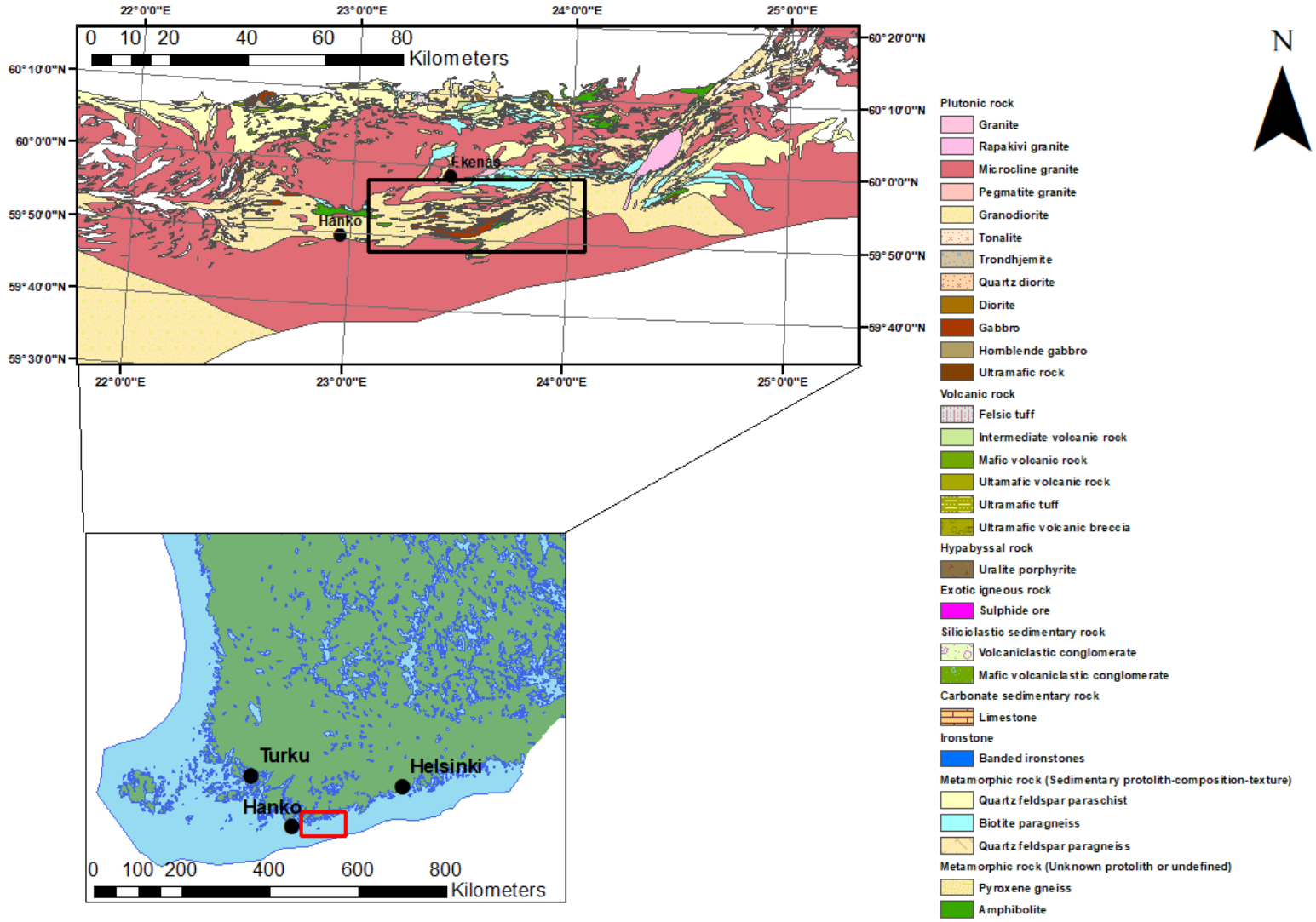

Figure 1. A broad map over the study area (modified after ESRI, 2018)

2. LITHOLOGICAL BACKGROUND

The bedrock in southernmost Finland was formed during the Svecofennian orogeny 1.92–1.77 Ga (Lahtinen et al., 2005). The Svecofennian orogeny began after or simultaneously with the Lapland-Kola orogeny 1.93–1.92 Ga. A collision between continental blocks Karelia and Norrbotten caused NNW–SSE-trending active continental margin to close. The change from divergent tectonics, which was caused by the attenuation and break-off of an Archean basement 2.1–2.05 Ga (Nironen, 2017), to convergent tectonics in ca. 1.9 Ga formed an island arc system that collided with the Archean basement (Gaál & Gorbatchev, 1987; Lahtinen, 1994). At the same time, more island arcs were formed from juvenile mantle material further southward and collided with each other 1.89–1.88 Ga

(Lahtinen, 1994). Because of this, Windley (1995) classified the Svecofennian orogeny as an arc-accretionary orogeny.

The southern Finland's accretionary arc complex consists of Paleoproterozoic supracrustal rocks aged 1.9–1.87 Ga. The supracrustal rocks are metasedimentary and metavolcanic rocks (1.9–1.88 Ga) in amphibolite and granulite facies, and synorogenic intrusive rocks (1.88–1.87 Ga) (Skyttä, 2007). There are several interpretations of how the Uusimaa belt formed, for example, Gaál (1990) suggested that the Uusimaa belt formed in a paleo-island arc terrane, whereas Nironen (1997) proposed that the Uusimaa belt formed in a back-arc basin.

The Uusimaa belt has been reshaped by several different regional metamorphic events. The early Svecofennian period (1.88–1.87 Ga) reached amphibolite facies and it can be observed throughout the Svecofennian province (Skyttä, 2007). During the late stage of Svecofennian orogeny (1.84–1.8 Ga), the highest metamorphic facies in the Uusimaa belt reached its peak (Kähkönen, 2005). Geobarometry indicates that the rocks in west Uusimaa reached granulite facies and were metamorphosed at ca. 750-800 ^{o}C at 4–5 kbar. However, the granulite facies is not restricted only to west Uusimaa, but continues to east Uusimaa (Hölttä & Heilimo, 2017). The period bears the stamp of high-temperature metamorphism and extension with associated mafic and felsic magmatism (Nironen, 2005). The metamorphism reached granulite facies and reshaped the previous rocks and structures (Kähkönen, 2005).

The deformation during the late stage of Svecofennian orogeny has been explained with, e.g., an oblique collision between protocontinents Fennoscandia and Volgo-Sarmatia (1.82–1.8 Ga) (Nironen et.al, 2002). The collision caused the post-collision magmatism in Southern Finland, which formed bimodal shoshonitic intrusions (1.81–1.77 Ga) (Eklund et.al, 1998).

The study area is in the Hanko archipelago in southernmost Finland (Fig 2.), which is a part of southern Finland's accretionary arc complex. The bedrock in the study area is dominated by migmatised metavolcanic and metasedimentary rocks, which have also been affected by fluids. Bedrocks are striking in the E-W direction, and foliation is usually subvertical. Even grained tonalites and granodiorites occur as large dikes and small plutons. Abundant deformed and migmatised granites occur north and south of the study area. However, leucogranites and granitic leucosomes occur in the proximity of the study

area. Amphibolites occur as thin layers in the gneisses or as thick formations that are deformed into large troughs that stretch several kilometres in the W-E direction. Gabbro also occurs as thin layers or large deformed troughs but is not as abundant as amphibolite. Together with amphibolite, gneisses form strongly deformed formations that contain fragments of ultramafic rocks. Limestone and skarn occur as lenses or discontinuous layers in amphibolites and gneisses (Edelman & Jaanus-Järkkälä, 1983; Saukko et.al, 2021).

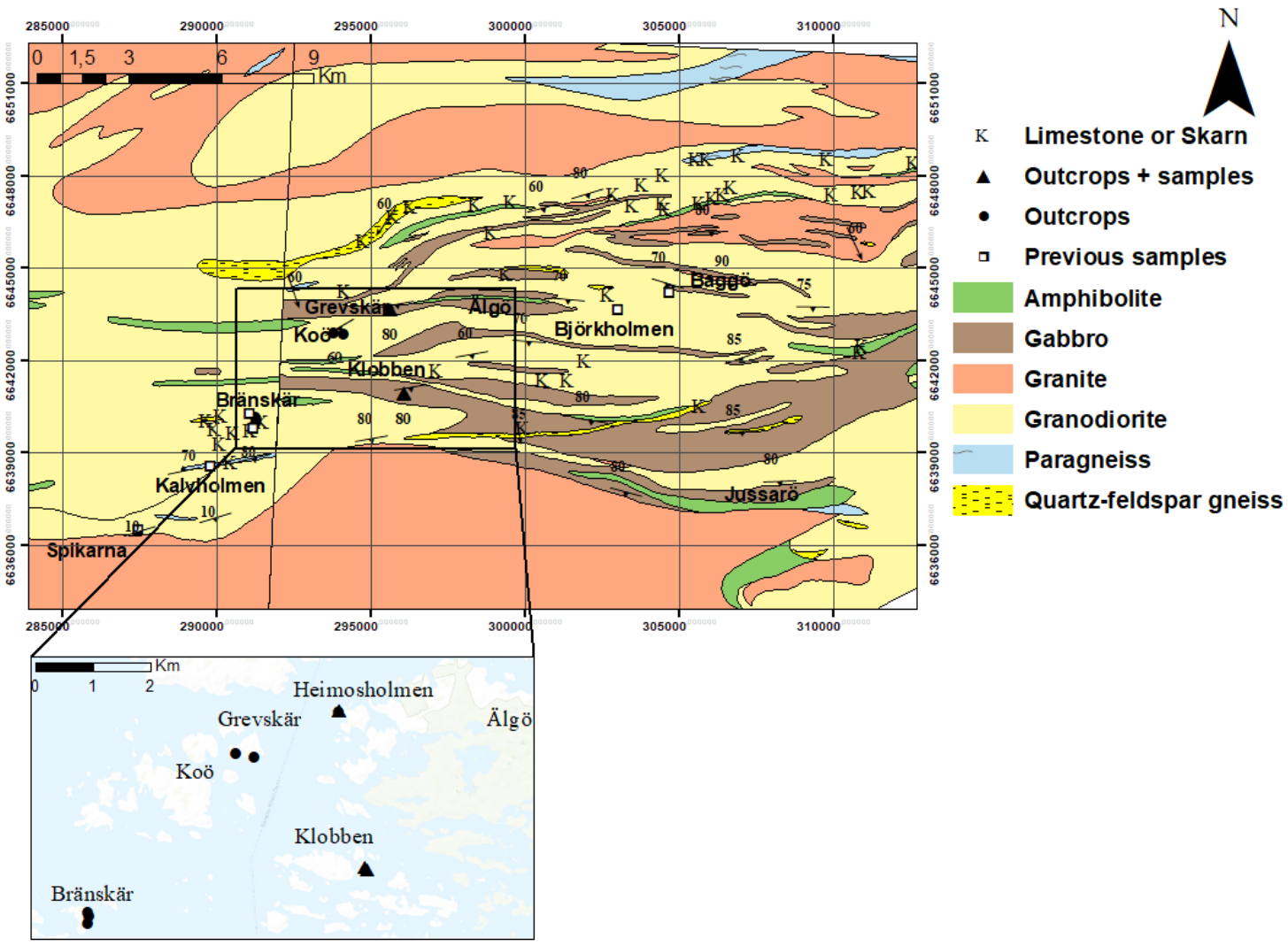

Figure 2. Bedrock map (top) and basic map (bottom) of the study area (modified after Laitila, 1973)

3. THEORETICAL BACKGROUND OF PARTIAL MELTING

Migmatite consists of two or several petrographically different parts and can be found in areas that have been affected by prograde metamorphism, i.e., change of mineral paragenesis [mineral assemblages] with increasing temperature and pressure conditions. Migmatites are formed when at least one part of the rock has been affected by anatexis, i.e., partial melting. Anatexis is a complex process that is affected by, for instance, temperature and pressure relation, presence of fluids and the composition of the protolith, i.e., the original rock. Since migmatite is formed in medium to high metamorphism, the protolith is usually an already metamorphosed rock (Sawyer, 2008).

Migmatite mainly consists of three petrographic parts. Paleosome represents the protolith and has either been partially or not at all affected by anatexis. Therefore, paleosome usually has conserved structures and textures which are older than anatexis. Neosome, i.e., "new rock", consists of components that have been exsolved by anatexis. Neosome can be divided into two segregations: leucosome and melanosome. Leucosome is the melt product of the anatexis, while melanosome is the remaining unmolten component of the protolith. Leucosome usually consists of light minerals, such as feldspars and quartz, while melanosome consists of darker minerals, such as amphiboles, pyroxene, garnet, and biotite (Sawyer, 2008).

Leucosome can be classified based on where it crystallised relative to where it was formed. Crystallisation that occurs in melt's original position is defined as in-situ. Melt that has migrated from its original prominence, but is still in its original layer, is called in-source leucosome. If the melt migrates to another layer in the same metamorphic region, leucocratic, i.e., rock that consists of at least 90% felsic minerals, veins and dikes are formed. Melt that has migrated from the original position forms sills with granitic (tonalitic, granodioritic, etc.) composition (Sawyer, 2008).

Migmatite can be classified as metatexite or diatexite based on the degree of anatexis. Metatexite migmatite consists of paleosome with well-preserved structures which are older than anatexis. By contrast, diatexite migmatite has been affected by a higher degree of partial melting and is, therefore, dominated by neosome. Paleosome can be completely missing from diatexite migmatite or it can be present in schollen structures, i.e., a

combination of rounded paleosome blocks and abundant mass of neosome which completely envelopes the paleosome blocks (Sawyer, 2008).

3.1 Amphibolite melting

Amphibolite is a phaneritic metamorphic rock type that consists mainly of hornblende, or another amphibole, and plagioclase. Depending on the protolith's bulk chemical composition, garnet, pyroxene, and quartz may occur; subordinated amounts of biotite, titanite, and Fe-Ti oxides may also be locally present. To be able to classify a rock as an amphibolite, it must consist of 75% amphibole and plagioclase (Best, 2003; Coutinho et al, 2007).

Partial melting of amphibolites at middle-lower crustal depths usually occurs due to dehydration of amphibole or the influx of externally derived hydrous fluids. Partial melting caused by breakdown of a hydrous mineral, such as amphibole, biotite, or muscovite, is referred to as dehydration melting. By contrast, partial melting caused by the presence of external hydrous fluids is called water-fluxed melting (Weinberg & Hasalová, 2015). Water-fluxed melting reactions and dehydration melting reaction of amphibolite are listed in Table 1.

3.1.1 Water-fluxed melting and dehydration melting

There are three major differences between water-fluxed melting and dehydration melting: (i) presence, type, and composition of peritectic minerals and melts, (ii) melting temperatures, (iii) initial water content of the melt (Weinberg & Hasalová, 2015).

All the water in dehydration melting reactions is derived from hydrous minerals and, therefore, the melt produced is water undersaturated. In comparison, in the presence of an aqueous fluid phase, water is only limited by the rate of inflow and, therefore, the melt produced is water-rich or water-saturated. Water-fluxed melting reactions are either congruent, i.e., the composition of the melt that forms is the same as the composition of the protolith, usually at low temperatures, or incongruent, i.e., the chemical composition

of the produced melt is not the same as the protolith, at higher temperatures where melts produced are water undersaturated. (Weinberg & Hasalová, 2015).

Dehydration melting reactions involve muscovite, biotite or amphibole as the hydrous reacting phase. Melts produced from dehydration melting vary in geochemical composition, depending on protolith composition and temperature. Melts formed from dehydration melting are usually dioritic to granodioritic and peralkaline to metaluminous in composition and have a lower K/Na ratio compared to other melts (Weinberg & Hasalová, 2015).

The influx of hydrous fluids decreases the melting temperature of amphibolite down to approximately 700–750 ºC at high-pressure conditions and down to 650 ºC at 6–10 kbar (Moyens & Stevens, 2006). Peritectic minerals, most commonly amphibole, form from water-fluxed incongruent melting reactions. Amphibole dehydration melting occurs at temperatures as high as 850–900 ºC, and typically produces peritectic clinopyroxene, orthopyroxene, and/or garnet. Therefore, it is possible to roughly distinguish water-fluxed melting and dehydration melting from each other by their peritectic minerals. Gardien et al (2000), however, showed with their experiment that water-fluxed melting of Bt (biotite) + Pl (plagioclase) + Qtz (quartz) banded gneiss at <800 ºC and 10 kbar produces peritectic garnet and hornblende. Therefore, it is plausible to influx of water trigger incongruent melting producing anhydrous peritectic minerals (Weinberg & Hasalová, 2015).

3.1.2 Melt composition of water-fluxed melting

The presence of an aqueous fluid phase affects the melting reaction and volume of the melt produced by a given protolith. Thus, water has a major role in controlling the geochemistry of granitic melts. Melting similar protoliths under variable $a\mathrm{H_2O}$, i.e., water activity, conditions give a wide variety of silicate compositions. Water-saturated melt has $a\mathrm{H_2O}$ =1, whereas water-undersaturated melts have $a\mathrm{H_2O}$ <1. The proportion of Ab (albite), An (anorthite), and Or (orthoclase) is the most significant difference between melt composition produced from water-fluxed melting and dehydration melting. The melts become richer in An and Ab and poorer in Or the higher $a\mathrm{H_2O}$ is. Therefore, added water-rich fluids produce more tonalitic to trondhjemitic melts in comparison to melts produced by dehydration melting (Weinberg & Hasalová, 2015). However, the formation

of tonalitic and trondjemitic melts is also related to high pressure melting conditions (≥8 kbar at 700 °C and ≥11 kbar at 750 °C) or protoliths' K-poor bulk compositions, rather than to the only influx of water (Bartoli, 2021).

Water influx plays a key role in the melting of amphibolite. Dehydration melting experiments of amphibolites, in the absence of free water, at 800–1000 ºC and 1–6.9 kbar conducted by Beard and Lofgren (1991) produced melts with Pl + Cpx (clinopyroxene) + Opx (orthopyroxene) + Mag (magnetite) restites and that had granodioritic to trondhjemitic compositions. In contrast, water-saturated melting experiments produced much more peraluminous, low-Fe melts which is different from most silicic igneous rocks, and amphibole-rich, plagioclase-poor residues. Beard and Lofgren (1991) concluded that water-saturated melting of amphibolite cannot produce low-K silicic rocks that are typical of magmatic arcs, whilst dehydration melting can.

3.1.3 Peritectic hornblende

Water-fluxed melting experiments have found that at low aH_2O, peritectic hornblende is stable near the solidus, i.e., ~850 ºC (Conrad et al., 1988). Experiments conducted by Naney (1983), and Naney and Swanson (1980) showed that peritectic hornblende is stable at a minimum of ~4 wt.% H_2O at 2 kbar, and 2.5 wt.% H_2O at 8 kbar. Therefore, the stability of peritectic hornblende shifts to lower aH_2O with increasing pressure. The experiment by Gardien et al. (2000) revealed that hornblende was stabilised above the water-saturated solidus only when 2-4 wt.% of water was added at ≥10 kbar. Johnston and Wyllie (1988) conducted a melting experiment of Westerly granite at 10 kbar, and the results showed that peritectic hornblende is present only if 10 wt.% of water is added. All these experiments show that the presence of peritectic hornblende indicates the addition of external hydrous fluids during partial melting.

3.1.4 Trace element

Major mineral phases that contribute to the melting reaction control concentrations of Rb, Sr and Ba and, therefore, have been used as possible indicators of the melting reaction. It

is known that micas are rich in Rb and poor in Sr, while plagioclase is poor in Rb and rich in Sr (Inger & Harris, 1993). Therefore, mica-dehydration reactions produce melts that have high Rb/Sr ratio, whereas water-fluxed melting produces melts that have low Rb/Sr ratio. Inger and Harris (1993) modelled biotite dehydration and water-present, i.e., water-fluxed, melting with Rb/Sr versus Ba and Sr diagrams. They showed that water-fluxed melting decreases Ba concentration and increases Sr with little change in Rb/Sr. In contrast, biotite dehydration showed a strong increase in Rb/Sr with little effect on Ba and Sr concentrations, because these are hosted mainly by plagioclase.

3.1.5 Structural control on water-fluxed melting

Regional faults or shear zones play an important role as fluid channels during water-fluxed melting (Sawyer, 2010). Active shear zones tend to attract hydrous fluids due to decreased pressure. Shear zones and thrust faults are also thought to be excellent pathways for both hydrous fluids that cause anatexis, and magma extraction (Mogk, 1992). The study area is situated in the southern Finland shear zone, where NW-SE trending major, minor and thrust faults could have functioned as fluid pathways down to middle-lower crust and initiated water-fluxed melting. Further studies are needed to prove this assumption.

Water-fluxed melting (Peritectic Hbl)						
	Pressure (kbar)	**Temperature (°C)**	**Reaction**	**Peritectic mineral**	**Rock type**	**Reference**
[1]	6-8	675-750	$Hbl_1 + Pl\ (An_{40}) + Bt + Qtz\ (+ H_2O) = Hbl_2 + Pl\ (An_{48}) + Qtz + melt$	Hbl	Amphibolite	Lappin & Hollister (1980); Kenah & Hollister (1983)
[2]	6-8	675-750	$Hbl + Qtz\ (+ H_2O) = Hbl + melt$	Hbl	Amphibolite	Lappin & Hollister (1980)
Dehydration melting						
	PT conditions	**Reaction**	**Melt composition**	**Peritectic mineral**	**Protolith type**	**Reference**
[3]	Variable, type of peritectic mineral depend on rock composition and PT	Hbl + Qtz = Pl + Opx + Cpx (+ Grt) + melt; Hbl + Pl = Cpx (+ Grt + Opx + Amp) + melt	Pl- rich melt	Pl, Opx, Cpx, Grt	Metabasakt; K-poor/Ca-rich amphibolite	Thompson (2001); Moyen & Stevens (2006); Wolf & Wyllie (1994)

Table 1. Water-fluxed and dehydration melting reactions of amphibolite, modified after Weinberg & Haslová (2015). (Hbl = Hornblende, Pl = Plagioclase, An = Anorthite, Bt = Biotite, Qtz = Quartz, Opx = Orthopyroxene, Cpx = Clinopyroxene, Grt = Garnet, Amp = Amphibole)

4. MATERIALS

4.1 Fieldwork

Fieldwork was conducted together with Prof. Olav Eklund and PhD. Kaisa Nikkilä in Spring 2021. During the fieldwork, ten different outcrops were observed, and nine different samples were collected from six outcrops. Four tonalite, two melanosome, one paleosome, and one leucosome sample were collected. Two of the tonalite samples, one homogenous and one heterogeneous, were collected from Heimosholmen, two tonalite and one melanosome samples from Brännskär, and one paleosome, one leucosome and one tonalite sample from Grevskär. The coordinates, field and sample description as well as what type of analysis were conducted for the collected samples are listed in table 2. Locations, where samples were collected, are marked as black triangles in figure 1. The samples names, samples descriptions, locations and coordinations of previously collected and analysed samples are listed in table 3.

4.1.1 Field observations

On the island Heimosholmen, three different outcrops were visited and observed. Outcrop 1 and 2 consisted of layered fine-grained amphibolite paleosome with coarse-grained hornblende-rich melanosome separating paleosome from fine-grained tonalitic leucosome. Outcrop 3, which is in southwestern Heimosholmen, consisted of a homogenous tonalite layer between two heterogenous tonalite layers. The homogenous tonalite was equigranular, i.e., even grained, and fine grained, whereas the heterogenous tonalite was more inequigranular, i.e., uneven grained, and coarse grained. No sample was collected from outcrops 1 and 2, however, samples of both tonalites from outcrop 3 were collected. In outcrop 1, which is in north-western Heimosholmen, small and larger fragments of ultramafic rocks were observed. The dip direction and dip for the foliation in tonalite were 110°/60°.

In outcrop 2, which is in western Heimosholmen, a 5-meter-wide layer of garnet-rich supracrustal rock was observed beside the leucosome margin with a sharp contact. Dip direction and dip for the foliation in the layered supracrustal rock were 120°/60°.

On the island Klobben, two outcrops were visited and observed. In both outcrops 4 and 5, amphibolite melting was observed. Coarse-grained hornblende-rich melanosomes were locally observed as narrow slivers along the tonalitic leucosome margins (Fig, 3 A). Both heterogeneous and homogeneous leucosomes were observed in the outcrops. Heterogenous leucosome consisted of porphyric hornblende grains embedded in the leucosome. In outcrop 5, which is north of outcrop 4, melt from paleosome migrating into partially melted paleosome was locally observed (Fig. 3 B). No sample from the outcrops was collected.

On the island Brännskär, three different outcrops were visited and observed. In outcrop 6, southeast of Brännskär, layered amphibolite paleosome, coarse-grained hornblende-rich melanosome, and tonalitic leucosome were observed. The layering was in the N-S direction, and dip direction and dip were 180°/80°. A tonalite sample was collected from the outcrop.

Outcrop 7, in east Brännskär, was similar to outcrop 5, but slivers of coarse-grained hornblende-rich melanosome are missing. Melanosome is mostly embedded in leucosome, and coarse-grained hornblende grains embedded in leucosome were observed (Fig. 4 A & B.). A sample that contained both melanosome and leucosome was collected from the outcrop.

Outcrop 8 consisted of large fragments of coarse-grained hornblende-rich melanosome (Fig. 4 C). There is no visible layering and fragments are irregular, but also slightly elongated. Between the fragments is heterogenous leucosome that has also intruded some of the fragments. A melanosome sample was collected from the outcrop.

Two outcrops were visited and observed on the island Grevskär. In outcrop 9, which is in southeast Grevskär, layered paleosome, melanosome, and tonalitic leucosome were observed. A sharp contact with plagioclase porphyry leucosome and homogenous leucosome was observed. In addition, an intraorogenic dike with sharp contacts with plagioclase porphyry leucosomes on both sides was observed. Three samples were collected from the outcrop: one melanosome, one paleosome, and one leucosome sample.

Outcrop 10, which is in southwest Grevskär, consisted of layered paleosome, melanosome, and tonalitic leucosome. The area most likely demonstrates partial melting of amphibolite paleosome. The layers' dip direction and dip were 180°/80°. A sample of tonalitic leucosome was collected from the outcrop.

Outcrop	Sample	Location	Coordinates (WGS84)	Field description	Sample description	Analysis type
Outcrop 1	No sample	Heimosholmen	59°52'49.1"N 23°20'52.8"E	Amphibolite melting and ultramafic rock fragments	-	No analysis
Outcrop 2	No sample	Heimosholmen	59°52'48.2"N 23°20'51.9"E	Amphibolite melting and garnet-rich supracrustal rock	-	No analysis
Outcrop 3	EA-2021-01 & -02	Heimosholmen	59°52'47.3"N 23°20'52.6"E	Homogenous and heterogenous tonalite	Homogenous and heterogenous tonalite	Petrographic description, SEM (EA-2021-01) & XRF
Outcrop 4	No sample	Klobben	59°51'19.8"N 23°21'32.9"E	Amphibolite melting, narrow slivers of melanosome	-	No analysis
Outcrop 5	No sample	Klobben	59°51'21.2"N 23°21'31.8"E	Amphibolite melting, melt migration	-	No analysis
Outcrop 6	EA-2021-03	Brännskär	59°50'41.9"N 23°16'28.5"E	Tonalitic leucosome, sinistral folding	Tonalite	Petrographic description & XRF
Outcrop 7	EA-2021-04	Brännskär	59°50'45.5"N 23°16'28.2"E	Melanosome imbedded in leucosome	Melanosome and leucosome	Petrographic description & XRF
Outcrop 8	EA-2021-05	Brännskär	59°50'47.2"N 23°16'27.0"E	Elongated fragments of melanosome	Melanosome	Petrographic description, SEM & XRF
Outcrop 9	EA-2021-06, -07 & -08	Grevskär	59°52'20.5"N 23°19'23.1"E	Amphibolite melting and intraorogenic dike	Melanosome, paleosome and leucosome	Petrographic description, SEM (EA-2021-07 & -08), XRF
Outcrop 10	EA-2021-09	Grevskär	59°52'20.2"N 23°19'00.9"E	Amphibolite melting	Tonalite/granodiorite	Petrographic description & XRF

Table 2. List of samples that were collected during the fieldwork.

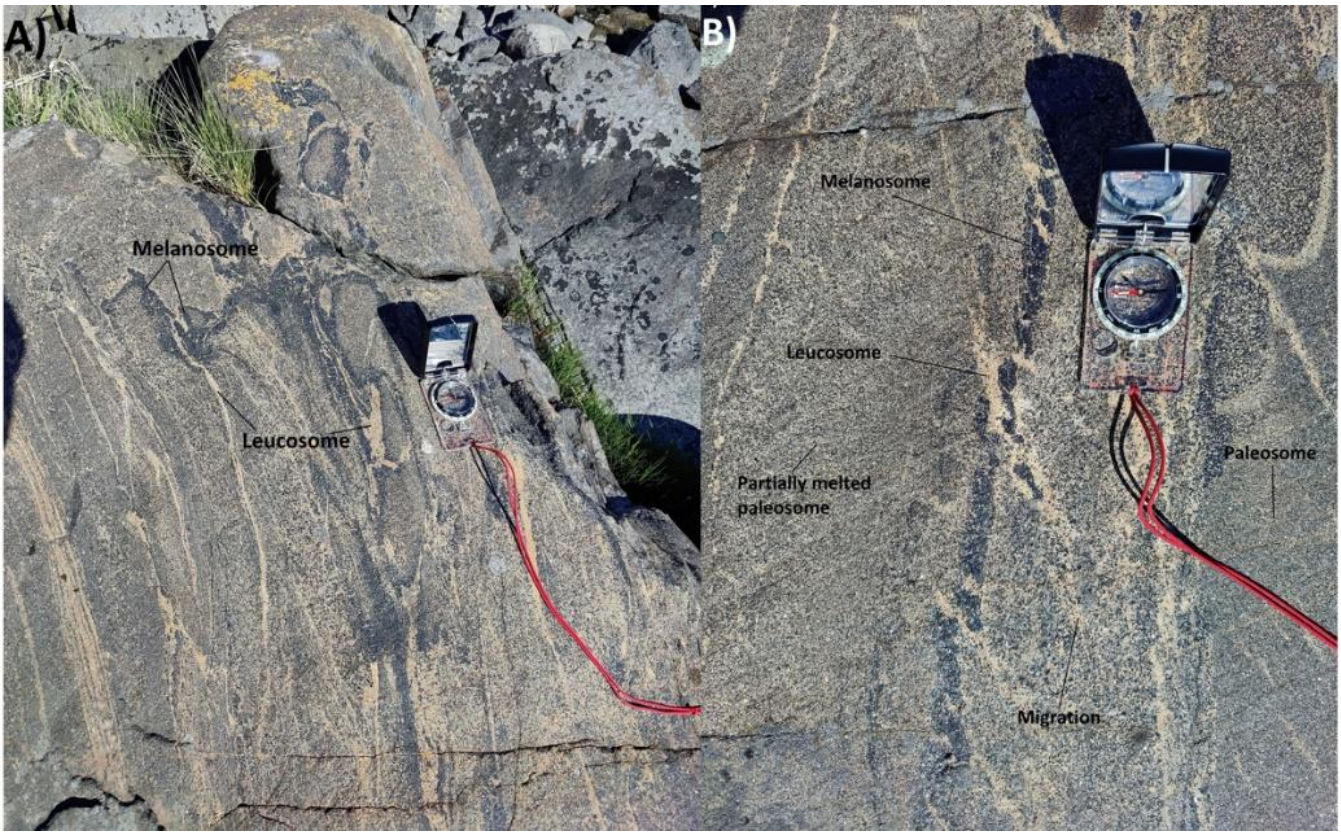

Figure 3 A) Coarse-grained hornblende-rich melanosomes as narrow slivers along leucosome margins. B) Melt from partial melted paleosome migrating into more partial melted paleosome. Leucosomes in the picture represent the last migmatisation that occurred around 1.83–1.81 Ga.

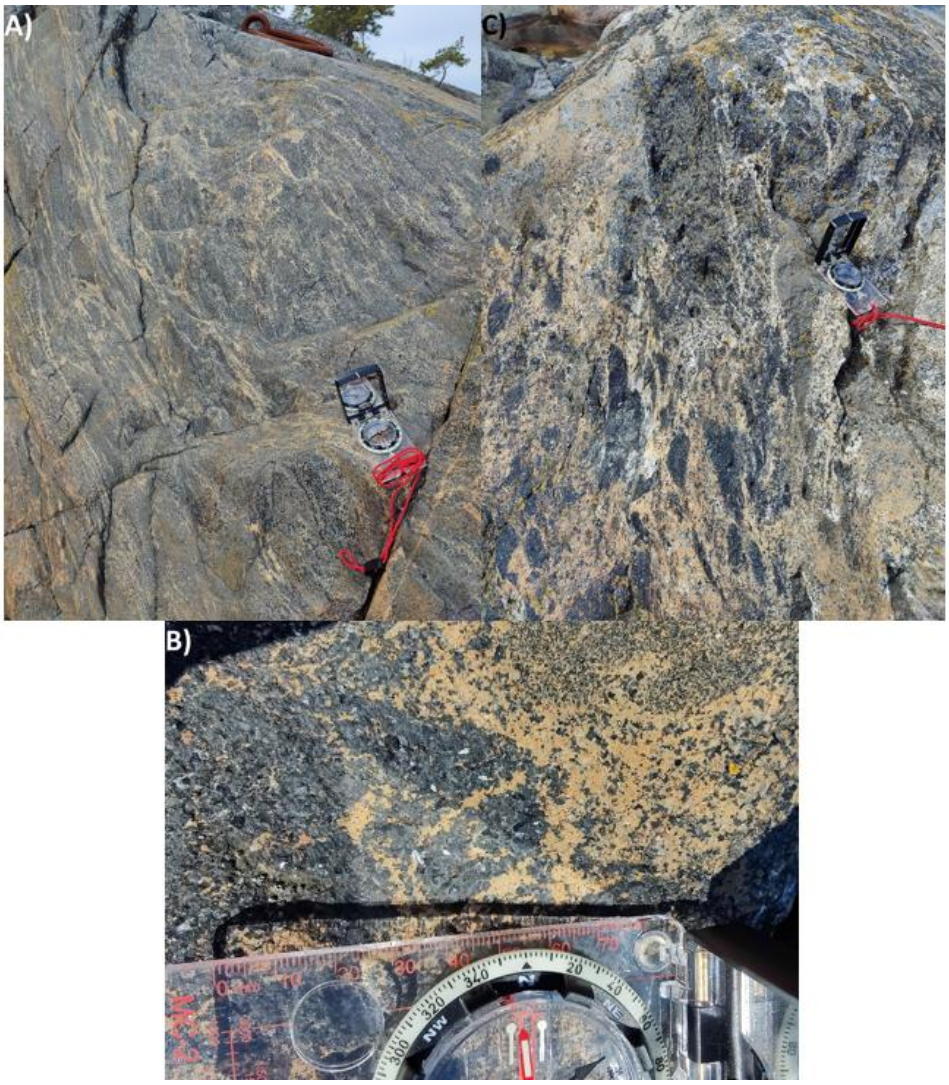

Figure 4 A) Coarse-grained hornblende-rich melanosome and tonalitic leucosome outcrop. B) Coarse-grained hornblende embedded in leucosome, grain size varies from <1mm up to 6mm. C) Fragments of coarse-grained hornblende-rich melanosome in leucosome.

4.2 Sample preparation

Samples were prepared in accordance with the method of analysis (Table 1.). Thin sections were needed for petrography description and SEM (Scanning Electron Microscopy) analysis. Twelve thin sections of the nine collected samples were made. The samples were sawn to approximately 3*5*2 cm pieces and were attached to glass sheets. The pieces were grinded and polished to the standard 0.03 mm thickness.

The collected samples from fieldwork and additional previously collected samples (Table 3) were sawn into smaller even-sized pieces, crushed and grinded into powder with Pulverisette 9, dried in a 105 ºC hot oven for approximately 24 h, mixed with wax, and

pressed in 20 kg x 1000 pressure with a minipress into briquets for trace element analysis with WDXRF (X-Ray Fluorescence). A total of 15 briquets were prepared for trace element analysis.

For major element analysis, glass disks of each sample were prepared. Approximately 4 g of each sample was scooped into their own Al_2O_3 crucibles which were placed into a 1000 ºC hot temperature-controlled furnace for one hour to evaporate water, carbonates and carbon from them. Afterwards, approximately 1 g of each sample was mixed with ca. 10.5 g of anhydrous lithium tetraborate with lithium metaborate and lithium bromide fused. The fusion mixtures were placed separately into a platinum crucible that was then placed into the Claisse LeNeo Fusion instrument, in which the heating chamber was approximately 1050 ºC hot. The instrument automatically poured the melted sample into a platinum mold, and let it cool down into glass disks. A total of 19 glass disks were prepared for major element analysis.

Sample	Sample description	Location	Coordinates (WGS84)
MIGMA-2015-01	Amphibolite	Kalvholmen	59°49'53.4"N 23°14'58.1"E
MIGMA-2015-21	Paleosome	Spikarna	59°48'42.3"N 23°12'36.0"E
MIGMA-2015-27	Garnet filled granodiorite	Hanko	59°51'48.7"N 23°04'34.1"E
MIGMA-2018-1.1	Amphibolite melting	Baggö Marina	59°53'22.4"N 23°30'32.9"E
MIGMA-2018-1.2	Leucosome from mafic protolith	Baggö Marina	59°53'22.4"N 23°30'32.9"E
MIGMA-2018-1.4	Melanosome	Baggö Marina	59°53'22.4"N 23°30'32.9"E
MIGMA-2018-1.6	Paleosome	Baggö Marina	59°53'22.4"N 23°30'32.9"E
MIGMA-2018-1.8	Tonalite	Baggö Marina	59°53'22.4"N 23°30'32.9"E
MIGMA-2018-1.9	Tonalite leucosome in amphibolite	Baggö Marina	59°53'22.4"N 23°30'32.9"E
MIGMA-2018-4.3	Tonalitic leucosome	Björkholmen	59°52'59.7"N 23°28'46.9"E
MIGMA-2018-5.4	Amphibolite	Brännskär	59°50'49.7"N 23°16'13.9"E
MIGMA-2018-5.5	Granodiorite leucosome	Brännskär	59°50'34.9"N 23°16'23.1"E
MIGMA-2018-6.1	TTG	Hanko	59°53'57.0"N 23°13'26.2"E

Table 3. Previously collected samples, TTG = Tonalite-Trondhjemite-Granodiorite. Locations are marked with rectangles in Figure 1.

5. METHODS

The thin sections were observed under polarised light microscopy for petrographic description and point analysis of individual minerals was done in SEM-EDX. The petrographic description was conducted to describe the textures and mineral content in the samples. Point analysis in SEM-EDX was done to investigate the elemental difference between biotite, amphibolite, and plagioclase in paelosome, melanosome, leucosome and heterogenous tonalite. Both major and trace element analyses were done in WDXRF to determine the elemental composition in the samples. GCDkit was used to create binary, tertiary, and spider plot diagrams of the analysis results.

5.1 Scanning electron microscope – Energy-dispersive X-ray (SEM-EDX)

A scanning electron microscope (SEM) is a variant of an electron microscope that produces images of a sample, in our case of the thin sections, by scanning the surface with a focused beam of electrons. SEM is also an important tool for identifying chemical signatures in individual mineral grains (Goodhew et al, 2001). SEM-EDX (Energy-dispersive X-ray) is a combination of scanning electron microscopy and energy-dispersive X-ray spectroscopy. SEM-EDX provides high quality picture of the microscopic surface structures of the sample as well as generates accurate information about its elemental composition (Shindo & Oikawa, 2002). The Phenom XL Desktop SEM in Geohouse was used to conduct mineral analysis of the samples.

The prepared thin sections were analysed with point analysis in SEM-EDX to compare the composition differences between biotite, amphibolite, and plagioclase in paleosome (EA-2021-07), melanosome (EA-2021-05A), leucosome (EA-2021-08) and heterogenous tonalite (EA-2021-02). Furthermore, the composition of amphiboles and coexisting plagioclases in leucosome and tonalite were analysed to determine PT conditions for the rocks. The rims of amphibole and plagioclase crystals that were located close to one another were analysed to obtain the most accurate PT estimations. SEM was operated at an accelerating voltage of 15 kV, high pressure (0.1 Pa), and counting duration for each point was 30 s. Individual mineral grains were analysed, and the chemical signature result was downloaded and transferred to CIPW calculators in Microsoft Excel.

The results were in oxide form and, therefore, CIPW calculators were necessary to calculate the ppm value for elements. Before the results could be inserted into the calculators, the results for biotite and amphibolite were multiplied by 0.95 and 0.975, respectively. This is because SEM does not consider water content in hydrous mineral grains, and it is known that biotite and hornblende contain approximately 5% and 2.5% water, respectively.

5.1.1 Plagioclase-amphibole geothermobarometer

Plagioclase-amphibole geothermobarometer is used to determine the PT conditions in which a rock has formed. Bulk composition of magma, temperature, pressure, and oxygen fugacity during crystallization affects amphibole composition. The four aforementioned factors affect the Al content in amphibole. Increased PT condition, which are the two main factors, increase the Al_2O_3 content in amphiboles (Moody et al., 1983). However, some amphiboles, such as actinolite and tremolite, are not suited for geothermobarometric studies, because they are created through subsolidus and secondary processes (Leake, 1971; Helmy et al., 2004). A general amphibole classification diagram was created to determine the composition of analysed amphiboles (Fig. 11 A). The mineral analysis results show that most of the amphiboles plot in the Ca amphibole field and, therefore, are classified as calcic amphibole. Calcic amphiboles can be distinguished into two separate groups: calcic amphibole with (Na + K) > 0.5, and calcic amphibole with (Na + K) < 0.5 (Leake et al., 1997 & 2004). The mineral analysis results of amphiboles show that all paleosome, melanosome and leucosome have (Na + K) < 0.5, whereas some amphiboles in tonalite have (Na + K) > 0.5 (Appendix VI). A diagram for calcic amphiboles with (Na + K) < 0.5 and another diagram for calcic amphiboles with (Na + K) > 0.5 were created to ensure that the analysed points were suitable for geothermobarometer study (Fig. 11 B & C).

The pressure estimation was calculated using geobarometer developed by Schmidt (1992). Schmidt's geobarometer have a standard deviation of ±0.6 kbar and, therefore, gives accurate pressure estimations. The initial temperature was calculated with thermometer developed by Blundy and Hollan (1990). The calculation considers the effect of pressure and have a standard deviation of ±40 ^{o}C and, therefore, is an accurate

plagioclase-amphibole thermometry. The geobarometry (1) and geothermometry (2) calculations are listed below:

(1) P (±0.6 kbar) = –3.01 + 4.76Al^{total} (Scmidt, 1992)

Where Al^{total} = Al^{IV} + Al^{VI}.

(2) $T(\pm 40°C) = \frac{0.677\,P - 48.98}{-0.0616 - 0.008314 \ln K}$ (Blundy and Holland, 1990)

Where $K = \left(\frac{Si-4}{8-Si}\right) \times X_{Ab}^{Plag}$.

The calculation results are shown in appendix VII. The results that are highlighted with green and red are the lowest and the highest value, respectively.

5.2 Wavelength-dispersive X-ray fluorescence (WDXRF)

WDXRF is an analytical technique used to determine the elemental composition of materials. The chemistry of a sample is determined by measuring the fluorescent X-ray emitted within a small wavelength range from a sample when it is excited by a primary X-ray source. Each element in a sample emits a set of characteristic fluorescent X-rays, i.e., a fingerprint, that is unique for that specific element (Brouwer, 2013). The Pananalytical Zetium Minerals edition in Geohouse in Turku was used for WDXRF analysis. The analysis results of major and trace element are shown in appendix II and III, respectively.

5.3 Geochemical data toolkit (GCDkit)

GCDkit is a comprehensive software designed for handling and recalculating whole-rock analyses for igneous rocks. It is written in R, which is a computer language and environment for statistical computing and graphics (Janoušek, V. et al., 2006). The main features of GCDkit used in this thesis are standard geochemical calculations involving major- and trace-element analysis. Common plots, such as binary, ternary and spider diagrams, of major- and trace-element analysis results from SEM-EDX and WDXRF were created with GCDkit.

6. RESULTS

6.1 Petrography

The minerals, textures and microstructures present in thin sections reveal if external hydrous fluids have participated in amphibolite partial melting or not. Furthermore, petrographical description along with field observations helps with the rock identification and reveals deformation events that have occurred. Sample EA-2021-07 represents the paleosome and will be petrographically described first. Paleosome is then followed by melanosome, which is represented by EA-2021-05A, B and C, and EA-2021-06. Afterwards, leucosome is described, which is represented by EA-2021-08. Tonalite will be described last and is represented by samples EA-2021-02 and -09.

6.1.1 Amphibolites

Amphibolites in the study area are medium-grained (~1–5 mm) and consist mainly of hornblende, plagioclase, biotite, and quartz together with small amounts of Fe-Ti oxides, zircons, and apatite as accessory minerals.

Prismatic hornblende and euhedral biotite are aligned parallel to a weak foliation (Fig. 5). The hornblende grains are mostly subhedral, rarely exceed 1 mm in size, and several grains contain quartz and rare plagioclase inclusions. Most of the hornblende grains are chloritised, but few unaltered grains occur.

Plagioclase grains are subhedral to anhedral and are not bigger than 1 mm in size. Several plagioclase grains have been sericitised and/or carbonatised, which are secondary alterations. Few plagioclase grains display oscillatory zoning. Both plagioclase and quartz grains display undulose extinctions. Undulatory extinction in minerals occurs in rocks that have been subjected to deformation (Nesse, 2004). Therefore, both plagioclase and quartz have been affected by plastic deformation events.

Quartz grains occur as subhedral to anhedral and are mostly less than 0.5 mm in size. Interstitial quartz fills space between rounded hornblende and plagioclase grains; this microstructure indicates dissolution at high temperatures (Sawyer, 2008).

Biotite occurs mostly as euhedral, but subhedral grains occurs as well. Small zircon and apatite inclusions occur in biotite. Some biotite grains display initial chloritisation.

6.1.2 Melanosome and leucosome

The melanosomes are enriched in large-grained (≥5 mm) poikilitic hornblende together with minor plagioclase and quartz, and both zircon and apatite occur as small accessory minerals. Plagioclase has been either partially or heavily sericitised, which is a secondary alteration. Hornblendes occur as subhedral to anhedral, and commonly contain quartz inclusions. Hornblende grain size ranges from 1.5 mm to approximately 5 mm, which is larger than what it is in amphibolites. Occasionally, crystallised melt can be observed in hornblende grain triple junctions (Fig. 6 A & B). Quartz display undulose extinction and have been dynamically recrystallised. Interstitial quartz can be observed along the grain boundaries of hornblende (Fig. 6 B); such a microstructure indicates an increase in the H_2O content of incipient melt that reduces the wetting angle of the quartz grains (Sawyer, 2001).

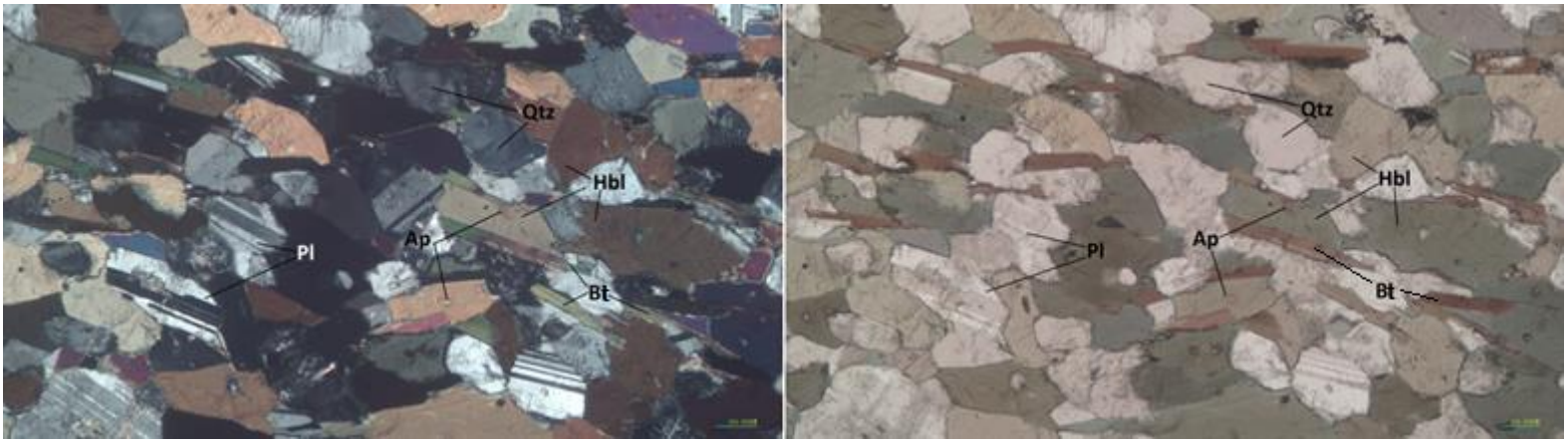

Figure 5. Photo of sample EA-2021-07. (Left) Amphibolite shown in XPL. (Right) Amphibolite shown in PPL. (Scale shown with 0.16mm long blue line on the bottom right corner of the photos; Pl = Plagioclase, Qtz = Quartz, Hbl = Hornblende, Bt = Biotite, Ap

The leucosomes mainly consist of plagioclase, hornblende, quartz, and biotite along with a minor amount of titanite, apatite and zircon. Poikilitic hornblende containing inclusions of plagioclase, quartz and rare biotite occurs in the leucosomes. Plagioclase mainly occurs

as subhedral grains and locally form framework structures with interstitial quartz aggregates (Fig. 6 C); such a microstructure can be interpreted as the presence of former melts crystallised into the leucosome (Vernon & Collins, 1988). Initial carbonatization in plagioclase occurs locally and is interpreted as secondary alteration. Plagioclase grains in the leucosomes often have straight grain boundaries with quartz (Fig. 5 D); such microstructure indicates that both plagioclase and quartz grew from a former melt phase (Holness & Sawyer, 2008; Sawyer, 2010; Holness et al., 2011).

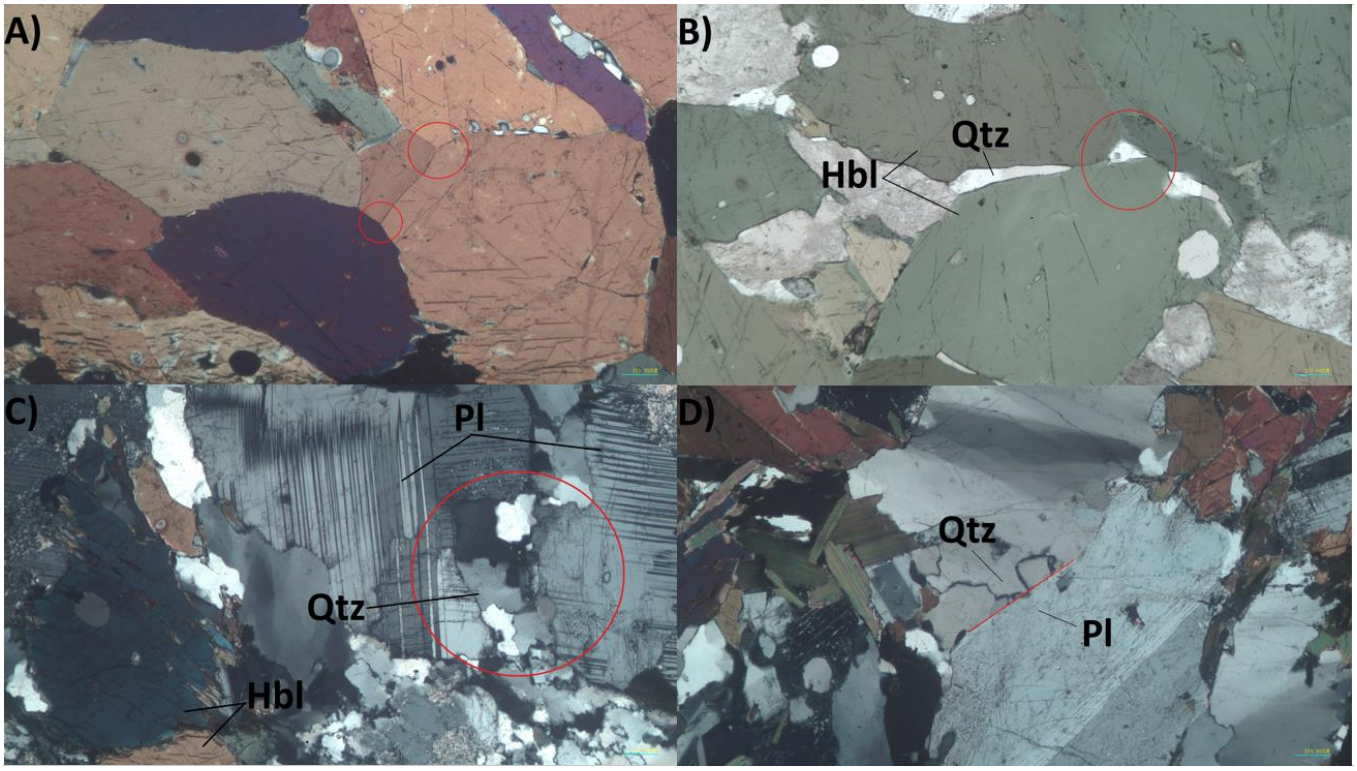

Figure 6. Photos A and B are from sample EA-2021-05 and C and D are from sample EA-2021-08. A) Triple junction between hornblende grains. B) Interstitial quartz between two hornblende grains and melt in triple junction highlighted with a red circle. C) Plagioclase form a framework structure with interstitial quartz aggregates. D) Straight grain boundary between a quartz and a plagioclase grain. (A, C and D are shown in XPL, and B is shown in PPL).

6.1.3 Tonalite

Tonalite mainly consists of plagioclase, hornblende, biotite, quartz, and minor amounts of Fe-Ti oxides. Plagioclase occurs as euhedral to subhedral and occasionally as phenocrysts. Some plagioclase phenocrysts have oscillatory zoning pattern (Fig. 7 A). Initial carbonatization and sericitization can be observed in some plagioclase grains (Fig.

7 D). Hornblende occurs as euhedral to subhedral and occasionally as phenocrysts with quartz, plagioclase, rare biotite, apatite, and Fe-Ti oxide inclusions (Fig. 7 C). Most of the hornblende grains have been completely or partially chloritised, however, few hornblende grains have not been altered. Biotite occurs as euhedral to subhedral grains and does not exceed 1 mm in length. Quartz occurs as 1-2 mm long anhedral grains and displays undulose extinction and have been dynamically recrystallised (Fig. 7 B). The modal abundance of plagioclase and quartz varies between 40-60% and 20-40% respectively. Based on classification after IUGS submission recommendations (1973), the rock can be classified as biotite-hornblende tonalite.

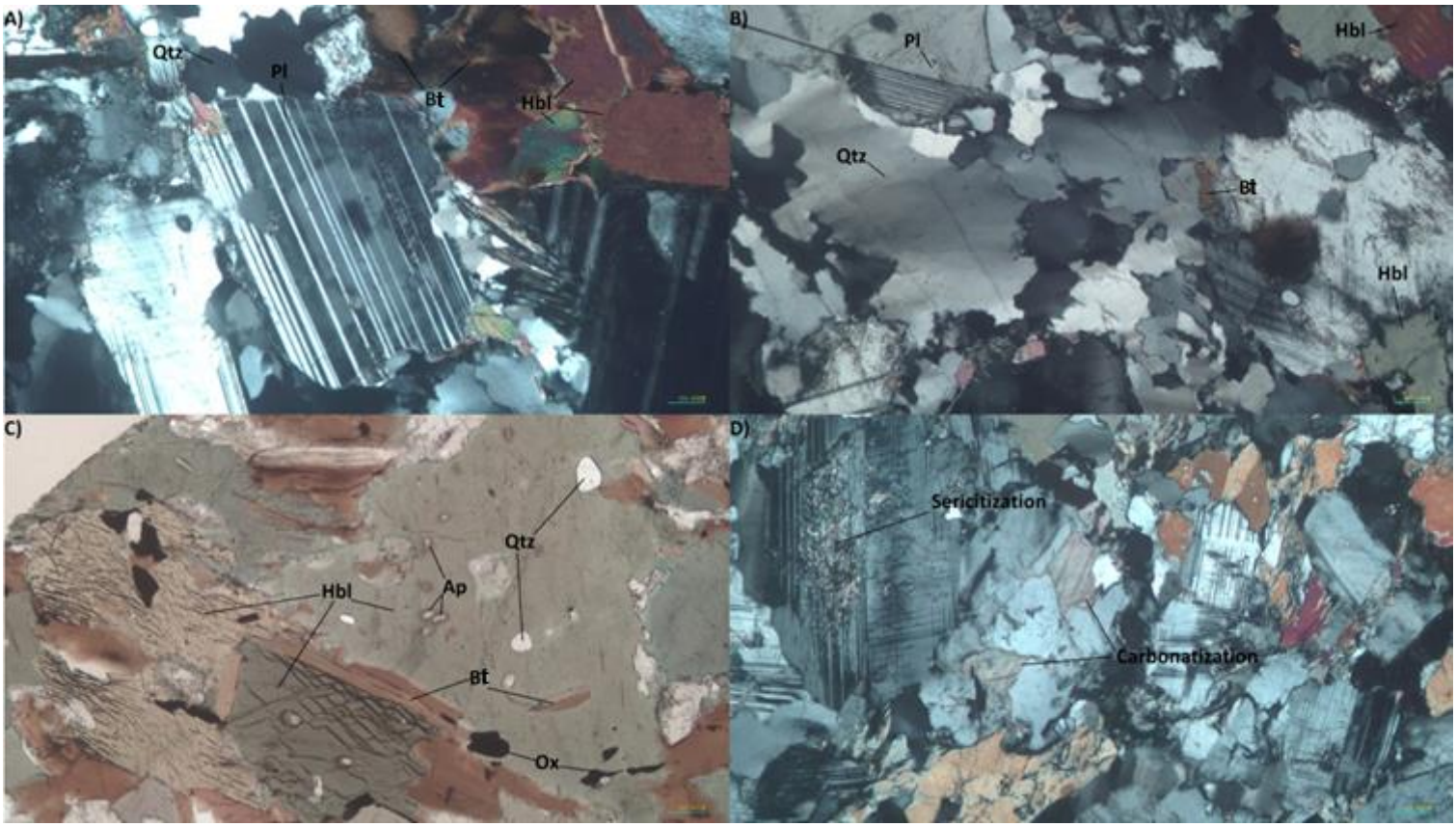

Figure 7. Photo of sample EA-20201-02. A) Oscillatory zoning pattern in plagioclase. B) Quartz display undulose extinction and have been dynamically recrystallised. C) Chloritised hornblende grains with quartz, biotite, apatite, and oxide inclusions. D) Initial carbonatization and sericitization in plagioclase grains. (A, B and D are shown in XPL, and C in PPL; Ox = Oxide)

6.2 Geochemical indications of partial melting

A plot of FeO_T + MgO versus K_2O is a useful diagram (Fig. 8) in determining the processes of migmatite evolution and anatectic granite formation from amphibolites (Sawyer, 1998). However, protoliths in the study area are depleted in potassium and produce tonalitic leucosomes through partial melting and, therefore, K_2O is replaced with Na_2O. Na_2O, that is present in plagioclase, is an incompatible element and, therefore, partition in the melt during partial melting. Iron and magnesium, that are present in mafic phases, are highly compatible elements and, therefore, partition in the solid during partial melting (Wolfram et al., 2018). Therefore, melanosome is depleted of Na_2O and enriched with FeO_T + MgO, whereas leucosome and tonalite are depleted in FeO_T + MgO and enriched in Na_2O. This creates a trend, where melanosome plot high on the top left corner of the FeO_T + Mgo vs. K_2O diagram, whereas leucosome and tonalite plot on the bottom left corner, and paleosome plot between these two quadrants (Fig. 8).

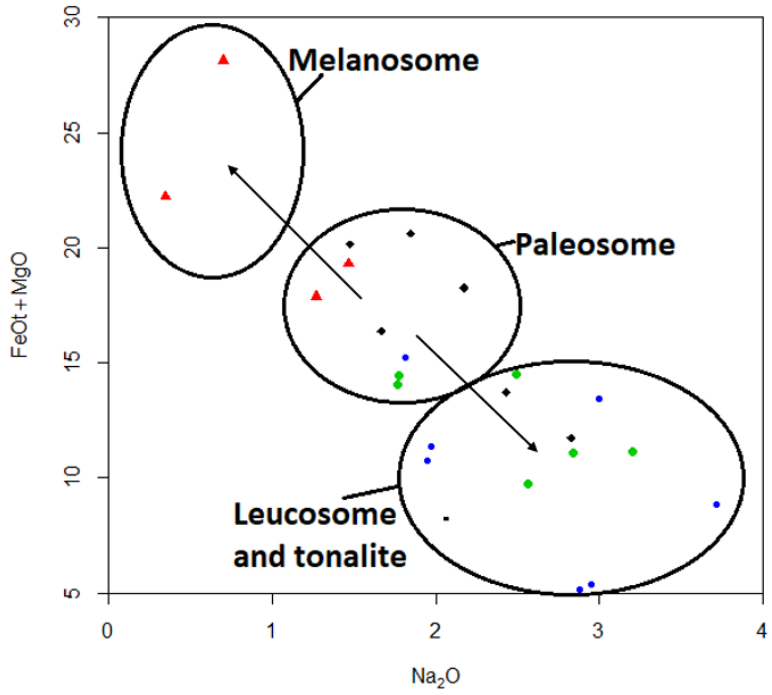

Figure 8. FeO_T + MgO vs. Na_2O binary diagram that show the partial melting evolution of paleosome (black circles). Leucosome (blue circles) and tonalites (green circles) are depleted in FeO_T and MgO, and enriched with Na_2O, whereas melanosomes (red triangles) are depleted in Na_2O and enriched in FeO_T and MgO.

It is known that Sr is compatible with plagioclase, K_D, i.e., distribution coefficient, for Sr in plagioclase is approximately 3, whereas Sc is highly compatible with amphibole, with K_D for Sc in amphibole is around 17. With a Sr/Sc vs. Sc diagram (Fig. 9) we can observe the evolution of the partial melting. Sc is compatible with amphiboles and, therefore, partition in the restite during partial melting, whereas Sr is compatible with plagioclase and, therefore, partition in melt.

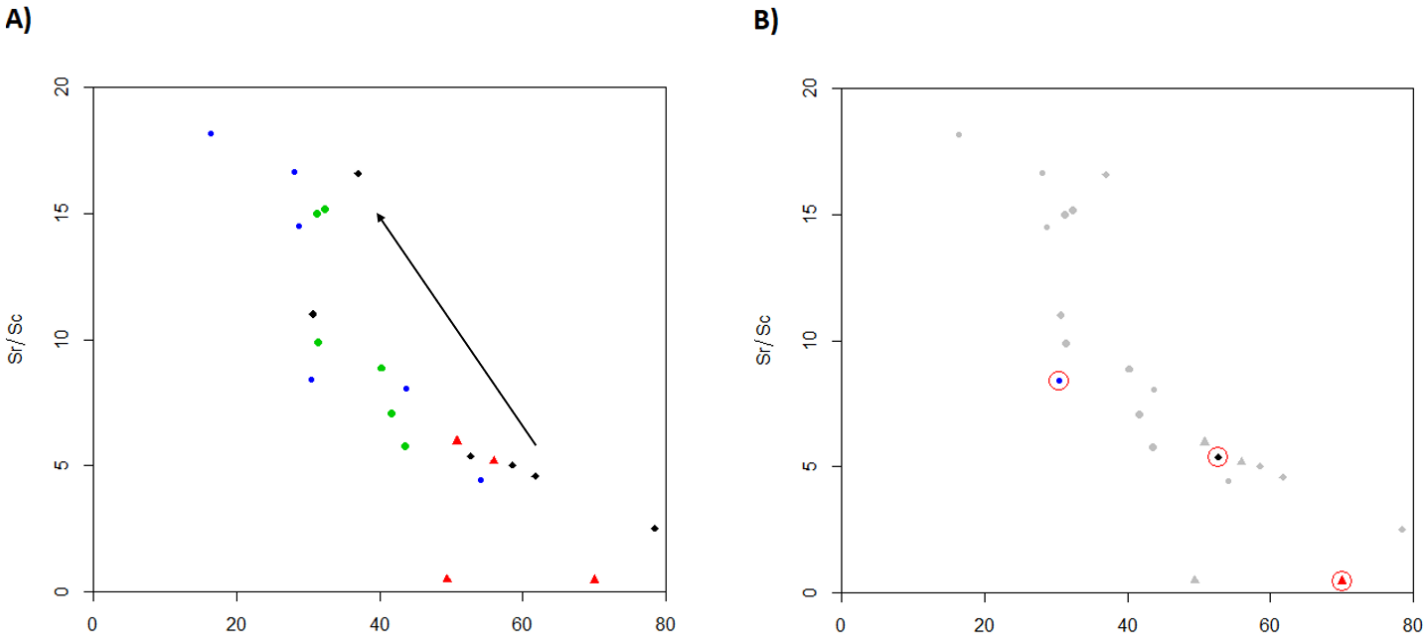

Figure 9. Sr/Sc – Sc diagram. A) A trend, which is illustrated with an arrow, can be seen, where paleosomes and melanosomes are enriched in Sc and have low Sc/Sr-index, whereas leucosomes and tonalites have high Sc/Sr-index and depleted in Sc. B) Samples EA-2021-05, -07 and -08 are highlighted.

It is important to note that some samples that are classified as paleosomes plot in the same proximity as leucosomes and tonalites. Some of these paleosome samples have been partially melted, such as MIGMA-2018-5.2, and, therefore, plot toward leucosome and tonalite. Some samples that are classified as amphibolite or paleosome, such as MIGMA-2015-01 and -21, that have been affected by K-metasomatism (Fig. 10). Spider diagram show a spike in potassium, that indicates contamination caused by K-metasomatism, i.e., chemical alteration of a rock caused by hydrothermal or other fluids (Pearce, 1996; Harlov & Austrheim, 2013). Therefore, paleosome samples that plot in the proximity of leucosomes and tonalites can be ignored in this study.

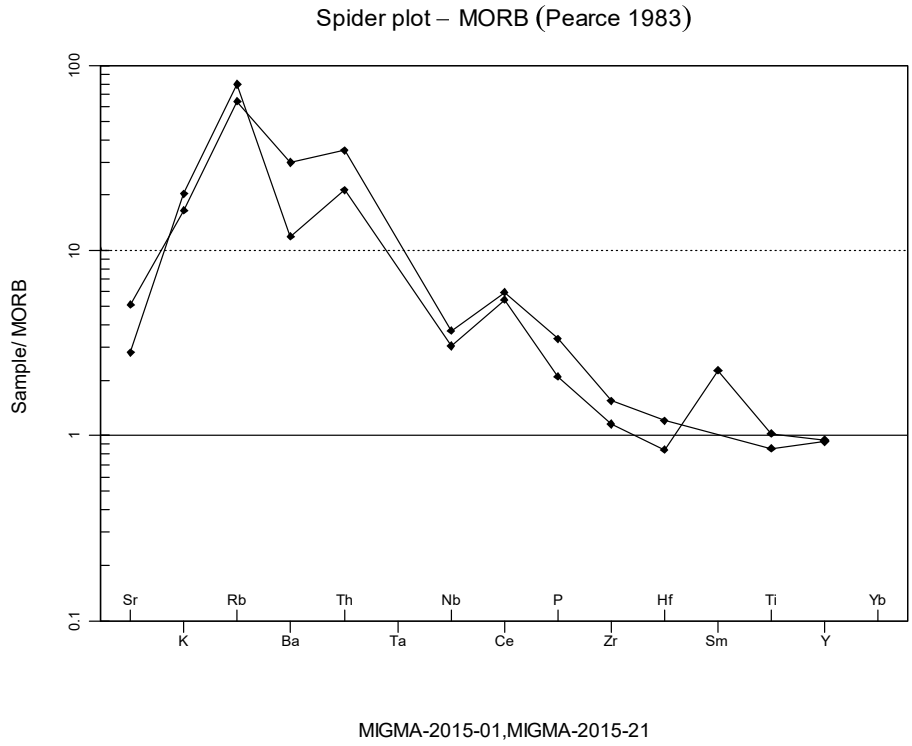

Figure 10. Samples MIGMA-2021-01 and -21 are plotted in the spider plot diagram (modified after Pearce, 1983).

6.3 SEM analysis

6.3.1 Biotite

The general composition of all biotites is phlogopite in the Fe/(Fe+Mg) vs. tot.Al diagram (Fig. 11 A). Biotite in leucosome has a lower Fe-index compared to paleosome and tonalite, and tonalite has a lower Fe-index than paleosome. Biotite in leucosome also have a higher Al-index than paleosome and tonalite, which have approximately the same Al-index.

In the FeO-10xTiO_2-MgO diagram, which separates the primary biotites from re-equilibrated primary biotite and secondary biotite, the majority of biotites in paleosome, leucosome and tonalite plot in the field of re-equilibrated primary biotite, except for a few that are deficient in Ti and plot in the field of secondary biotite (Fig. 11 B). Melanosome did not bear any biotite; therefore, it was not considered in biotite analysis.

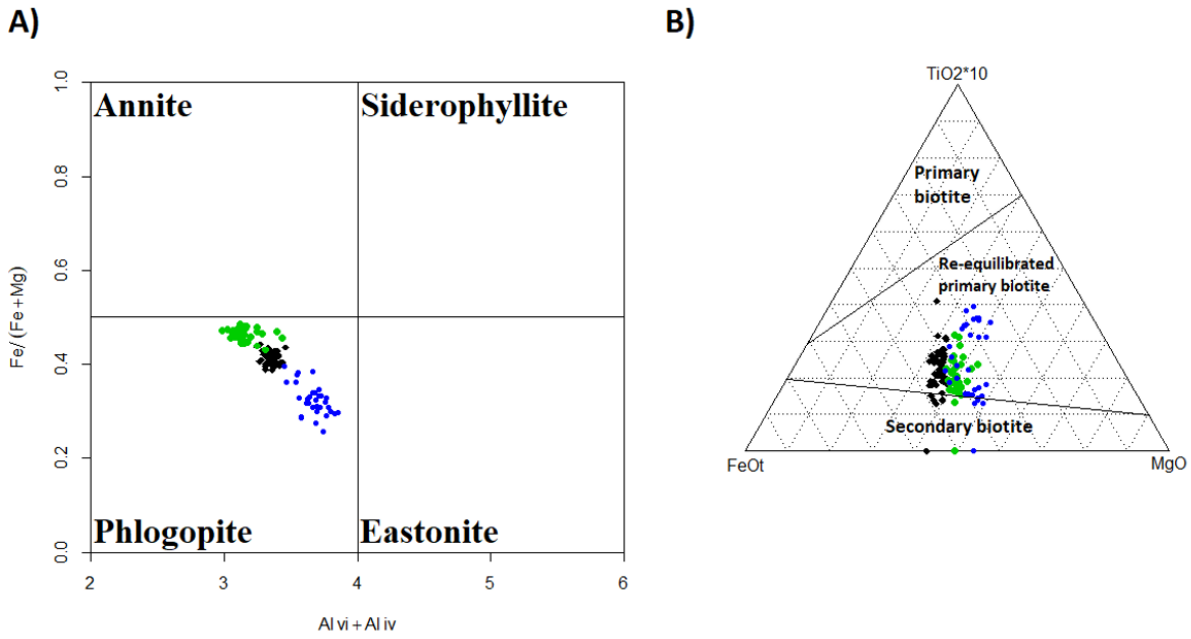

Figure 11. SEM analysis of biotites in paleosome, leucosome and tonalie.. A) Biotites are classified as phlogopites according to the Fe/(Fe+Mg) vs. total Al diagram. B) Diagram separating primary biotite from re-equilibrated primary biotite and secondary biotite

The fO_2, i.e. fugacity, and aluminosity variation diagram (Fig. 12) reflects the environment biotite grew in and is reflected by FeO/MgO ratio and Al_2O_3/(FeO+MgO) index. Bell et al. (2017) used the fO_2 value 3.5 to distinguish reduced and oxidised environment, and aluminosity values >0.55 for peraluminous rocks and <0.45 for metaluminous rocks. All biotites have formed in an oxidizing environment and crystallised from a peraluminous magma. The aluminosity in leucosome is higher compared to tonalite and paleosome.

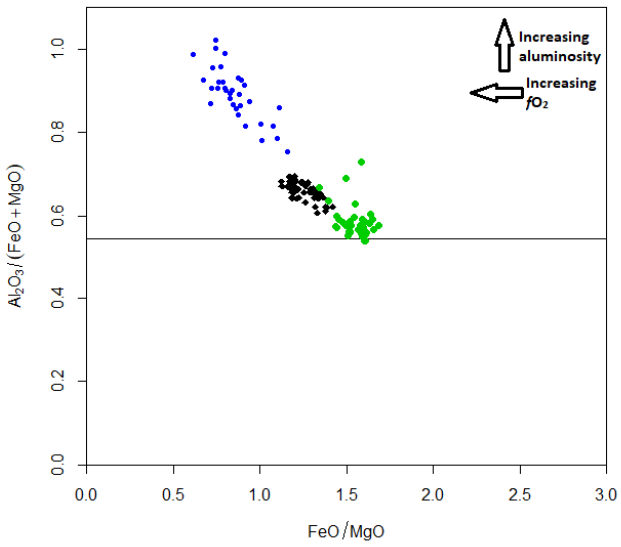

Figure 12. Diagram illustrating variations in fO_2 and aluminosity. Coloured arrows indicate trends.

The Ti content and Mg# are excellent indicators for crystallisation temperature of biotite. High Ti and high Mg# indicates a high crystallisation temperature. By using the Ti-in-biotite geothermometer (Fig. 13) developed by Henry et al. (2005), half of the analysed biotites in paleosome and leucosome gave temperatures below 500 ºC. The other half of biotite in palesome reached above 500 ºC, and the other half of biotite in leucosome reached 600 ºC. In contrast, biotites in tonalite gave temperatures well over 500 ºC and even reaching 650 ºC.

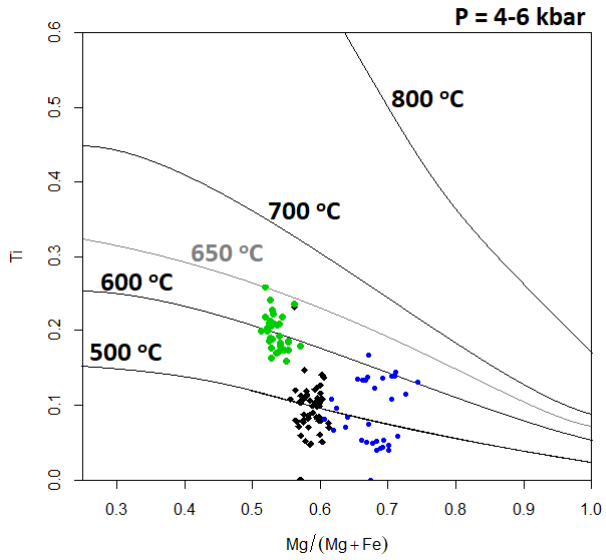

Figure 13. Ti-in-biotite geothermometer modified after Henry et al. (2005).

6.3.2 Amphibole

The majority of analysed amphiboles plot in the Ca-amphibole field in the Ca-Mn^{2+}-Na ternary diagram (Fig. 14 A), however, most of the amphiboles in melanosome plot in the Ca-Na-amphibole field. This indicates that the amphiboles in paleosome, leucosome and tonalite are Ca-rich in composition and, therefore, classified as calcic amphiboles, whereas most amphiboles in melanosome are Na- and Ca-rich in composition. The calcic amphiboles, that have (Na + K) < 0.5, plot in the Mg-hornblende field in the $Mg/(Mg+Fe^{2+})$ vs. Si calcic amphibole classification diagram (Fig. 14 B), however, a few amphiboles in tonalite plot in the tschermakite field. A few amphiboles in tonalite have (Na + K) > 0.5 and, therefore, plot in the edenite field and pargasite/magnesiohastingsite field (Fig. 14 C). Because Al^{VI} is lower than Fe^{3+}, the amphiboles that plot in pargasite/magnesiohastingsite field are classified as magnesiohastingsite. Most of the amphiboles are suitable for geothermobarometry study, however, tschermakite do not coexist with plagioclases (Leake et al., 1997). The petrographic observations have proved that amphibole and plagioclase coexist in the samples and, therefore, amphiboles classified as tchermakite are most likely errors and, therefore, are not suitable for the geothermobarometry.

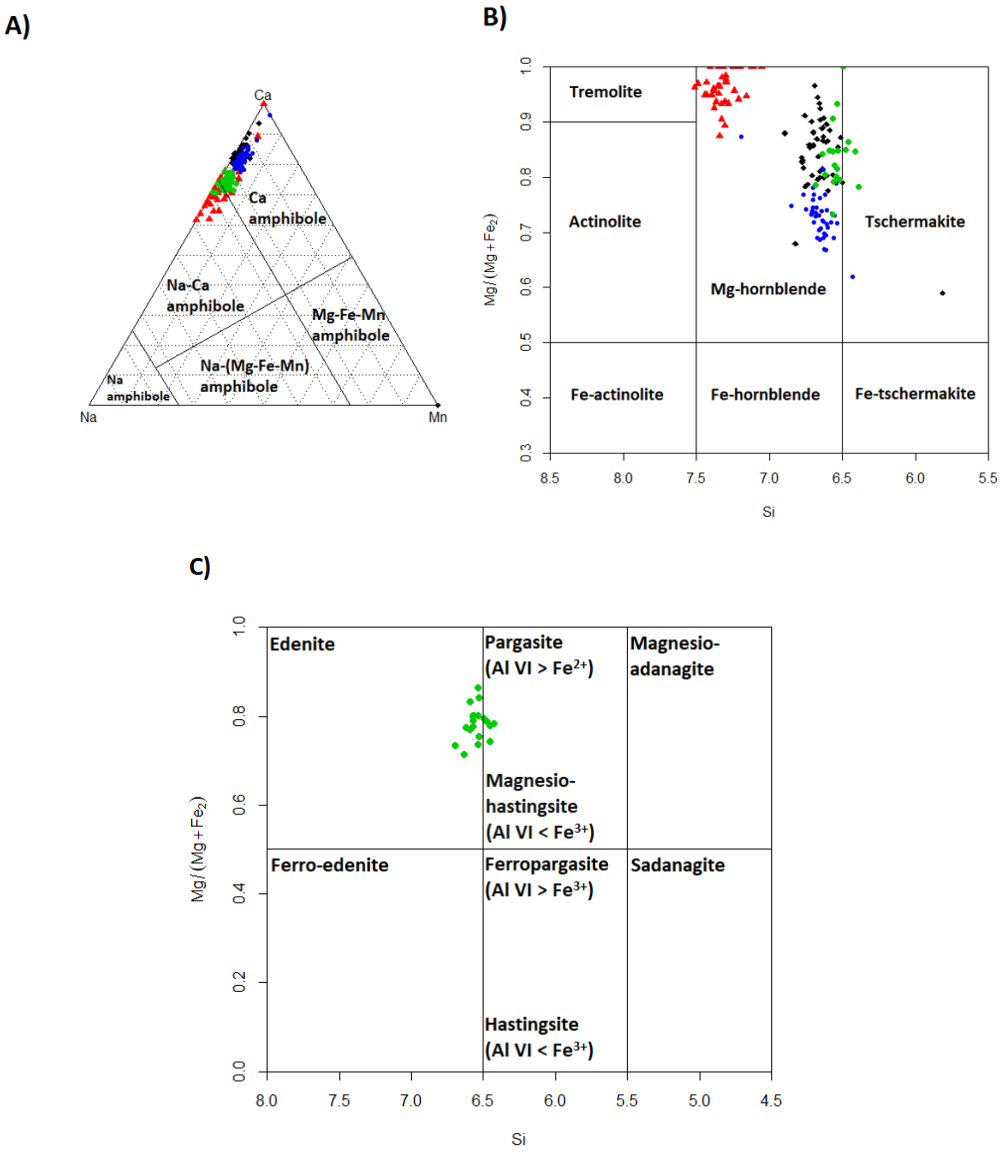

Figure 14. Amphibole classification diagrams. A) Ca-Mn^{2+}-Na ternary diagram [modified after Banno et al. (2019)] showing a compositional range of amphibole from paleosome, melanosome, leucosome and tonalite. B) Calcic amphibole classification diagram where (Na + K) < 0.5. C) Calcic amphibole classification diagram where (Na + K) > 0.5 (B & C modified after Leake et al., 1997).

By using the calculations (1) and (2), the PT conditions for leucosome and tonalite melting could be determined. The geobarometry calculation developed by Schmidt (1992) has a deviation of ±0.6 kbar, and the geothermometry calculation developed by Blundy and Holland (1990) has a deviation of ±40 °C. The average pressure and temperature for leucosome melting was calculated to be approximately 8.3±0.6 kbar and 543±40 °C, respectively, whereas the average pressure and temperature for tonalite melting was calculated to be approximately 6.7±0.6 kbar and 553±40 °C, respectively (Fig. 15).

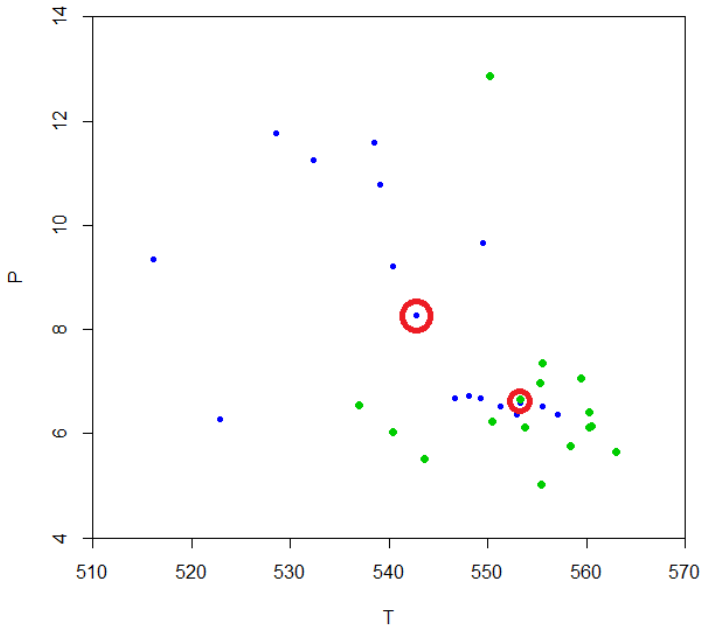

Figure 15. PT diagram. P = pressure in kbar and T = temperature in °C. The highlighted samples are the average result of leucosome (blue) and tonalite (green).

6.3.3 Plagioclase

The composition of the analysed plagioclase in paleosome, melanosome, leucosome and tonalite varied (Appendix V). In the ternary feldspar diagram (Fig. 16), paleosome plots in the andesine (30-50 An%) and labradorite (50-70 An%) field, whereas the majority of plagioclase in leucosome plots in the andesine field. The majority of plagioclase in tonalite plot in the andesine field, few grains are An-richer and plot in the labradorite field. Plagioclase in melanosome are An-poor compared to plagioclase in paleosome, leucosome and tonalite. The majority of plagioclase in melanosome plot in the andesine field, and a few grains plot in the oligoclase (10-30 An%) and albite (0-10 An%) field. Analysed plagioclase that plot in the empty space have most likely been affected by K-metasomatism.

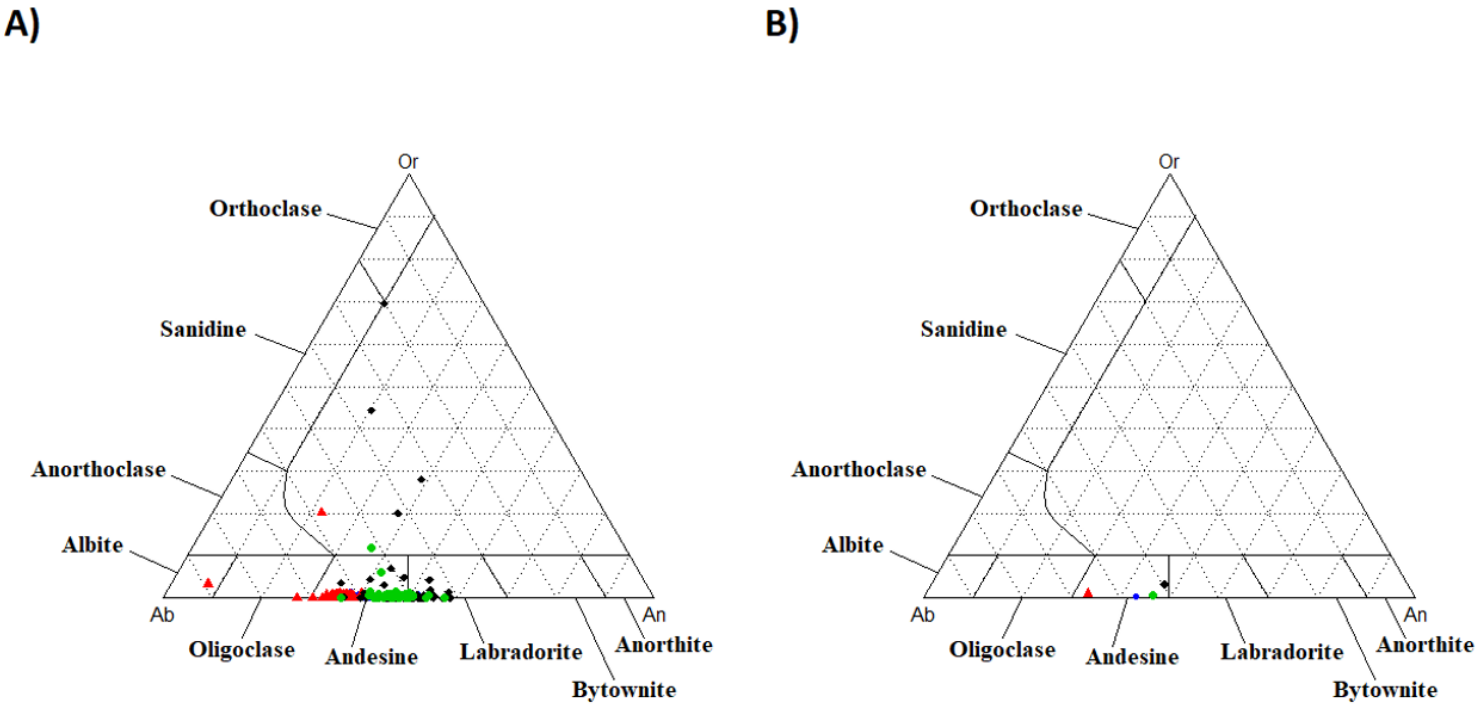

Figure 16. Ternary feldspar diagram. A) All analysed plagioclase plotted. B) The average result of analysed plagioclase.

6.4 WDXRF analysis

The major element analysis of EA-2021-07, -05 and -08 revealed that they are a gabbro, gabbroic norite and tonalitic leucosome respectively. It was also confirmed that the tonalite, EA-2021-02, is an actual tonalite (Fig. 17). Most paleosome plot in gabbro, gabbroic norite and gabbroic diorite field, however, a few are much more felsic and plot in the diorite field. Leucosomes are in composition tonalitic to granodioritic, however, a few samples are more intermediate and plot in the diorite field. A few assumed tonalites, such as the earlier mentioned homogenous tonalite in outcrop 3, plot in gabbroic diorite and diorite field.

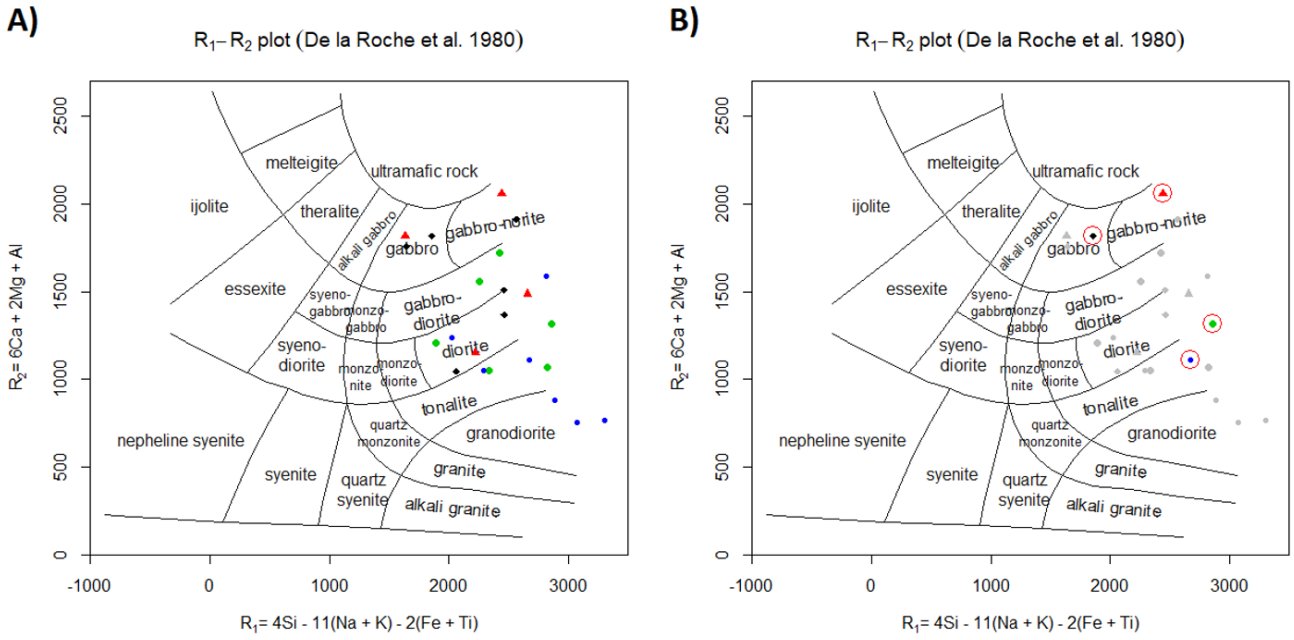

Figure 17. R_1-R_2 plot diagram modified after De la Roche et al. (1980). A) All sample plotted in the plot diagram. B) EA-2021-02, -05, -07 and -08 are highlighted with red circles.

The feldspar triangle diagram further supported the assumption of tonalite being an actual tonalite and leucosome having a tonalitic composition (Fig. 18). The majority of leucosomes and tonalite plot in the tonalite field, with a few exceptions that plot in granodiorite, trondhjemite and granite field.

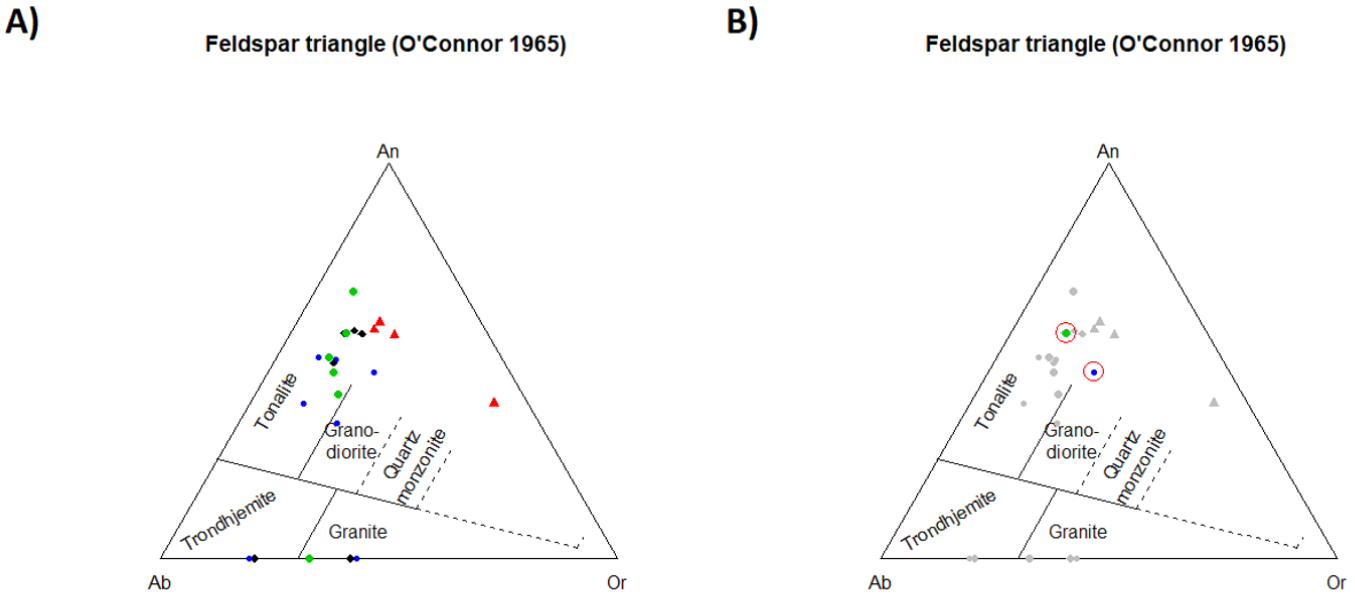

Figure 18. Feldspar triangle diagram modified after O'Connor (1965). A) All samples plotted in the diagram. B) Samples EA-2021-02 (green) and -08 (blue) are highlighted with red circles.

Most of the samples plot in the calc-alkaline series when plotted in the $SiO_2 - K_2O$ binary diagram (Fig. 19). All the analysed samples plot in the VAG (Volcanic Arc Granite) field in the granite tectonic discrimination diagrams (Fig. 20). According to Pearce et al. (1984), granites from the calc-alkaline arcs plot in the calc-alkaline series, whether it be oceanic or continental.

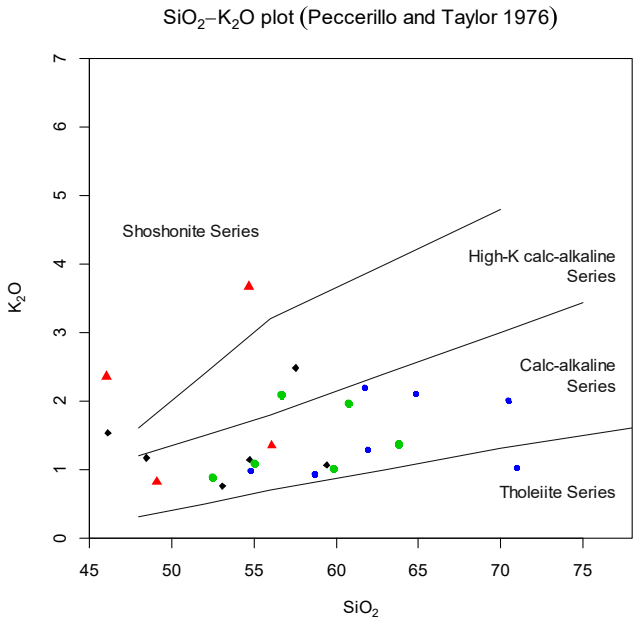

Figure 19. SiO_2-K_2O plot diagram modified after Perccerillo & Taylor (1976).

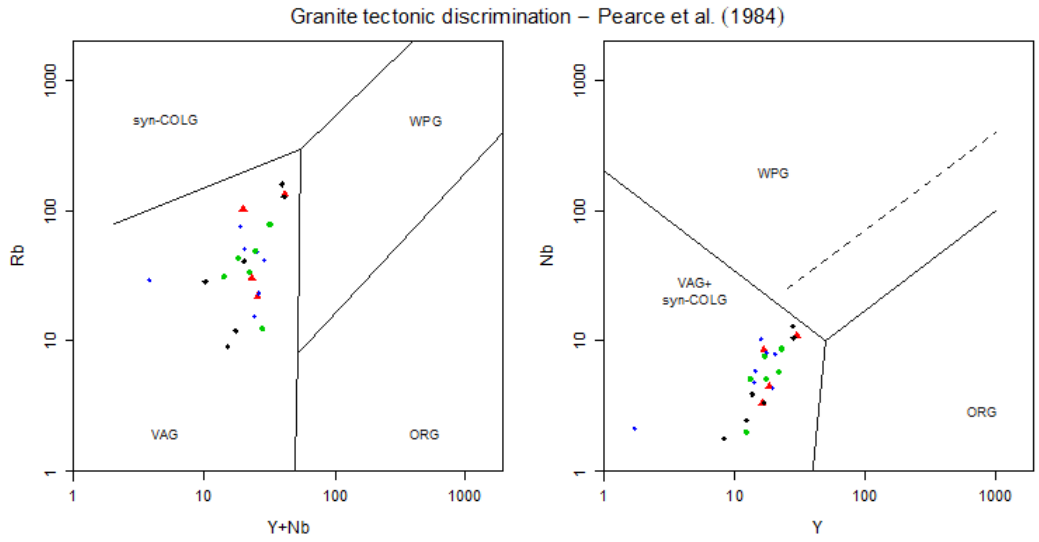

Figure 20. Granite tectonic discrimination diagram modified after Pearce et al. (1984). Ocean ridge granites (ORG), volcanic arc granites (VAG), within plate granites (WPG) and syn-collisional granites (syn-COLG).

The ORG (Ocean Ridge Granite) referenced spider plot (Fig. 21) shows that leucosome and tonalite are enriched in Rb, Ba and Th, and Ce relative to Ta, Nb, Zr, Y and Yb. This indicates that both leucosome and tonalite are calc-alkaline collisional granitic rocks (Pearce et al., 1984).

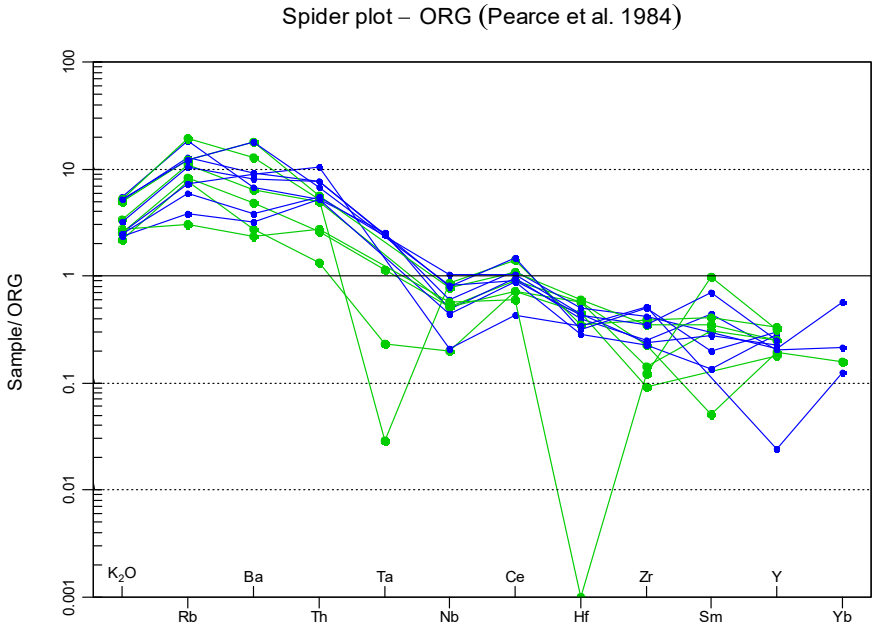

Figure 21. Trace element analysis results of leucosome and tonalite plotted onto ocean ridge granite (ORG) referenced spider plot (modified after Pearce et al., 1984).

Breakdown of muscovite in the absence of hydrous fluids increases the Rb/Sr ratio and decreases Ba and Sr. Figure 22 and figure 23 show trends suggesting that both leucosome and tonalite derive from vapour-present melting.

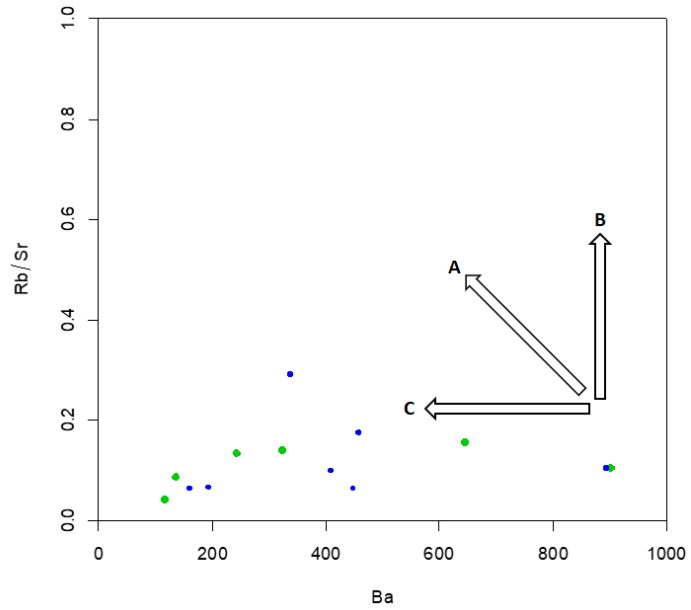

Figure 22. Melting reactions can be observed through Rb/Sr ratio and Ba index (modified after Inger & Harris, 1993). A) Vapour-absent Ms-dehydration melting. B) Vapour-absent Bt-dehydration melting. C) Vapour-present melting.

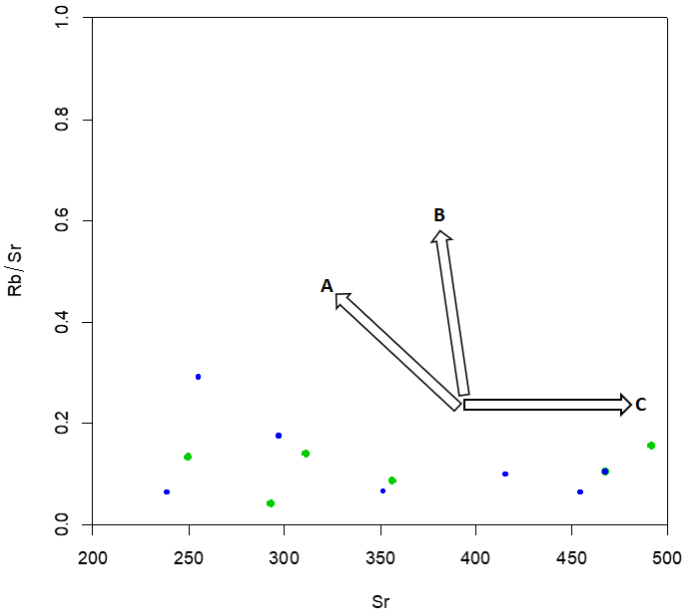

Figure 23. Melting reaction can be observed through Rb/Sr ratio and Sr index (modified after Inger & Harris, 1993). A) Vapour-absent Ms-dehydration melting. B) Vapour-absent Bt-dehydration melting. C) Vapour-present melting.

A Sr/Y–Y discrimination diagram (Fig. 24) is used to discriminate adakites and rocks that form in island arc domains. The results show that both leucosome and tonalite derive from a normal island arc setting, however, one leucosome sample plot in the adakites field.

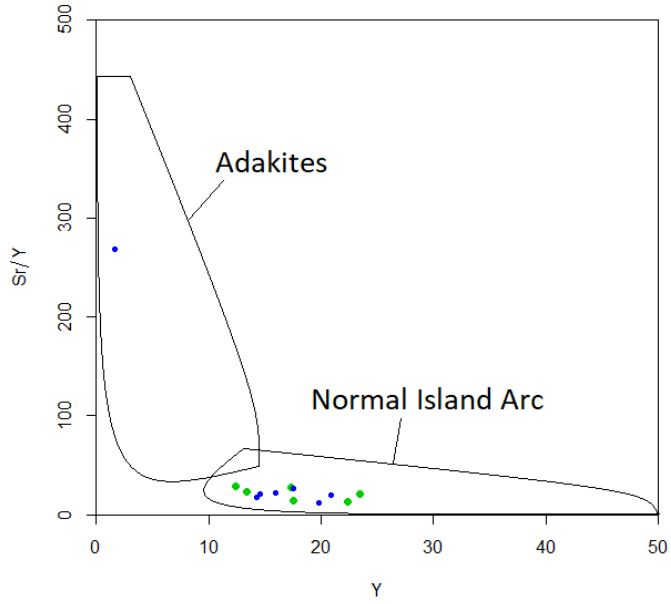

Figure 24. Sr/Y – Y discrimination diagram (modified after Defant & Drummond, 1990).

7. DISCUSSION

Field observations showed that tonalitic leucosomes are in the proximity of protoliths and indications of partial melting are present, whereas protoliths were not observed to be nearby the larger tonalite areas. Field observations and petrographical descriptions showed that both tonalitic leucosomes and tonalites are similar in composition, texture, and microstructure. Field observations in addition with petrographical descriptions indicate that tonalite is more volumetrically larger in the study area than tonalitic leucosome and there are no indications that they derive from the same source, however, they have similar petrographical attributes that indicate they have formed in similar processes.

Geochemical data combined with field and petrographic observations reveal that external fluids have participated in the partial melting of amphibolite in Hanko archipelago. Hornblende-rich melanosomes are volumetrically minor and locally present as narrow slivers along the leucosome margin. Hornblendes occur as a peritectic phase in the absence of other mafic phases, suggesting that these hornblende-rich melanosomes are the product of water-fluxed melting (Slagstad. 2005). Because hornblende is the only mafic phase present, the reaction [3] (Table 1) does not apply in this study.

Petrographic observation showed that amphibolites mainly contain hornblende, plagioclase, biotite, and quartz. Reaction [2] (Table 1) requires that hornblende and quartz are the only melting components participating in the water-fluxed melting, whereas reaction [1] suggest that hornblende, plagioclase, quartz, and biotite participate in the melting reaction. Therefore, reaction [1] applies better in this study.

Petrographic observation revealed coarse-grained poikilitic hornblende containing rounded inclusions of plagioclase, quartz, and biotite in the absence of anhydrous peritectic minerals. Such microstructure is attributed to the water-fluxed melting reaction [1] (Table 1): $Hbl_1 + Pl\ (An_{40}) + Bt + Qtz\ (+ H_2O) = Hbl_2 + Pl\ (An_{48}) + Qtz + melt$ (Lappin & Hollister, 1980). Furthermore, the occurrence of quartz interstitial to the rounded grains of hornblende and plagioclase further confirms the participation of external fluids in partial melting (Sawyer, 2001). In addition, microstructure such as triple junctions and melt occurring between triple junctions indicate that partial melting has taken place (Sawyer, 2008).

The absence of potassium feldspar and the low potassium content (Appendix II) in amphibolites indicates that the influx of external water is not the only factor that caused the production of tonalitic melt. Because of low potassium content in amphibolites, the melt that is produced from partial melting is bound to be K-poor in composition. Therefore, K-poor bulk composition in amphibolites is an important factor in tonalitic melt production in the study area.

Plagioclase phenocrysts in tonalite show common lamellar twins and oscillatory zoning patterns, indicating that tonalite was produced by fractional crystallisation (Haraguchi et al., 2003). In addition, experimental studies conducted by Naney (1983), and Naney and Swanson (1980) suggest that peritectic hornblende is stable for melting in the mafic rocks with a minimum water amount of ~4 wt.% at 2 kbar, and 2.5 wt.% at 8 kbar. The experiment conducted by Gardien et al. (2000) revealed that the addition of water into the melt has stabilised the amphibole solid solution. Therefore, the occurrence of peritectic hornblende in the absence of other mafic phases in leucosomes is attributed to the presence of external hydrous fluid during partial melting.

The SEM analysis results revealed that biotites in paleosome, melanosome, leucosome and tonalite are phlogopite. Tonalites have higher Fe-index and lower Al-index than leucosome, indicating that they grew in different environments. The majority of biotites

are re-equilibrated primary biotites due to Ti deficiency, indicating that they have been altered by hydrothermal alteration (Nachit et al., 2005).

FeO/MgO ratio and Al_2O_3/(FeO+MgO) index in biotites revealed that the biotites grew in an oxidised environment from a peraluminous source. The high fO_2 indicates that hydrous fluids have been available during biotite crystallisation, however, due to biotites being re-equilibrated primary biotites this could also indicate hydrothermal alteration (Weinberg & Hasalová, 2015). Tonalite has higher FeO/MgO ratio and lower Al_2O_3/(FeO+MgO) index compared to leucosome. This reflects that the fO_2 and access to aluminium was different during the formation, thus tonalite and leucosome formed in different environments (Eklund & Nikkilä, 2021).

The amphiboles in leucosome have higher Ca- and Mn-content and lower Mg/(Mg+Fe^{2+}) index than amphiboles in paleosome, supporting the reaction [1] where $Hbl_1 \rightarrow Hbl_2$. However, amphiboles in tonalite have higher Na- and Si-content and higher Mg/(Mg+Fe^{2+}) index than amphiboles in leucosome, suggesting that they derive from different sources.

According to the reaction [1] where Pl (An_{40}) → Pl (An_{48}), the An content in the melt product should be higher than in the paleosome. The SEM analysis results show that plagioclase in leucosome (An_{42}) and tonalite (An_{46}) have lower An content than plagioclase in paleosome (An_{47}) (Fig. 16) and, therefore, the reaction suggested by Lappin and Hollister (1980) does not apply in our case. However, it is important to note that the An content in paleosome, leucosome and tonalite are in the same order of magnitude and, therefore, a conclusion is hard to make. Furthermore, the reaction suggested by Lappin and Hollister (1980) could be Hbl_1 + Pl (An_{x1}) + Bt + Qtz (+ H_2O) = Hbl_2 + Pl (An_{x2}) + Qtz + melt, where An content (X1) varies depending on several factors, such as source and PT conditions.

The results plotted in Ti-in-biotite geothermometer by Henry et al. (2005) show that tonalite has formed in approximately between 450 and 650 ºC, whereas leucosome has formed in approximately ~550–650 ºC. According to Moyens and Stevens (2006), the influx of hydrous fluids decreases the melting point of amphibolite down to ~700–750 ºC at high-pressure conditions and down to 650 ºC at 6–10 kbar. Furthermore, the reaction [1] requires PT conditions of 675–750 ºC at 6–8 kbar to occur. Therefore, the results indicates that conditions have been sufficient for water-fluxed melting. However, it is

important to consider the fact that the results showed in Ti-in-biotite geothermometer could be false since analysed biotites are re-equilibrated primary biotites.

The plagioclase-amphibole PT calculations show that leucosome has melted in approximately 543±40 ºC at 8.3±0.6 kbar, whereas tonalite has melted in approximately 553±40 ºC at 6.7±0.6 kbar (Fig. 15). These PT conditions would be sufficient for water-fluxed melting reaction for both leucosome and tonalite if the highest deviation of temperature and/or pressure applies. Therefore, the results indicates that water-fluxed melting has taken place but leucosome and tonalite derive from different sources. However, the PT results could also indicate the PT conditions for the well-preserved metamorphic cumulation that occurred in 1.83 Ga.

Peritectic hornblende and PT conditions shown in figures 13 and 15 indicate that approximately ~2.5–3 wt% H_2O have been present (Naney, 1983; Naney & Swanson, 1980). Furthermore, low Or content and high Ab and An in plagioclase indicates that aH_2O has been 1 or more (Weinberg & Hasalová, 2015). However, these assumptions are concluded from a small amount of data, thus, the volume of water that participated in water-fluxed melting requires further studies.

Major element analysis results show that paleosome plots in the gabbro, gabbro-norite, gabbro-diorite and diorite fields (Fig. 17). Paleosome samples that plots in the diorite field has most likely been contaminated and, therefore, does not represent the original rock. Paleosomes in the study area have most likely been gabbroic rocks that have been metamorphosed into amphibolite. Most of leucosome are dioritic to granodioritic in composition, and some assumed tonalites plot in the gabbro-diorite and diorite fields (Fig. 18). However, samples EA-2021-02 and -08 plot in the tonalite field, which supports the assumption that some tonalitic leucosome and tonalite have derived from the same source.

Samples were plotted in the feldspar triangle diagram (Fig. 16) developed by O'Connor (1965). The results show that sample EA-2021-02 is tonalitic, whereas sample EA-2021-08 is slightly granodioritic. However, the difference in composition is not significantly enormous and, therefore, it is acceptable to consider leucosome and tonalite to be similar in composition. The results shown in figure 16 and 17 suggests that the samples are similar in composition.

Results shown in figures 19–21 indicate that both leucosome and tonalite are collisional granitic rocks. Collisional granitic rocks can be subdivided into continent-continent,

continent-arc, and arc-arc, and geochemically resemble VAG. However, there are a few distinctive characteristics, namely the high contents of Rb and low contents of Ce, Zr, Hf and Sm. In conclusion, leucosome and tonalite are calc-alkaline (Fig. 19) and are classified as VAG (Fig. 20) with distinctive geochemical characteristics, which indicates that they are formed in a collisional setting (Fig. 21). In addition, knowing the study area's geological history, the reasonable conclusion to be drawn from these results is that both leucosome and tonalite formed in a continent-arc or arc-arc setting (Pearce et al., 1984).

When plotting leucosome and tonalite in Rb/Sr – Ba and Rb/Sr – Sr diagrams, the Rb/Sr ratio for leucosome and tonalite is low, showing that both rocks have derived from water-fluxed melting. There is a little change in Rb/Sr ratio, however, it is not significantly big enough a change to be counted as Bt-dehydration melting. Furthermore, there is no significant decrease or increase in Ba and Sr respectively to indicate Bt-dehydration melting. Therefore, both rocks have derived from water-fluxed melting.

The Sr/Y–Y discrimination diagram (Fig. 24) is a useful tool to distinguish adakitic tonalites and calc-alkaline tonalites from each other. Calc-alkaline tonalites derive from a differentiated island arc magma chamber, whereas adakites represent melting of a previous crust (Zhang et al., 2021). The results show that all samples, except for one leucosome sample, plot in the normal island arc field, indicating that both leucosome and tonalite are derived from a differentiated island arc magma chamber. Furthermore, the oscillatory zoned plagioclase in both leucosome and tonalite supports this assumption.

8. CONCLUSION

Field observations, petrographic description, mineral analysis, major and trace element analysis revealed that both tonalitic leucosome and biotite-hornblende tonalite are results of water-fluxed melting and formed in a continent-arc or arc-arc setting. Major and trace element analysis together with mineral analysis and petrographic observations revealed that both leucosome and tonalite have derived from a differentiated oxidised calc-alkaline peraluminous magma source. The leucosome and tonalite contain peritectic hornblende, share the same microstructures and textures, and have geochemical characteristics in trace element that are attributed to water-fluxed melting. However, geochemistry in biotite, amphibole and plagioclase differs, suggesting that they derived from different sources,

therefore, there is no correlation between leucosome and tonalite in Hangö archipelago other than that both are products of water-fluxed melting. Furthermore, PT conditions, fO_2 and aluminosity variations have been different for both rocks, indicating that they crystallised in different environments. Further studies of how much melt has been produced, how much water has participated in water-fluxed melting and the structural controls on water-fluxed melting in Hangö archipelago is needed to completely understand water-flux melting in the area.

9. ACKNOWLEDGMENTS

I would like to thank first and foremost Professor Olav Eklund who offered me the chance to participate in the MIGMA project at Åbo Akademi University and who introduced me to the interesting and exciting subject. I also want to thank my supervisor PhD Kaisa Nikkilä for excellent guidance and counselling. A huge thanks goes to both MSc Arto Peltola, who helped me to prepare thin sections, and MSc Sören Fröjdö, who guided me on how to prepare glass disks for WDXRF analyses, how to use SEM-EDX and who carried out the WDXRF analyses for me.

10. SUMMARY IN SWEDISH - SAMMANFATTNING PÅ SVENSKA

10.1 Tonalitisk smältbildning från amfiboliter i Hangö skärgård

Ökad vattenflux eller dehydrering av amfibol är den vanligaste orsaken till en partiell uppsmältning av amfiboliter i nedresta och mellersta skorpan. Denna anatexi tros vara den främsta orsaken till den utbredda förekomsten av tonalitiska och trondhjemitiska smältor i orogeniska bälten. Partiell uppsmältning orsakad av vattenflux har varit i mindre fokus än dehydreringsmältning fastän vattenfluxsmältning har en av de största rollerna i smältformningsprocesserna i nedresta och mellersta skorpan under orogenesen. Processerna för vavattenfluxsmältning och dehydreringsmältning är avgörande för att förstå smältbildning under orogenesen (Yuyoung & Moonsup, 2020).

Studieområdet för denna avhandling är beläget i Hangö skärgård i sydligaste Finland (Fig. 1). Studieområdet består huvudsakligen av amfibolit, tonalit och granodiorit. Tonalitisk leukosom har observerats i området och tros vara en del av amfibolit partiell smältning under den tidiga Svekofenniska deformation ca 1.88 Ga.

I södra Finland finns två migmatitbälten som bildades under den svekofenniska orogenin. I sydligaste Finland finns granit migmatitbältet och norr om det finns tonalit/granodiorit migmatitbältet (Mouro et al., 1999). Migmatitbältena skiljer sig från varandra genom deras sammansättning och ålder. Tonalit/granodiorit migmatitbältet har en kaliumfattig leukosom, medan granit migmatitbältet har en mer kaliumrik leukosom (Ehlers et al., 1993; Mouri et al., 1999).

Åldern för regional metamorfos och smältbildning söder om det sydligaste Finlands granit migmatitbälte har fastställts till ca 1.89–1.86 Ga (Hopgood et al., 1983; Bredenberg, 2019). Det har föreslagits att den tidigare metamorfismen har raderats helt och hållet från södra Finland och den välbevarade metamorfa kulmination ägde rum cirka 1.83 Ga. Dessutom har Hopgood et. al (1983) hävdat att en tidigare partiell smältning ägde rum i södra Finland. MIGMA-projektet har också hävdat att en tidigare partiell uppsmältning har inträffat och undersöker bevis på den.

Granit migmatitbältet är en del av Nylandsbältet. Nylandsbältets sydkust skär genom södra Finlands stora skjuvzon. Skjuvzonen representerar den södra gränsen för granit migmatitbältet (Ehlers et al., 1993). Skärgård söder om den stora skjuvzonen är studieområdet för denna avhandling. Området utgör ett stort intresse för studier på grund av indikationer om en tidig migmatisering som hittats av Hopgood et al. (1983) och Bredenberg (2019). Detta tyder på att området inte har påverkats i samma grad av deformationen som orsakades av den postsvekofenniska orogenes som resten av Nylandsbältet (Kähkönen, 2005).

Syftet med avhandlingen är att studera tonalitsmältbildningen i Hangö skärgård och undersöka om det finns ett samband mellan den tonalitiska leukosomen och områden som består av ett större tonalitbatoliter. För att studera detta har jag fokuserat på tonalitiska leukosomer som finns i områden som består av amfibolit, tonalit och granodiorit. Tonalitisk leukosom har observerats i området och tros vara en del av amfibolit partiell uppsmältning under den tidiga svekofenniska deformationen som ägde rum ca. 1.89 Ga. För att studera sambanden mellan tonalitiska leukosomer och tonaliter som förekommer

inom studieområdet har jag utfört fältobservationer, petrografiska beskrivningar, huvud- och spårelementanalys samt mineralanalys. Dessutom studeras arten av den partiella uppsmältningen för att lära sig om externa vattenhaltiga fluider har deltagit i smältningen eller om den har orsakats av dehydreringsmältning. Detta är viktigt eftersom endast en liten mängd vätskor kan inverka oerhört mycket på de fysikaliska och kemiska egenskaperna hos en sten, såsom smälttemperaturer, smältkemi, viskositet och densitet. Därför påverkar tillströmningen av vatten grundläggande magmatiska processer som anatexi, magmauppstigning, kristallisering och utbrott (Weinberg & Hasalová, 2015).

10.2 Migmatit

Migmatit består av två eller flera petrografiskt olika delar som finns i områden som har påverkats av progradisk metamorfos, det vill säga förändring av mineralparagenes med ökande temperatur- och tryckförhållanden. Migmatiter bildas när minst en del av bergarten har påverkats av anatexi. Anatexi är en komplex process som påverkas av till exempel temperatur- och tryckförhållanden, närvaro av vätskor och protolitens sammansättning. Eftersom migmatit bildas i medelhög till hög metamorfosgrad är protoliten vanligtvis en redan metamorfoserad bergart (Sawyer, 2008).

Migmatit består huvudsakligen av tre petrografiska delar. Paleosomen representerar protoliten och har vanligtvis delvis eller inte alls påverkats av anatexi. Därför har paleosomen vanligtvis bevarade strukturer och texturer som är äldre än anatexin. Neosom, det vill säga ”ny bergart”, består av komponenter som har exsolverat av anatexi. Neosom kan delas in i två segregeringar: leukosom och melanosom. Leukosom är smältprodukten av anatexi, medan melanosom är restit av osmält paleosom. Leukosom består vanligtvis av lätta mineraler, såsom fältspat och kvarts, medan melanosom består av mörkare mineraler, såsom amfiboler, pyroxen och biotit (Sawyer, 2008).

Leukosomen kan klassificeras enligt var den kristalliserades i förhållande till var den bildades. Kristallisering som sker i smältans originalposition definieras som in situ. Smälta som har migrerat från sin ursprungliga position, men är fortfarande i sitt ursprungliga lager, kallas ”in-source” leukosom. Om smältan migrerar till ett annat lager i samma metamorfregion bildas leukokratiska ådror och gångar, det vill säga bergarter som består av minst 90 % felsiska mineraler. Smälta som har migrerat från den

ursprungliga positionen bildar lagergångar med granitisk (tonalitisk, granodioritisk osv.) sammansättning (Sawyer, 2008).

Migmatit kan klassificeras som metatexit eller diatexit baserat på graden av anatexi. Metatexitisk migmatit består av paleosom med välbevarade strukturer som är äldre än anatexin. Diatexitisk migmatit har däremot påverkats av en högre grad av partiell uppsmältning och domineras därför av neosom (Sawyer, 2008).

10.3 Amfibolit vattenfluxsmältning och dehydreringsmältning

Amfibolit är en faneritisk metamorfisk bergart som huvudsakligen består av hornblände, eller en annan amfibol och plagioklas. Beroende på protolitens kemiska sammansättning, granat, pyroxen och kvarts kan uppstå. Dessutom kan små mängder biotiter, titanit och Fe-Ti oxider kan också vara lokalt närvarande. För att kunna klassificera en sten som en amfibolit måste bergarten bestå av totalt 75 % amfibol och plagioklas (Best, 2003; Coutinho et al., 2007).

Partiell uppsmältning av amfiboliter vid nedersta och mellersta skorpan uppstår vanligtvis på grund av dehydrering av amfiboler eller influx av externa vattenrika fluider. Partiell uppsmältning orsakad av nedbrytning av ett vattenhaltig mineral, såsom amfibol, biotit eller muskovit, kallas för dehydreringsmältning. Däremot kallas partiell uppsmältning orsakad av närvaron av externa vattenrika fluider för vattenfluxsmältning (Weinberg & Hasalová, 2015). Smältning med vattenflux och dehydreringsmältreaktion av amfibolit förtecknas i Table 1.

Allt vatten i dehydreringssmältningsreaktioner härrör från vattenhaltiga mineraler, och därför är den smälta som produceras vatten undermättad. I jämförelse, begränsas vattenfluxsmältning endas av vatteninflödet, och därför är smältan som produceras från vattenfluxsmältning vattenrik eller vattenmättad. Vattenfluxsmältreaktioner är antingen kongruenta, det vill säga sammansättningen av smältan som bildas är densamma som protolitens sammansättning, vanligtvis vid låga temperaturer, eller inkongruenta, det vill säga den kemiska sammansättningen av den producerade smältan är inte densamma som protolitens, vid högre temperaturer där smältan som produceras är undermättad (Weinberg & Hasalová, 2015).

Dehydreringssmältningsreaktioner involverar muskovit, biotit eller amfibol som en vattenrik facies. Smälta som produceras genom dehydrering varierar i geokemisk sammansättning, beroende på protolitens sammansättning och temperatur. Smältor som bildas genom dehydreringssmältning är vanligtvis till sin sammansättning dioritiska till granodioritiska och peralkalina till metaluminösa och har ett lägre K/Na-förhållande jämfört med andra smältor (Weinberg & Hasalová, 2015).

Tillströmningen av vatten sänker smälttemperaturen för amfibolit ner till cirka 700–750 ^{o}C vid högtryckförhållanden och ner till 650 ^{o}C vid 6–10 kbar (Moyens & Stevens, 2006). Peritektiska mineraler, oftast amfiboler, bildas genom inkongurenta vattenfluxsmältningsreaktioner. Amfibol dehydreringsmältning sker vid 850–900 ^{o}C och producerar vanligtvis peritektiska pyroxener och/eller granat. Därför är det möjligt att grovt skilja vattenfluxsmältning och dehydreringssmältning från varandra genom deras periktetiska mineraler. Reaktionen [1] visar att vid vattenfluxsmältning av en amfibolit, förändras Hbl_1 vid reaktionen till Hbl_2 samt att An-halten i plagioklas ökar i leukosomen jämfört med paleosomen.

10.4 Material och metoder

Fältarbete genomfördes tillsammans med prof. Olav Eklund och FD Kaisa Nikkilä under våren 2021. Under fältarbetet observerades tio olika hällar och nio olika prover samlades in från sex hällar. Fyra tonalit-, två melanosom-, en paleosom- och ett leukosomprov samlades in. Två av tonalitproverna, ett homogent och ett heterogent, togs från Heimosholmnen, två tonalitprover och ett melanosomprov från Brännskär samt ett paleosom-, ett leukosom- och ett tonalitprov från Grevskär. Koordinaterna, fält- och provbeskrivning samt vilken typ av analys utfördes för de insamlade proverna förtecknas i Table 2. Platserna, där proven samlades in, markeras med svarta trianglar i Figure 1.

Tunnslip observerades under polariserade mikroskop för petrografisk beskrivning, och punktanalys av enskilda mineraler gjordes med SEM (svepelektronmikroskop). Den petrografiska beskrivningen utfördes för att beskriva texturerna och mineralsammansättningen i proverna. Punktanalys i SEM gjordes för att undersöka den elementära skillnaden mellan biotit, amfibolit och plagioklas i paleosom, leukosom och

heterogena tonalit. Både huvud- och spårelementanalys gjordes i WDXRF för att bestämma sammansättningen i proverna.

10.5 Diskussion och sammanfattning

Fältobservationer visade att tonalitiska leukosomer ligger i närheten av protoliter och indikationer på partiell uppsmältning är närvarande, medan större tonalitområden inte observerades vara i närheten av protoliter. Fältobservationer och petrografiska beskrivningar visade att både tonalitiska leukosomerna och tonaliterna har likadana sammansättning, textur och mikrostruktur. Fältobservationer tillsammans med petrografiska beskrivningar indikerar att tonaliter är mer volumetriskt större i studieområdet än tonalitiska leukosomer och det finns inga bevis för att de härrör från samma källa, men de har liknande petrografiska attribut vilket indikerar att de har producerats genom likadana processer.

Hornbländerika melanosomer är volumetriskt få och förekommer lokalt som smala strimlor längs leukosomens marginaler. Hornblände uppstår som en peritetisk fas i avsaknad av andra mafiska faser, vilket indikerar att dessa hornbländerika melanosomer är produkten av vattenfluxsmältning (Slagstad, 2005). Eftersom hornblände är den enda mafiska fasen som finns närvarande, gäller inter reaktionen [3] (Table 1) i denna studie.

Petrografiska observationer visade att amfiboliter huvudsakligen består av hornblände, plagioklas, biotit och kvarts. Reaktion [2] (Table 1) tyder på att hornblände och kvarts är de enda smältkomponenterna i reaktionen, medan reaktion [1] tyder på att hornblände, plagioklas, kvarts och biotit deltar i smältreaktionen. Därför gäller reaktion [1] i denna studie.

Petrografiska observationer visade grovkorniga poiklitiska hornbländen som innehåller rundade inneslutningar av plagioklas, kvarts och biotit i avsaknad av vattenfri periktetiska mineraler. En sådan mikrostruktur hänförs till vattenfluxsmältningsreaktion [1] (Lappin & Hollister, 1980).

Amfiboliterna är kalifältspatfattiga och har låga K sammansättning (Appendix II), vilket indikerar att inflöde av vatten inte är den enda faktorn som orsakade produktionen av tonalitisk smälta. På grund av lågt K-innehåll i amfiboliterna, är smältan som producerats

från partiell uppsmältning bunden att vara K-fattig. Därför är K-fattiga sammansättningen i amfiboliterna en viktig faktor i tonalitisk smältproduktion i Hangö skärgård.

SEM-analysresultaten visade att biotiter i paleosom, melanosom, leukosom och tonalit är flogopiter. Biotiterna i tonaliterna har högre Fe-index och lägre Al-index än biotiterna i leukosomerna, vilket indikerar att de två bergarterna bildades i olika miljöer.

FeO/MgO-förhållanden och Al_2O_3/(FeO+MgO)-indextet i biotiterna visade att biotiterna växte i en oxiderad miljö från en peraluminös källa. Den höga fO_2 indikerar att vattenrika vätskor har varit tillgängliga under biotitkristallisering, men på grund av att biotiterna är återbalanserade primära biotiter kan detta också indikera hydrotermal alteration (Weinberg & Hasalová, 2015). Tonaliterna har högre FeO/MgO-förhållande och lägre Al_2O_3/(FeO+MgO)-index än leukosomerna. Detta återspeglar att fO_2 och tillgång till aluminium har varit olika under formationerna, således bildades tonaliterna och leukosomerna i olika miljöer (Olav & Nikkilä, 2021).

Amfibolerna i leukosomerna har högre Ca- och Mn-koncentration och lägre Mg/(Mg+Fe^{2+})-index än amfiboler i paleosomerna, vilket stöder reaktionen [1] där Hbl_1 → Hbl_2. Amfibolerna i tonaliterna har dock högre Na- och Si-koncentration och högre Mg/(Mg+Fe^{2+}) index än amfibolerna i leukosomerna som indikerar att de härrör från olika källor.

Enligt reaktionen [1] bör An-halten i smältprodukten vara högre än i paleosomen. SEM-analysresultaten visar att leukosomerna och tonaliterna har lägre An-innehåll än palosomerna, således gäller inte den reaktionen som Lappin och Hollister (1980) föreslagit i det här fallet. Reaktionen kan dock vara istället Hbl_1 + Pl (An_{x1}) + Bt + Qtz (+H_2O) = Hbl_2 + Pl(An_{x2}) + Qtz + smälta, där An-innehållet varierar beroende på källa och PT förhållanden. Det är dock viktigt att notera att An-innehållet för paleosomerna, leukosomerna och tonaliterna är i samma storleksordning och därför är det svårt att dra stora slutsatser av dessa resultat.

Ti i biotit geotermometer av Henry et al. (2005) och geotermobarometer av Pylusina (1982) visar att tonalit har bildats i cirka 450–650 ºC, medan leukosom har bildats i cirka 550–650 ºC. Enligt Moyens och Stevens (2006) minskar tillströmningen av vattenvätskor smältpunkten för amfibolit ner till 700–750 ºC vid högtryckförhållanden och ner till 650 ºC vid 6–10 kbar. Dessutom kräver reaktionen [1] PT förhållanden på 675–750 ºC vid 6–8 kbar för att inträffa. Således har förutsättningarna varit tillräckliga för

vattenfluxsmältning i Hangö skärgård. Det är dock viktigt att beakta att resultaten som visas i Ti i biotit geotermometer kan vara falska eftersom de analyserade biotiter är återbalanserade primära biotiter.

Tryck- och temperaturförhållande beräkningarna visar att leukosomen har smultit i cirka 543±40 ºC vid 8,3±0,6 kbar, medan tonaliten har smultit i cirka 553±40 ºC vid 6,7±0,6 kbar (Fig. 15). Dessa PT-förhållanden skulle vara tillräckliga för vattenfluxsmältning för både leukosomen och tonaliten om den högsta avvikelsen för temperatur- och/eller tryckförhållanden gäller. Således indikerar resultaten att vattenfluxsmältning har ägt rum, men att leukosomen och tonaliten härrör från olika källor. PT-resultaten kan emellertid också indikera PT-förhållandena för den välbevarade metamorfa kumulationen som inträffade i 1.83 Ga.

Leukosomerna och tonaliterna är kalkalkaliska (Fig. 19) och klassificeras som VAG (Fig. 20), det vill säga granitiska bergarter som härstammar från öbågar, med distinkta geokemiska egenskaper, såsom hög koncentration av Rb och låga halter av Ce, Zr, Hf och Sm, som indikerar att de bildades i en kollisionsmiljö (Fig. 21).

Proverna plottades i fältspatdiagrammen (Fig. 16) utvecklad av O'Connor (1965). Resultaten visar att prov EA-2021-02 är tonalitiskt, medan prov EA-2021-08 är lite mer granodioritiskt. Skillnaden i sammansättning är inte signifikant enorm och därför är det acceptabelt att betrakta leukosomer och tonaliter som likartade i sammansättning. Tillsamman med de resultat som visas i figur 17 kan vi dra slutsatsen att de liknar i sammansättning.

Rb/Sr-förhållandena för leukosomerna och tonaliterna är låga, vilket indikerar att båda bergarterna härrör från vattenfluxsmältning. Det finns en liten förändring i Rb/Sr-förhållanden., men den är inte en tillräckligt stor förändring för att räcknas som biotit dehydreringssmältning. Dessutom finns det ingen signifikant minskning eller ökning av Ba respektive Sr för att indikera biotit dehydreringssmältning. Således har båda bergarterna härletts från vattenfluxsmältning.

Sr/Y–Y diagrammet (Fig. 24) är ett användbart verktyg för att skilja adakitiska och kalkalkaliska tonaliter från varandra. Kalkalkaliska tonaliter härrör från en differentierad öbåge magmakammare, medan adakiter representerar smältning av en tidigare skorpa (Zhang et al., 2021). Resultaten visar att alla prover, förutom en leukosomprov, befinner sig i det normala öbågefältet, vilket tyder på att både leukosom och tonalit härrör från en

differentierad öbågemagmakammare. Dessutom stöder oskillatorisk zonerad plagioklas i både leukosom och tonalit detta antagande.

Sammanfattningsvis har fältobservationer, petrografisk beskrivning, mineralanalys, huvud- och spårelementanalys bevisat att tonalitiska leukosomer och biotit-hornblände tonaliter är resultat av vattenfluxsmältning. Resultanterna också indikerar att både leukosom och tonalit härstammar från en differentierad oxiderad kalkalkalisk peraluminös magmakammare. Både leukosomerna och tonaliterna innehåller peritektisk hornblände utan vattenfria peritektiska mineraler, har samma mikrostukturer och texturer, och har geokemisk karaktäristik som hänförs till vattenfluxsmältning. Geokemin i biotit, amfibol och plagioklas skiljer sig dock åt, vilket indikerar att de härrör från olika källor, således finns det inget samband mellan leukosom och tonalit i Hangö skärgård förutom att båda är produkter av vattenfluxsmältning. Dessutom har PT-förhållanden, fO_2 och aluminiumvariatoner varit olika för båda bergarterna, vilket indikerar att de kristalliserades i olika miljöer.

REFERENCES

Banno, Y., Momma, K. & Ritsuro, M. (2019) New data on ferri-ghoseite in Sanbagawa quartz schist from the Iimori region, Wakayama Prefecture, Japan: Solid solution between magnesio-riebeckite and clino-suenoite. Journal of Mioneralogical and Petrological Sciences 114, pp. 5.

Bartoli, O. (2021) Granite geochemistry is not diagnostic of the role of water in the source. Earth and Planetary Science Letters, Volume 564, pp. 1–9.

Beard, J.S. & Lofgren, G.E. (1991) Dehydration melting and water-saturated melting of basaltic and andesitic greenstones and amphibolites at 1, 3, and 6. 9 kb. Journal of Petrology vol. 32, pp. 365–401.

Best, M.G. (2003) Igneous and metamorphic petrology. 2nd edition. Blackwell Science Ltd. pp. 460.

Bredenberg, E. (2019) Tonalit migmatite i södra Finland – åldersbestämning och petrografisk analys. Master's thesis, Åbo Akademi University, pp. 3–33.

Brouwer, P. (2013) Theory of XRF. PANanalytical B.V. The Netherlands. Vol 4, pp. 7.

Conrad, W.K., Nicholls, I.A. & Wall, V.J. (1988) Water-saturated and -undersaturated melting of metaluminous and peraluminous crustal compositions at 10 kbar; Evidence for the origin of silicic magmas in the Taupo volcanic zone, New Zeland, and other occurrences. Journal of Petrology 29, pp. 765–803.

Coutinho, J., Kräutner, H., & Sassi, F., & Schmid, R. & Sen, S. (2007) Recommendations by the IUGS Subcommission on the Systematics of Metamorphic Rocks. Amphibolite and Granulite: Web version 01.02.07.

Ehlers, C., Lindroos, A. & Selonen, O. (1993) The late Svecofennian granite-migmatite zone of southern Finland – a belt of transpressive deformation and granite emplacement. Precambrian Research 64, pp. 295–309.

Eklund, O., Konopelko, D., Rutanen H., Fröjdö S. & Shebanov, A.D., (1998) 1.8 Ga Svecofennian post-collisional shoshonitic magmatism in the Fennoscandian shield. Lithos 45, pp. 87–108.

Eklund, O. & Nikkilä, K. (2021) Biotite as petrogenetic tool in granite-migmatite areas. LITHOSPHERE 2021, 11th Symposium. Institute of Seismology, University of Helsinki. Helsinki, Finland. Vol. 71, pp. 15–18.

Gaál, G. & Gorbatschev, R. (1987) An outline of the Precambrian evolution of the Baltic Shield. Precambrian Research vol. 35, pp. 15–52.

Gaál, G. (1990) Tectonic styles of early Proterozoic ore deposition in the Fennoscandian Shield. Precambrian Research, vol. 46, pp. 83–114.

Gardien, V., Thompson, A.B., Ulmer, P. (2000) Melting of biotite + plagioclase + quartz gneisses; the role of H_2O in the stability of amphibole. Journal of Petrology vol. 41, pp. 651–666.

Goodhew, P.J., Humphreys, J. & Beanland, R. (2001) Electron Microscopy and Analysis 3rd Edition. Taylor and Francis, pp. 265.

Harlov, D.E. & Austrheim, H. (2013) Metasomatism and the Chemical Transformation of Rock: Rock-Mineral-Fluid Interaction in Terrestrial and Extraterrestrial Environments. In: Metasomatism and the Chemical Transformation of Rock. Lecture Notes in Earth System Sciences. Springer, Berlin, Heidelberg. pp. 1–16.

Helmy, H.M., Ahmed, A.F., El Mahallawi, M.M. & Ali, S.M. (2004) Pressure, temperature and oxygen fugacity conditions of calc-alkaline granitoids, Eastern Desert of Egypt, and tectonic implication. Journal of African Earth Science, 38, pp. 255–268.

Henry, D.J., Guidotti, C.V. & Thomson, J.A. (2005) The Ti-saturation surface for low-to-medium pressure metapelitic biotites: Implications for geothermometry and Ti-substitution mechanisms. American Mineralogist, vol. 90, pp. 316–328.

Hopgood, A., Bowes, D.R., Kouvo, O., (1983) U–Pb and Rb–Sr isotopic study of polyphase deformed migmatites in the Svecokarelides, southern Finland. I: M.P. Atherton, C.D. Gribble (Eds.), Migmatites, Melting and Metamorphism. Shiva, Cheshire, pp. 80–92.

Hölttä, P. & Heilimo, E. (2017) Metamorphic map of Finland. Geological Survey of Finland, Special Paper 60, pp. 75–126.

Inger, S. & Harris, N. (1993) Geochemical constraints on leucogranite magmatism in the Langtang Valley, Nepal Himalaya. Journal of Petrology 34, pp. 345–368.

Janoušek, V. et al. (2006) Interpretation of whole-rock geochemical data in igneous geochemistry: introducing Geochemical Data Toolkit (GCDkit). Journal of Petrology. Vol 47. pp. 1255–1259.

Kähkönen, Y. (2005) Svecofennian supracrustal rocks. I: Lehtinen, M., Nurmi, P. A. & Rämö, O. T. (eds) Precambrian Geology of Finland – Key to the Evolution of the Fennoscandian Shield. Developments in Precambrian Geology 14. Elsevier, pp. 43–406.

Lahtinen, R. (1994) Crustal evolution of the Svecofennian and Karelian domains during 2.1 – 1.79 Ga, with special emphasis on the geochemistry and origin of 1.93–1.91 Ga gneissic tonalites and associated supracrustal rocks in the Rautalampi area, central Finland. Geological Survey of Finland, Bulletin 378, pp. 128.

Lahtinen, R., Korja, A. & Nironen, M. (2005) Paleoproterozoic tectonic evolution. In: Lehtinen, M., Nurmi, P.A. & Rämö,O.T. Precambrian Geology of Finland – Key to the Evolution of the Fennoscandian Shield. Elsevier B.V., pp. 481–532.

Leake, B.E. (1971) On aluminous and edenitic hornblendes. Mineralogical Magazine, 38, pp. 389–407.

Leake, B.E., Woolley, A.R., Arps, C.E., Birch, W.D., Gilber, M.C., Grice, J.D., Linthout, K., Laird, J., Mandarino, J., Maresch, W.V., et al. (1997) Nomenclature of amphiboles: Report of the subcommittee on amphiboles of the international mineralogical association, commission on new minerals and mineral names. Can. Mineral.vol. 35, pp. 219–246.

Leake, B.E., Woolley, A.R., Birch, W.D., Burke, E.A.J., Ferraris, G., Grice, J.D., Hawthorne, F.C., Kisch, H.J., Krivovichev, V.G., Schumacher, J.C., Stephenson, N.C.N. & Whittaker, E.J.W. (2004) Nomenclature of amphiboles: Additions and revisions on the International Mineralogical Association's amphibole nomenclature. American Mineralogist, 89, pp. 883–887.

Nachit, H., Ibhi, A., Abia, E.H. & Ohoud, M.B. (2005) Discrimination between primary magmatic biotites, reequilibrated biotites and neoformed biotites. Comptes Rendus Geoscience, vol. 337, no. 16, pp. 1415–1420.

Naney, M.T. (1983) Phase equilibria of rock-forming ferromagnesian silicates in granitic systems. American Journal of Science 283, pp. 993–1033.

Naney, M.T & Swanson, S.E. (1980) The effect of Fe and Mg on crystallization in granitic systems. American Mineralogist 65, pp. 639–653.

Nesse, W.D. (2004) Introduction to Optical Mineralogy. 3rd edition, Oxford University Press, Inc. Oxford, New York, USA. pp. 47.

Nironen, M. (1997) The Svecofennian Orogen: a tectonic model. Precambrian Research vol. 86, pp. 21–44.

Nironen, M., Lahtinen, R. & Korja, A. (2002) Paleoproterozoic Tectonic Evolution of the Fennoscandian Shield – Comparison to Modern Analogues.Institute of Seismology, University of Helsinki, Report S-42, pp. 95–97.

Nironen, M. (2005) Proterozoic orogenic granitoid rocks. I: Lehtinen, M., Nurmi, P.A. & Rämö, O.T. (eds.) Precambrian Geology of Finland – Key to the Evolution of the Fennoscandian Shield. Elsevier B.V., Amsterdam, pp. 443–480.

Moody, J.B., Meyer, D. & Jenkins, J.E. (1983) Experimental characterization of the greenschist/amphibolite boundary in mafic systems. American Journal of Science, 283, pp. 48–92.

Mogk, D.W. (1992) Ductile shearing and migmatization at midcrustal levels in an Archean high-grade gneiss belt, Northern Gallatin Range, Montana, USA. Journal of Metamorphic Geology 10, pp. 427–438.

Mouri, H., Korsman, K. & Huhma, H. (1999) Tectono-metamorphic evolution and timing of the melting processes in the Svecofennian Tonalite Trondhjemite Migmatite Belt: An example from Luopioinen, Tampere area, southern Finland. Bulletin of the Geological Society of Finland 71, Part 1, pp. 31–56.

Moyen, J.F. & Stevens, G. (2006) Experimental Constraints on TTG Petrogenesis: Implications for Archean Geodynamics. In: Benn, K., Mareschal, J.-C., Condie, K.C. (Eds.), Archean Geodynamics and Environments, Monographs. American Geophysical Union, Washington, D. C., pp. 149–178.

Pearce, J.A., Harris, N.B.W. & Tindle A.G. (1984) Trace Element Discrimination Diagrams for the Tectonic Interpretation of Granitic Rocks. Oxford, England. Journal of Petrology, vol. 25, pp. 956–983.

Saukko, A., Nikkilä K., Eklund O. & Väisänen M. (2021) Granites of southernmost Finland. LITHOSPHERE 2021 Symposium, pp. 125&126.

Sawyer, E.W. (1998) Formation and evolution of granite magmas during crustal reworking: the significance of diatexis. Journal of Petrology vol. 39, pp. 1147–1167.

Sawyer, E.W. (2001) Melt segregation in the continental crust: distribution and movement of melt in anatectic rocks. Journal of Metamorphic Geology, vol. 19, no. 3, pp. 291–309.

Sawyer, E.W. (2008) Atlas of Migmatites: The Canadian Mineralogist Special Publication 9. Canadian Science Publishing. pp. 371.

Sawyer, E.W. (2010) Migmatites formed by water-fluxed partial melting of a leucogranodiorite protolith: microstructures in the residual rocks and source of the fluid. Lithos, vol. 116, no. 3–4, pp. 273–286.

Schmidt, M.W. (1992) Amphibole composition in tonalite as a function of pressure: An experimental calibration of the Al-in-hornblende barometer. Contributions to Mineralogy and Petrology, 110, pp. 304–310.

Shindo, D. & Oikawa, T. (2002) Energy Dispersive X-ray Spectroscopy. Analytical Electron Microscopy for Materials Science. Springer, Tokyo. pp. 82–102.

Skyttä, P. (2007) Svecofennian crustal evolution in the Uusimaa Belt area, S W Finland. Geological Survey of Finland, pp. 17.

Slagstad, T., Jamieson R.A. & Culshaw, N.G. (2005) Formation, crystallization, and migration of melt in the mid-orogenic crust, Muskoka domain migmatites, Grenville Province, Ontario. Journal of Petrology, vol. 46, no. 5, pp. 893–919.

Vernon, R.H. & Collins, W.J. (1988) Igneous microstructures in migmatites. Geology, vol. 16, no. 12, pp. 1126–1129.

Weinberg, R.F. & Hasalová, P. (2015) Water-fluxed melting of the continental crust: A review, Lithos 212–215, ss. 158–188.

Windley, B. F. (1995) The Evolving Continents. 3rd edition. Chichester: John Wiley & Sons, pp. 526.

Wolfram, L.C., Weinberg, R.F., Hasalová, P. & Becchio, R. (2018) How Melt Segregation Affects Granite Chemistry: Migmatites from the Sierra de Quilmes, NW Argentina. Journal of Petrology, Vol. 58, No. 12, pp. 2339–2364.

Yuyoung, L. & Moonsup C. (2020) Fluid-Present Partial Melting of Paleoproterozoic Okbang Amphibolite in the Yeongnam Massif, Korea. Lithosphere, Vol. 2020, pp 1–21.

Zhang, L., Li, S. & Zhao, Q. (2021) A review of research on adakites. International Geology Review, vol. 62, pp. 47–64.

Appendix I – Map of the study area (ESRI, 2018)

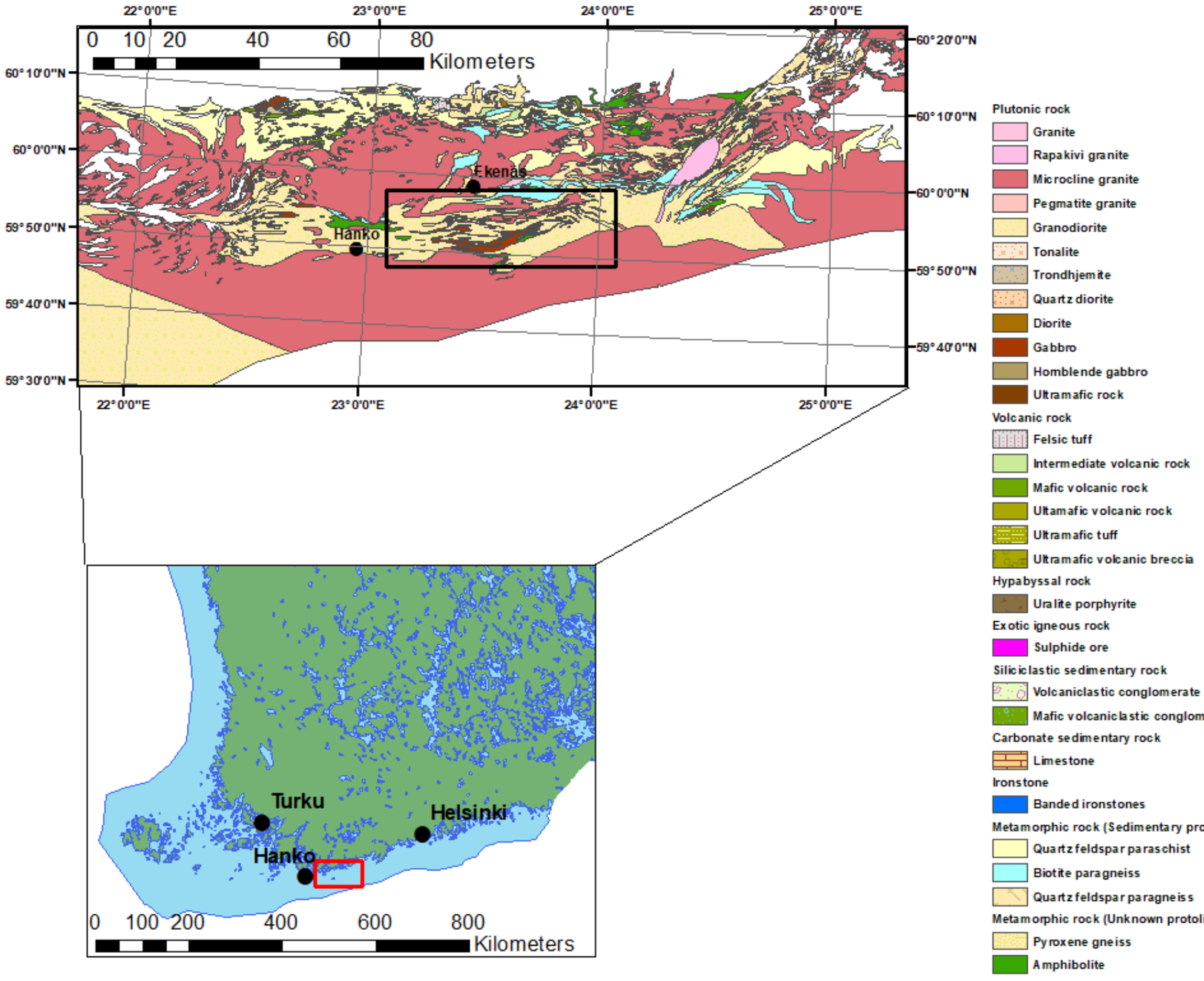

Appendix II - Major element analysis results (wt%)

Sample name	Rock type	SiO_2	TiO_2	Al_2O_3	Fe_2O_3	MgO	MnO	CaO	Na_2O	K_2O	P_2O_5
EA-2021-01	Gabbro-diorite	52.46	0.30	19.43	9.10	6.23	0.15	9.66	1.77	0.88	0.04
EA-2021-02	Heterogen tonalite	59.80	0.54	14.11	10.13	4.93	0.17	7.48	1.76	1.00	0.07
EA-2021-03	Tonalite	56.65	0.90	17.70	9.36	2.69	0.15	6.83	3.20	2.08	0.44
EA-2021-04	Melanosome	46.05	1.12	17.56	13.18	7.45	0.24	10.31	1.47	2.36	0.27
EA-2021-05	Melanosome	49.07	0.58	7.91	14.76	14.84	0.38	10.91	0.70	0.82	0.06
EA-2021-06	Melanosome	54.69	1.19	10.35	16.21	7.65	0.27	5.32	0.35	3.67	0.28
EA-2021-07	Paleosome	48.44	0.73	17.17	12.14	7.36	0.20	10.43	2.17	1.17	0.18
EA-2021-08	Leucosome	61.72	0.56	15.32	8.42	3.76	0.13	5.81	1.97	2.20	0.12
EA-2021-09	Tonalite/Granodiorite	63.80	0.50	15.47	7.24	3.20	0.10	5.65	2.56	1.36	0.11
MIGMA-2018-1.1	Amphibolite melting	64.83	0.80	13.88	9.00	2.66	0.13	4.41	1.95	2.10	0.23
MIGMA-2018-1.2	Leucosome from mafic protolith	70.44	0.34	14.42	4.63	0.99	0.07	3.93	2.88	2.02	0.09
MIGMA-2018-1.4	Melanosome	56.08	0.61	13.01	11.70	7.36	0.26	8.11	1.27	1.35	0.18
MIGMA-2018-1.6	Paleosome	54.72	0.75	14.48	12.09	5.52	0.26	8.91	1.67	1.14	0.14
MIGMA-2018-1.8	Tonalite	55.04	0.62	15.75	10.20	5.31	0.15	9.25	2.49	1.09	0.09
MIGMA-2018-1.9	Tonalitic leucosome in amphibolite	58.63	0.32	11.81	8.58	7.51	0.18	9.22	1.81	0.94	0.07
MIGMA-2018-4.3	Tonalitic leucosome	54.78	1.11	17.85	12.03	2.57	0.21	7.16	3.00	0.98	0.32
MIGMA-2018-5.2	Amphibolite partially melted	53.09	0.50	9.37	10.17	11.02	0.21	11.06	1.48	0.75	0.09
MIGMA-2018-5.3	Granodioritic melt	70.93	0.38	14.17	4.97	0.88	0.04	4.12	2.95	1.02	0.08
MIGMA-2018-5.4	Amphibolite	46.12	0.91	16.69	15.43	6.76	0.25	10.25	1.85	1.53	0.21
MIGMA-2018-5.5	Granodiorite leucosome	61.90	0.61	16.65	7.82	1.82	0.13	5.87	3.72	1.29	0.21
MIGMA-2015-01	Amphibolite	59.42	0.29	15.66	9.21	3.44	0.16	8.36	2.83	1.06	0.26
MIGMA-2015-21	Paleosome	57.53	1.28	15.11	11.73	3.14	0.26	5.52	2.43	2.48	0.41
MIGMA-2015-27	Garnet filled granodiorite	60.75	0.74	15.97	8.90	3.04	0.13	5.45	2.84	1.96	0.23

Appendix III – Trace element analysis results (ppm)

Sample name	EA-2021-01	EA-2021-02	EA-2021-03	EA-2021-04	EA-2021-05	EA-2021-06	EA-2021-07	EA-2021-08	EA-2021-09
Rock type	Gabbro-diorite	Heterogenous tonalite	Tonalite	Melanosome	Melanosome	Melanosome	Paleosome	Leucosome	Tonalite/Granodiorite
Ag	0.00	-4.55	0.71	6.01	0.00	0.04	-7.21	2.47	0.44
Al	139934.50	110171.90	129697.00	132451.00	58715.09	85309.48	127397.50	116336.90	117091.70
As	2.69	4.64	4.99	3.01	0.52	4.37	5.31	4.93	4.14
Ba	136.36	242.03	645.10	440.60	78.71	658.01	156.71	337.32	323.89
Ca	70394.85	57479.03	50441.18	78478.14	81139.20	37834.59	77293.19	43073.61	43042.39
Cd	3.10	0.95	8.73	6.56	2.89	6.39	-1.40	5.33	-1.01
Ce	25.44	25.12	48.72	32.83	11.23	62.82	25.96	33.69	31.52
Cl	131.72	338.89	843.98	273.79	289.27	708.40	236.15	251.15	157.48
Co	36.06	25.93	16.03	35.08	50.31	39.55	36.24	19.90	17.71
Cr	34.45	155.58	8.43	72.30	539.79	222.19	86.37	97.54	77.17
Cs	-4.69	-2.51	-7.71	-8.05	-1.19	-2.20	-13.32	6.02	1.08
Cu	18.67	16.15	22.70	50.09	3.89	38.06	37.34	12.09	10.15
F	-387.11	-393.80	-54.06	-335.10	-747.32	-456.91	-542.93	-259.90	-207.85
Fe	90130.42	98961.95	94094.00	131274.30	144289.80	161692.00	118658.90	83042.79	71487.59
Hf	4.06	5.08	3.13	1.96	0.09	5.76	0.16	3.59	5.08
K	8247.09	10047.31	22814.62	19882.03	6926.22	39282.77	10746.54	23245.53	13885.73
La	9.41	6.23	27.06	8.83	6.45	23.66	10.31	18.20	21.88
Mg	44406.56	36333.01	22002.88	50471.42	98826.46	56469.22	49021.32	29632.07	25420.73
MnO	1490.10	1607.80	1509.51	2304.06	3703.27	2605.43	1986.47	1362.03	1041.05
Mo	-0.54	0.60	-0.24	-0.21	-0.08	0.68	-0.21	-0.07	-0.70
Na	8375.01	9987.75	17800.04	6407.53	872.91	-591.15	11633.61	10699.57	14580.84
Nb	2.00	5.09	8.68	3.38	8.66	11.11	1.79	4.82	5.09
Nd	15.14	16.06	20.86	19.42	9.94	33.41	12.27	11.81	15.57
Ni	10.68	33.29	4.07	25.34	225.77	48.37	26.06	21.81	17.12
P_2O_5	337.64	594.07	4203.06	2382.64	480.55	2257.75	1750.51	1116.50	1025.51
Pb	8.39	6.45	6.61	5.30	4.52	26.53	8.83	9.13	9.11
Rb	30.97	33.26	76.65	104.35	21.80	134.88	28.83	74.41	43.45
S	406.58	365.29	49.07	409.66	39.90	364.92	309.74	149.96	21.25
Sc	40.20	43.52	32.35	55.91	69.97	49.41	52.72	30.39	31.43
Si	489725.20	578289.30	517698.90	436218.80	472674.70	529596.90	456775.20	585272.20	598281.30
Sm	-0.99	2.78	3.69	6.48	3.19	4.38	-2.42	4.00	0.46
Sn	4.05	3.69	4.77	6.56	6.28	8.76	3.12	6.74	4.93
Sr	356.11	249.53	491.74	287.52	30.90	23.07	282.55	255.02	311.34
Ta	0.16	0.79	0.02	-0.40	0.18	1.59	0.26	1.78	-0.18
Th	1.06	2.08	4.18	1.38	0.05	3.04	2.00	4.13	3.94
Ti	3117.16	5440.85	9595.80	11200.89	5700.46	11634.52	7342.17	5914.92	5439.44
U	0.53	1.59	2.48	2.49	0.97	2.27	0.56	1.34	0.76
V	169.13	137.48	86.63	297.33	249.88	297.25	255.97	147.63	126.01
W	1.49	2.53	0.19	1.41	1.74	1.38	1.74	0.95	-0.39
Y	12.45	17.58	23.47	16.34	16.95	30.06	8.34	14.26	13.40
Yb	-3.76	-2.10	-1.86	-2.03	1.05	0.08	-1.09	1.72	1.27
Zn	78.82	97.76	99.33	133.93	176.34	199.30	99.27	88.30	70.39

Sample name	MIGMA-2018-1.1	MIGMA-2018-1.2	MIGMA-2018-1.4	MIGMA-2018-1.6	MIGMA-2018-1.8	MIGMA-2018-1.9	MIGMA-2018-4.3	MIGMA-2018-5.2	MIGMA-2018-5.3	MIGMA-2018-5.4	MIGMA-2018-5.5	MIGMA-2015-01	MIGMA-2015-21	MIGMA-2015-27
Rock type	Amphibolite melting	Leucosome from mafic protolith	Melanosome	Paleosome	Tonalite	Tonalitic leucosome in amphibolite	Tonalitic leucosome	Amphibolite partially melted	Granodioritic melt	Amphibolite	Granodiorite leucosome	Amphibolite	Paleosome	Garnet filled granodiorite
Ag	-0.22	-0.05	0.37	1.98	6.75	-0.49	-5.06	-1.38	-0.35	-3.91	2.95	0.34	-	-1.68
Al	130711.00	118855.20	116180.90	125398.60	122258.70	93811.66	147360.40	73108.41	121071.70	134972.80	134323.90	138698.90	-	131739.50
As	3.18	-0.66	0.08	3.33	-4.09	0.71	0.63	-0.83	2.33	4.40	4.55	2.65	3.76	1.96
Ba	893.70	458.13	172.36	111.22	116.27	160.27	192.70	104.87	448.19	186.70	407.76	239.96	601.00	900.78
Ca	41555.48	30614.45	76237.38	81250.49	70606.16	70468.23	55238.81	84047.70	32650.15	75392.01	44563.07	49141.27	-	41561.36
Cd	5.09	-8.00	1.48	1.06	5.25	-1.31	-4.20	-3.90	-2.00	-2.38	2.87	4.66	3.97	0.22
Ce	31.88	39.46	32.94	20.10	20.96	31.21	35.76	20.51	15.20	26.67	51.69	54.43	59.68	37.57
Cl	563.55	343.72	345.37	989.75	466.36	183.71	364.87	174.29	75.38	534.10	599.33	863.15	829.00	577.01
Co	16.08	6.45	38.65	37.86	32.61	28.51	16.13	36.72	6.38	41.54	11.73	14.23	20.00	18.08
Cr	16.75	9.53	261.77	75.66	29.58	569.81	30.95	732.91	17.96	19.81	13.81	174.65	21.00	17.61
Cs	3.62	6.04	-2.57	1.08	3.26	-0.42	0.98	0.13	-4.11	0.29	9.20	3.77	9.21	6.82
Cu	16.04	7.38	27.32	47.70	76.15	6.67	11.00	2.37	3.96	5.67	11.34	-0.39	1.00	15.71
F	134.74	-37.97	-241.65	-79.37	-196.31	-273.73	-131.69	-337.70	-123.16	-443.18	200.93	1362.24	1469.00	120.89
Fe	84703.54	43187.49	112008.00	112583.50	98196.93	83412.17	113390.80	100343.50	45343.39	149537.30	74595.42	92562.98	-	84743.29
Hf	3.84	4.48	-0.46	1.07	0.01	2.54	3.98	2.10	3.06	-0.55	2.85	2.01	2.89	5.37
K	19800.51	21584.84	12607.15	10315.07	10691.27	9495.79	9678.11	7490.40	11251.90	15489.97	13032.29	25277.65	-	19850.30
La	18.45	16.64	8.91	7.77	5.00	12.37	10.53	7.58	5.86	9.57	22.39	23.98	18.22	13.44
Mg	25071.43	9270.15	64818.49	47309.89	39282.82	57191.81	19835.31	79031.34	9309.35	45715.03	14998.89	28850.21	-	25267.17
MnO	1225.81	654.98	2020.91	1956.18	1557.15	1775.22	1872.49	2012.72	459.10	2391.38	1265.08	1883.93	-	1226.93
Mo	0.29	0.07	0.12	0.24	0.17	0.46	0.00	-0.27	-0.28	0.13	0.20	0.75	2.09	-0.21
Na	18354.92	19809.65	11076.84	14151.92	14695.62	10372.49	21000.89	7233.68	21531.04	10389.28	25739.24	17989.23	-	18574.02
Nb	8.16	5.98	4.56	2.48	5.70	4.35	10.43	3.89	2.12	3.39	8.01	10.71	12.98	7.70
Nd	18.58	18.42	24.73	15.04	12.64	18.56	23.18	13.68	5.95	13.40	28.63	29.10	35.74	17.68
Ni	12.45	3.36	109.75	38.74	30.50	84.40	12.02	112.97	2.95	27.31	8.86	37.62	15.00	11.93
P_2O_5	2144.69	858.69	1427.16	1094.46	822.36	607.83	3126.92	736.58	848.71	1795.72	2022.71	2876.29	-	2157.30
Pb	3.54	7.22	4.28	6.13	4.23	3.16	6.14	1.48	5.00	3.10	10.22	10.61	12.93	4.71
Rb	48.47	51.93	30.52	9.11	12.28	15.41	23.52	12.14	29.30	41.22	41.69	159.15	129.00	48.92
S	144.21	77.62	225.99	410.28	607.47	74.63	17.02	19.16	39.09	28.44	306.72	58.22	72.00	153.14
Sc	28.08	16.34	50.77	58.53	41.70	54.13	43.66	78.44	7.30	61.75	28.63	30.67	37.00	31.13
Si	610301.50	718007.90	508632.10	481682.70	539834.40	595722.30	555547.10	532235.80	719980.30	455942.10	613487.80	543295.80	-	614665.90
Sm	6.34	-1.08	0.95	6.16	8.76	1.21	2.48	5.74	-6.55	0.20	1.78	7.43	0.00	3.18
Sn	9.25	2.11	2.80	3.48	9.53	2.04	5.49	0.80	1.42	1.41	5.97	10.92	13.90	5.96
Sr	467.61	296.94	300.97	292.77	292.85	238.26	351.39	195.52	454.25	280.97	415.00	338.02	614.00	467.61
Ta	-0.69	1.71	-1.70	-1.84	-1.30	-0.41	-2.96	-1.01	-0.78	-2.77	-1.11	-2.28	-	-1.60
Th	5.36	6.19	2.72	2.02	2.21	4.16	4.35	2.05	8.34	0.07	6.12	4.26	6.97	4.45
Ti	7554.08	3664.48	5826.02	6848.12	6261.45	3369.95	10502.02	4913.19	4056.92	8897.28	6154.97	9224.09	-	7555.26
U	2.05	2.89	1.08	2.35	1.47	3.44	2.33	2.68	2.41	2.78	2.59	1.98	3.49	1.11
V	124.70	35.27	194.38	272.60	269.64	132.73	95.62	185.81	39.53	407.76	68.19	154.85	230.00	123.26
W	38.79	0.25	74.08	72.68	55.89	1.51	78.40	-0.51	-0.45	125.24	28.45	50.74	91.00	37.51
Y	17.56	14.62	18.41	12.50	22.36	19.80	15.94	13.64	1.69	16.74	20.86	28.36	28.00	17.30
Yb	-86.31	4.56	-161.62	-161.50	-120.86	-0.61	-174.51	1.52	0.99	-275.71	-59.57	-105.75	-	-85.55
Zn	91.11	42.40	89.77	81.94	72.32	77.11	111.58	132.28	44.34	115.13	71.68	153.32	193.00	91.38
Zr	119.67	141.69	43.37	36.90	41.40	77.33	80.01	24.64	174.00	32.44	169.77	104.08	139.00	119.73
Zr	30.98	48.29	130.63	35.73	21.47	235.12	22.63	84.73	75.85					

Appemdix IV – Plagioclase mineral analysis results (wt%)

Sample name	SiO_2	TiO_2	Al_2O_3	FeO	MnO	MgO	CaO	Na_2O	K_2O
Leucosome 1	51.55	0.00	32.18	0.00	0.00	0.57	10.77	4.93	0.00
Leucosome 2	52.64	0.00	31.00	0.24	0.08	0.68	9.84	5.53	0.00
Leucosome 3	51.15	0.00	32.45	0.00	0.00	0.56	11.32	4.52	0.00
Leucosome 4	53.97	0.11	29.92	0.00	0.12	0.80	8.50	6.52	0.06
Leucosome 5	54.27	0.00	29.70	0.15	0.14	0.73	8.20	6.74	0.08
Leucosome 6	55.02	0.00	29.11	0.00	0.00	0.62	7.94	7.11	0.19
Leucosome 7	54.21	0.00	30.07	0.30	0.10	0.60	8.11	6.61	0.00
Leucosome 8	54.02	0.29	29.76	0.00	0.00	0.78	8.47	6.66	0.03
Leucosome 9	54.61	0.00	29.85	0.00	0.00	0.68	8.04	6.75	0.08
Leucosome 10	54.39	0.28	29.52	0.00	0.08	0.72	8.16	6.83	0.00
Leucosome 11	55.35	0.00	28.74	0.00	0.00	0.69	8.10	6.99	0.13
Leucosome 12	55.46	0.00	28.89	0.00	0.00	0.59	8.12	6.78	0.16
Leucosome 13	55.06	0.00	29.01	0.11	0.15	0.64	8.23	6.72	0.09
Leucosome 14	55.20	0.07	28.87	0.27	0.00	0.62	7.93	6.94	0.10
Leucosome 15	54.98	0.00	28.92	0.00	0.08	0.66	8.28	6.96	0.11
Leucosome 16	55.70	0.00	28.87	0.00	0.00	0.60	8.03	6.79	0.00
Leucosome 17	54.94	0.00	29.09	0.32	0.27	0.63	8.03	6.68	0.04
Leucosome 18	55.16	0.00	29.04	0.00	0.00	0.72	8.28	6.72	0.08
Leucosome 19	55.13	0.00	29.13	0.00	0.08	0.60	8.40	6.67	0.00
Leucosome 20	54.06	0.18	29.70	0.15	0.32	0.53	8.53	6.54	0.00
Leucosome 21	53.78	0.00	30.40	0.00	0.00	0.70	8.67	6.36	0.09
Leucosome 22	54.93	0.00	29.34	0.00	0.00	0.72	8.15	6.76	0.09
Leucosome 23	54.56	0.00	30.11	0.00	0.00	0.62	8.05	6.66	0.00
Leucosome 24	53.32	0.00	30.61	0.16	0.00	0.74	9.00	6.12	0.05
Leucosome 25	54.10	0.09	29.86	0.00	0.00	0.64	8.69	6.57	0.05
Leucosome 26	53.96	0.00	30.14	0.00	0.00	0.75	8.48	6.57	0.09
Leucosome 27	53.58	0.00	30.62	0.00	0.00	0.75	9.15	5.87	0.04
Leucosome 28	51.86	0.00	31.78	0.00	0.00	0.67	10.52	5.06	0.11
Leucosome 29	52.55	0.18	30.94	0.00	0.15	0.72	9.89	5.41	0.15
Leucosome 30	52.10	0.00	31.48	0.19	0.00	0.65	10.21	5.23	0.14
Leucosome 31	55.68	0.00	28.82	0.11	0.00	0.63	7.59	6.88	0.28
Leucosome 32	55.53	0.00	28.92	0.00	0.00	0.66	7.69	7.15	0.05
Leucosome 33	54.67	0.00	29.72	0.00	0.00	0.57	8.49	6.55	0.00
Leucosome 34	52.81	0.00	31.09	0.12	0.00	0.70	9.77	5.41	0.10
Leucosome 35	53.48	0.00	30.35	0.16	0.00	0.66	9.33	6.02	0.00
Leucosome 36	55.13	0.09	28.79	0.00	0.18	0.57	8.22	6.98	0.04
Melanosome 1	56.81	0.00	27.85	0.17	0.00	0.61	7.04	7.52	0.00
Melanosome 2	56.62	0.00	27.58	0.54	0.00	0.83	7.10	7.20	0.14
Melanosome 3	56.03	0.14	28.15	0.16	0.23	0.64	7.20	7.37	0.08
Melanosome 4	56.77	0.00	27.98	0.00	0.00	0.64	7.01	7.49	0.10
Melanosome 5	56.48	0.05	27.94	0.00	0.00	0.66	7.41	7.39	0.06
Melanosome 6	55.07	0.00	31.54	0.00	0.11	0.57	3.99	5.70	3.02
Melanosome 7	56.40	0.00	28.47	0.00	0.00	0.57	7.14	7.29	0.13
Melanosome 8	56.45	0.07	28.13	0.00	0.00	0.69	7.11	7.50	0.05

Melanosome 9	56.99	0.14	27.74	0.13	0.00	0.46	7.04	7.43	0.06
Melanosome 10	57.10	0.00	27.64	0.00	0.00	0.64	6.78	7.84	0.00
Melanosome 11	58.68	0.00	26.61	0.00	0.12	0.62	5.64	8.33	0.00
Melanosome 12	62.50	0.00	23.68	0.00	0.00	0.73	1.66	10.83	0.60
Melanosome 13	56.35	0.00	28.21	0.00	0.00	0.63	7.21	7.54	0.06
Melanosome 14	55.99	0.00	28.22	0.00	0.15	0.56	7.64	7.33	0.10
Melanosome 15	56.99	0.00	27.87	0.00	0.00	0.62	7.18	7.29	0.05
Melanosome 16	56.69	0.00	27.79	0.00	0.24	0.68	7.12	7.44	0.04
Melanosome 17	56.89	0.00	28.00	0.00	0.00	0.57	6.93	7.61	0.00
Melanosome 18	57.15	0.10	27.37	0.33	0.08	0.67	6.32	7.98	0.00
Melanosome 19	56.12	0.00	28.27	0.31	0.00	0.66	7.43	7.12	0.10
Melanosome 20	56.45	0.00	27.89	0.18	0.00	0.59	6.99	7.78	0.13
Melanosome 21	55.87	0.07	28.22	0.21	0.18	0.60	7.62	7.10	0.12
Melanosome 22	55.92	0.17	28.31	0.00	0.00	0.52	8.20	6.70	0.17
Melanosome 23	56.41	0.00	28.43	0.00	0.00	0.55	7.77	6.83	0.00
Melanosome 24	56.29	0.20	27.72	0.41	0.17	0.56	7.49	7.00	0.15
Melanosome 25	55.91	0.15	28.12	0.34	0.00	0.58	7.76	7.01	0.12
Melanosome 26	55.88	0.00	28.17	0.00	0.00	0.68	7.97	7.17	0.14
Melanosome 27	56.76	0.00	27.89	0.08	0.00	0.58	7.28	7.21	0.21
Melanosome 28	56.30	0.00	28.14	0.00	0.00	0.69	7.75	7.07	0.05
Melanosome 29	57.31	0.00	27.52	0.09	0.00	0.64	6.86	7.58	0.00
Melanosome 30	56.29	0.14	28.27	0.00	0.00	0.60	7.37	7.34	0.00
Melanosome 31	56.74	0.05	27.57	0.17	0.07	0.59	7.16	7.53	0.13
Melanosome 32	56.27	0.00	28.12	0.00	0.08	0.58	7.56	7.24	0.15
Melanosome 33	57.09	0.00	27.93	0.00	0.00	0.70	7.08	7.17	0.04
Melanosome 34	55.85	0.00	28.39	0.24	0.13	0.68	7.48	7.18	0.06
Melanosome 35	56.16	0.00	28.40	0.00	0.12	0.66	7.75	6.82	0.10
Melanosome 36	56.71	0.00	28.01	0.22	0.00	0.69	7.26	7.11	0.00
Melanosome 37	56.60	0.00	28.02	0.00	0.00	0.54	7.67	7.12	0.05
Melanosome 38	56.78	0.26	27.73	0.00	0.00	0.64	7.27	7.24	0.09
Melanosome 39	56.24	0.09	28.19	0.00	0.15	0.59	7.39	7.22	0.14
Melanosome 40	56.45	0.14	27.98	0.00	0.13	0.64	7.46	7.12	0.07
Melanosome 41	56.63	0.00	28.08	0.09	0.00	0.69	7.49	7.02	0.00
Melanosome 42	56.24	0.00	28.27	0.21	0.26	0.58	7.39	6.89	0.15
Melanosome 43	57.82	0.00	27.26	0.00	0.00	0.56	7.06	7.31	0.00
Melanosome 44	56.36	0.00	28.46	0.00	0.12	0.62	7.41	6.96	0.07
Paleosome 1	53.57	0.08	32.02	0.20	0.00	0.00	8.13	5.52	0.48
Paleosome 2	54.15	0.00	31.58	0.00	0.00	0.00	8.28	5.88	0.12
Paleosome 3	54.44	0.00	30.86	0.00	0.23	0.00	8.13	6.34	0.00
Paleosome 4	53.32	0.00	32.25	0.00	0.00	0.00	9.16	5.27	0.00
Paleosome 5	52.34	0.00	33.02	0.00	0.00	0.07	9.52	5.05	0.00
Paleosome 6	58.32	0.00	29.12	0.00	0.00	0.17	1.58	1.73	9.08
Paleosome 7	53.08	0.00	32.31	0.00	0.00	0.11	9.20	5.21	0.09
Paleosome 8	52.90	0.00	32.01	0.36	0.19	0.15	8.77	5.63	0.00
Paleosome 9	51.52	0.28	33.01	0.18	0.00	0.00	10.31	4.64	0.05
Paleosome 10	53.26	0.00	32.20	0.27	0.09	0.00	8.99	5.18	0.00
Paleosome 11	52.60	0.15	33.03	0.00	0.00	0.00	9.24	4.99	0.00
Paleosome 12	53.05	0.00	31.95	0.54	0.13	0.00	9.29	5.03	0.00
Paleosome 13	53.58	0.00	31.52	0.26	0.00	0.00	8.99	5.65	0.00
Paleosome 14	54.11	0.00	31.44	0.00	0.00	0.00	8.52	5.87	0.05

Paleosome 15	52.02	0.00	33.26	0.00	0.00	0.00	10.38	4.33	0.00
Paleosome 16	52.05	0.17	33.01	0.13	0.16	0.00	9.67	4.82	0.00
Paleosome 17	53.07	0.15	32.39	0.00	0.00	0.00	9.70	4.60	0.09
Paleosome 18	52.74	0.00	32.79	0.00	0.00	0.00	9.44	4.99	0.04
Paleosome 19	52.00	0.00	33.19	0.00	0.00	0.00	10.05	4.65	0.11
Paleosome 20	52.60	0.00	32.41	0.28	0.00	0.09	9.52	5.03	0.07
Paleosome 21	52.23	0.00	33.28	0.00	0.00	0.00	10.00	4.49	0.00
Paleosome 22	52.34	0.00	32.96	0.00	0.00	0.00	9.87	4.84	0.00
Paleosome 23	54.21	0.00	31.20	0.24	0.11	0.00	8.27	5.97	0.00
Paleosome 24	52.38	0.00	32.73	0.00	0.00	0.00	10.10	4.69	0.11
Paleosome 25	54.08	0.00	31.50	0.00	0.00	0.00	8.70	5.73	0.00
Paleosome 26	53.06	0.00	31.80	0.26	0.00	0.00	9.58	5.13	0.17
Paleosome 27	53.54	0.00	32.04	0.21	0.00	0.00	8.93	5.22	0.05
Paleosome 28	53.56	0.00	31.88	0.24	0.00	0.00	8.60	5.71	0.00
Paleosome 29	53.57	0.00	32.08	0.00	0.00	0.00	9.18	5.10	0.07
Paleosome 30	51.06	0.00	33.98	0.00	0.00	0.00	10.57	4.17	0.22
Paleosome 31	54.30	0.09	31.02	0.00	0.00	0.00	8.78	5.81	0.00
Paleosome 32	51.49	0.00	32.75	0.56	0.14	0.00	10.25	4.70	0.11
Paleosome 33	54.01	0.00	30.90	0.00	0.00	0.14	9.22	5.64	0.09
Paleosome 34	52.75	0.00	32.55	0.00	0.00	0.00	9.96	4.70	0.04
Paleosome 35	53.00	0.00	32.44	0.00	0.00	0.00	9.63	4.94	0.00
Paleosome 36	52.63	0.00	32.75	0.00	0.00	0.00	9.74	4.88	0.00
Paleosome 37	55.38	0.22	30.12	0.00	0.00	0.00	7.88	6.35	0.05
Paleosome 38	50.89	0.00	36.81	0.23	0.00	0.00	5.79	2.76	3.53
Paleosome 39	53.78	0.00	31.32	0.41	0.20	0.00	8.85	5.44	0.00
Paleosome 40	54.91	0.00	30.31	0.26	0.00	0.00	7.96	6.37	0.19
Paleosome 41	53.91	0.00	31.78	0.24	0.21	0.00	7.44	5.41	1.01
Paleosome 42	56.50	0.00	29.21	0.19	0.00	0.00	6.77	6.74	0.60
Paleosome 43	52.30	0.15	32.37	0.00	0.13	0.05	10.01	4.87	0.12
Paleosome 44	52.80	0.00	32.43	0.24	0.18	0.09	8.58	4.93	0.75
Paleosome 45	52.33	0.00	32.66	0.00	0.00	0.00	10.09	4.64	0.29
Paleosome 46	52.47	0.00	34.42	0.46	0.18	1.00	3.03	2.92	5.51
Paleosome 47	52.28	0.00	32.37	0.15	0.17	0.00	10.34	4.62	0.08
Paleosome 48	52.37	0.09	32.62	0.00	0.00	0.00	9.96	4.84	0.12
Paleosome 49	52.04	0.00	32.49	0.20	0.18	0.00	10.32	4.72	0.04
Paleosome 50	52.87	0.00	31.97	0.00	0.00	0.11	9.89	5.13	0.04
Paleosome 51	54.75	0.00	30.38	0.10	0.00	0.00	8.28	5.34	1.14
Paleosome 52	53.17	0.00	31.98	0.00	0.00	0.00	9.73	5.01	0.10
Paleosome 53	53.00	0.00	31.96	0.20	0.10	0.11	9.09	5.51	0.04
Paleosome 54	55.29	0.00	30.32	0.32	0.14	0.00	7.65	6.29	0.00
Paleosome 55	52.14	0.00	34.25	0.28	0.13	0.14	6.34	3.91	2.81
Paleosome 56	53.06	0.15	32.02	0.00	0.00	0.00	9.18	5.46	0.13
Paleosome 57	56.68	0.00	29.26	0.00	0.00	0.00	7.20	6.81	0.05
Paleosome 58	52.25	0.00	32.21	0.44	0.30	0.09	9.75	4.96	0.00
Paleosome 59	54.31	0.22	31.55	0.00	0.31	0.00	7.32	5.61	0.68
Paleosome 60	53.35	0.00	31.94	0.00	0.00	0.00	9.49	5.17	0.05
Paleosome 61	51.67	0.00	33.52	0.30	0.00	0.00	9.48	4.38	0.65
Paleosome 62	54.27	0.16	31.04	0.11	0.00	0.00	8.70	5.71	0.00
Paleosome 63	50.94	0.00	33.94	0.29	0.00	0.00	10.65	4.18	0.00
Paleosome 64	53.81	0.00	31.65	0.00	0.00	0.00	8.79	5.67	0.08

Tonalite 1	53.10	0.00	30.49	0.00	0.00	0.69	9.60	5.88	0.25
Tonalite 2	52.66	0.00	31.13	0.00	0.14	0.11	10.14	5.60	0.22
Tonalite 3	52.69	0.00	31.81	0.00	0.00	0.00	10.47	5.04	0.00
Tonalite 4	52.72	0.11	30.96	0.00	0.00	0.68	9.56	5.87	0.10
Tonalite 5	53.03	0.00	30.87	0.00	0.00	0.67	9.19	6.14	0.10
Tonalite 6	53.81	0.00	30.34	0.00	0.00	0.62	9.03	6.08	0.12
Tonalite 7	52.73	0.00	31.07	0.00	0.00	0.69	9.27	6.09	0.15
Tonalite 8	53.73	0.00	31.06	0.00	0.00	0.00	9.69	5.48	0.04
Tonalite 9	52.91	0.00	30.71	0.20	0.10	0.59	9.71	5.78	0.00
Tonalite 10	53.80	0.00	30.46	0.00	0.00	0.71	8.76	6.27	0.00
Tonalite 11	52.16	0.00	31.49	0.00	0.16	0.70	9.88	5.53	0.08
Tonalite 12	54.02	0.13	30.02	0.00	0.07	0.56	8.94	6.21	0.05
Tonalite 13	52.72	0.00	30.88	0.00	0.00	0.59	10.08	5.56	0.18
Tonalite 14	53.09	0.00	30.99	0.23	0.20	0.11	9.72	5.53	0.14
Tonalite 15	51.89	0.00	32.26	0.00	0.00	0.00	11.21	4.63	0.00
Tonalite 16	54.60	0.33	29.21	0.14	0.24	0.00	8.72	6.61	0.16
Tonalite 17	52.85	0.19	31.40	0.16	0.00	0.00	10.43	4.89	0.09
Tonalite 18	53.64	0.08	29.95	0.28	0.00	0.55	8.99	6.34	0.17
Tonalite 19	52.10	0.00	31.42	0.29	0.00	0.65	10.05	5.37	0.12
Tonalite 20	52.01	0.00	31.47	0.27	0.00	0.58	10.16	5.45	0.06
Tonalite 21	52.72	0.14	31.05	0.00	0.00	0.45	9.98	5.66	0.00
Tonalite 22	55.34	0.00	29.09	0.00	0.00	0.67	7.55	7.35	0.00
Tonalite 23	53.23	0.00	31.45	0.00	0.32	0.64	7.88	5.53	0.96
Tonalite 24	54.36	0.00	29.66	0.00	0.00	0.51	8.94	6.47	0.06
Tonalite 25	53.05	0.06	30.36	0.13	0.00	0.60	10.04	5.71	0.05
Tonalite 26	53.37	0.00	30.68	0.00	0.00	0.50	9.31	5.99	0.16
Tonalite 27	53.31	0.00	30.10	0.18	0.19	0.76	8.61	6.59	0.26
Tonalite 28	53.47	0.08	30.72	0.00	0.00	0.58	8.64	6.45	0.07
Tonalite 29	53.47	0.08	30.72	0.00	0.00	0.58	8.64	6.45	0.07
Tonalite 30	53.12	0.00	30.61	0.00	0.09	0.78	9.45	5.95	0.00
Tonalite 31	52.47	0.00	31.52	0.00	0.00	0.56	9.95	5.50	0.00
Tonalite 32	53.86	0.13	29.67	0.24	0.41	0.44	8.73	6.46	0.07
Tonalite 33	53.57	0.00	30.45	0.00	0.00	0.72	8.78	6.49	0.00
Tonalite 34	52.64	0.18	30.85	0.00	0.00	0.77	9.71	5.85	0.00
Tonalite 35	53.34	0.00	30.76	0.12	0.09	0.65	9.19	5.85	0.00
Tonalite 36	52.25	0.16	31.17	0.13	0.09	0.67	9.70	5.72	0.11
Tonalite 37	53.15	0.08	32.39	0.00	0.00	0.56	6.71	5.27	1.84
Tonalite 38	53.74	0.00	30.01	0.00	0.07	0.73	8.67	6.64	0.14
Tonalite 39	53.40	0.00	30.60	0.09	0.00	0.71	8.91	6.28	0.00
Tonalite 40	53.04	0.00	30.76	0.18	0.31	0.59	9.68	5.44	0.00
Tonalite 41	53.85	0.00	30.00	0.19	0.12	0.62	8.86	6.35	0.00
Tonalite 42	53.61	0.00	30.18	0.00	0.00	0.61	9.02	6.52	0.05
Tonalite 43	53.35	0.00	30.85	0.30	0.00	0.60	8.87	6.04	0.00
Tonalite 44	53.52	0.00	30.04	0.00	0.19	0.68	9.29	6.20	0.09
Tonalite 45	51.95	0.00	31.83	0.00	0.00	0.72	9.87	5.63	0.00

Appendix V – Anorthite, albite and orthoclase content in samples (mole %)

Sample name	An	Ab	Or
Leucosome 1	54.70	45.30	0.00
Leucosome 2	49.56	50.44	0.00
Leucosome 3	58.05	41.95	0.00
Leucosome 4	41.72	57.90	0.38
Leucosome 5	40.01	59.54	0.45
Leucosome 6	37.73	61.17	1.10
Leucosome 7	40.38	59.62	0.00
Leucosome 8	41.22	58.63	0.15
Leucosome 9	39.53	60.02	0.45
Leucosome 10	39.76	60.24	0.00
Leucosome 11	38.75	60.54	0.71
Leucosome 12	39.47	59.59	0.94
Leucosome 13	40.16	59.33	0.51
Leucosome 14	38.49	60.93	0.58
Leucosome 15	39.41	59.95	0.64
Leucosome 16	39.54	60.46	0.00
Leucosome 17	39.83	59.95	0.22
Leucosome 18	40.34	59.22	0.44
Leucosome 19	41.04	58.96	0.00
Leucosome 20	41.85	58.15	0.00
Leucosome 21	42.72	56.75	0.52
Leucosome 22	39.77	59.71	0.52
Leucosome 23	40.03	59.97	0.00
Leucosome 24	44.70	55.00	0.30
Leucosome 25	42.13	57.57	0.30
Leucosome 26	41.42	58.07	0.52
Leucosome 27	46.18	53.59	0.23
Leucosome 28	53.09	46.22	0.69
Leucosome 29	49.79	49.29	0.91
Leucosome 30	51.46	47.70	0.84
Leucosome 31	37.24	61.12	1.64
Leucosome 32	37.24	61.12	1.64
Leucosome 33	41.73	58.27	0.00
Leucosome 34	49.64	49.75	0.62
Leucosome 35	46.13	53.87	0.00
Leucosome 36	39.35	60.44	0.21
Melanosome 1	34.11	65.89	0.00
Melanosome 2	34.96	64.19	0.85
Melanosome 3	34.90	64.67	0.44
Melanosome 4	33.90	65.52	0.58
Melanosome 5	35.52	64.12	0.36
Melanosome 6	22.27	57.65	20.08
Melanosome 7	34.86	64.40	0.73
Melanosome 8	34.28	65.43	0.29
Melanosome 9	34.26	65.38	0.36

Melanosome 10	32.36	67.64	0.00
Melanosome 11	27.24	72.76	0.00
Melanosome 12	7.57	89.21	3.23
Melanosome 13	34.45	65.19	0.36
Melanosome 14	36.33	63.09	0.58
Melanosome 15	35.12	64.59	0.29
Melanosome 16	34.50	65.28	0.22
Melanosome 17	33.49	66.51	0.00
Melanosome 18	30.44	69.56	0.00
Melanosome 19	36.37	63.04	0.58
Melanosome 20	32.94	66.35	0.71
Melanosome 21	36.98	62.31	0.70
Melanosome 22	39.93	59.07	1.00
Melanosome 23	38.60	61.40	0.00
Melanosome 24	36.85	62.28	0.87
Melanosome 25	36.85	62.28	0.87
Melanosome 26	37.77	61.46	0.77
Melanosome 27	35.39	63.40	1.21
Melanosome 28	37.63	62.09	0.28
Melanosome 29	33.34	66.66	0.00
Melanosome 30	35.70	64.30	0.00
Melanosome 31	34.21	65.08	0.71
Melanosome 32	36.27	62.88	0.85
Melanosome 33	35.24	64.54	0.22
Melanosome 34	36.41	63.23	0.36
Melanosome 35	38.35	61.07	0.58
Melanosome 36	36.05	63.95	0.00
Melanosome 37	37.19	62.53	0.29
Melanosome 38	35.52	63.98	0.50
Melanosome 39	35.86	63.36	0.78
Melanosome 40	36.52	63.05	0.43
Melanosome 41	37.08	62.92	0.00
Melanosome 42	36.90	62.22	0.88
Melanosome 43	34.80	65.20	0.00
Melanosome 44	36.88	62.69	0.44
Paleosome 1	43.51	53.46	3.03
Paleosome 2	43.41	55.85	0.74
Paleosome 3	41.46	58.54	0.00
Paleosome 4	48.96	51.04	0.00
Paleosome 5	51.03	48.97	0.00
Paleosome 6	10.18	20.20	69.62
Paleosome 7	49.09	50.33	0.59
Paleosome 8	46.27	53.73	0.00
Paleosome 9	54.93	44.74	0.34
Paleosome 10	48.96	51.04	0.00
Paleosome 11	50.58	49.42	0.00
Paleosome 12	50.50	49.50	0.00
Paleosome 13	46.79	53.21	0.00
Paleosome 14	44.37	55.30	0.33
Paleosome 15	56.97	43.03	0.00

Paleosome 16	52.60	47.40	0.00
Paleosome 17	53.50	45.89	0.61
Paleosome 18	50.99	48.75	0.26
Paleosome 19	54.03	45.29	0.68
Paleosome 20	50.88	48.70	0.42
Paleosome 21	55.14	44.86	0.00
Paleosome 22	53.00	47.00	0.00
Paleosome 23	43.35	56.65	0.00
Paleosome 24	53.99	45.34	0.67
Paleosome 25	45.64	54.36	0.00
Paleosome 26	50.21	48.71	1.08
Paleosome 27	48.43	51.23	0.34
Paleosome 28	45.44	54.56	0.00
Paleosome 29	49.66	49.92	0.42
Paleosome 30	57.50	41.05	1.45
Paleosome 31	45.50	54.50	0.00
Paleosome 32	54.29	45.03	0.67
Paleosome 33	47.20	52.25	0.55
Paleosome 34	53.79	45.96	0.25
Paleosome 35	51.88	48.12	0.00
Paleosome 36	52.43	47.57	0.00
Paleosome 37	40.55	59.12	0.32
Paleosome 38	38.65	33.32	28.03
Paleosome 39	47.34	52.66	0.00
Paleosome 40	40.38	58.49	1.13
Paleosome 41	40.38	58.49	1.13
Paleosome 42	34.43	61.97	3.60
Paleosome 43	52.80	46.45	0.75
Paleosome 44	46.66	48.46	4.88
Paleosome 45	53.58	44.57	1.84
Paleosome 46	20.38	35.54	44.08
Paleosome 47	55.03	44.47	0.49
Paleosome 48	52.80	46.45	0.75
Paleosome 49	54.54	45.21	0.25
Paleosome 50	51.45	48.30	0.24
Paleosome 51	42.90	50.09	7.02
Paleosome 52	51.40	47.95	0.66
Paleosome 53	47.59	52.16	0.25
Paleosome 54	40.19	59.81	0.00
Paleosome 55	37.85	42.19	19.96
Paleosome 56	47.78	51.39	0.83
Paleosome 57	36.73	62.94	0.32
Paleosome 58	52.09	47.91	0.00
Paleosome 59	40.02	55.55	4.43
Paleosome 60	50.19	49.48	0.33
Paleosome 61	52.14	43.60	4.26
Paleosome 62	45.74	54.26	0.00
Paleosome 63	58.50	41.50	0.00
Paleosome 64	45.91	53.60	0.49
Tonalite 1	46.74	51.81	1.45

Tonalite 2	49.38	49.35	1.28
Tonalite 3	53.44	46.56	0.00
Tonalite 4	47.09	52.32	0.59
Tonalite 5	45.00	54.41	0.58
Tonalite 6	44.76	54.53	0.71
Tonalite 7	45.29	53.84	0.87
Tonalite 8	49.30	50.46	0.24
Tonalite 9	48.14	51.86	0.00
Tonalite 10	43.57	56.43	0.00
Tonalite 11	49.44	50.08	0.48
Tonalite 12	44.18	55.53	0.29
Tonalite 13	49.52	49.43	1.05
Tonalite 14	48.86	50.30	0.84
Tonalite 15	57.23	42.77	0.00
Tonalite 16	41.78	57.31	0.91
Tonalite 17	53.80	45.65	0.55
Tonalite 18	43.50	55.52	0.98
Tonalite 19	50.48	48.81	0.72
Tonalite 20	50.56	49.08	0.36
Tonalite 21	49.35	50.65	0.00
Tonalite 22	36.21	63.79	0.00
Tonalite 23	41.41	52.59	6.01
Tonalite 24	43.15	56.51	0.34
Tonalite 25	49.14	50.57	0.29
Tonalite 26	45.77	53.29	0.94
Tonalite 27	41.30	57.21	1.49
Tonalite 28	42.36	57.23	0.41
Tonalite 29	42.36	57.23	0.41
Tonalite 30	46.74	53.26	0.00
Tonalite 31	49.99	50.01	0.00
Tonalite 32	42.58	57.02	0.41
Tonalite 33	42.78	57.22	0.00
Tonalite 34	47.84	52.16	0.00
Tonalite 35	46.47	53.53	0.00
Tonalite 36	48.06	51.29	0.65
Tonalite 37	36.39	51.72	11.88
Tonalite 38	41.58	57.62	0.80
Tonalite 39	43.95	56.05	0.00
Tonalite 40	49.58	50.42	0.00
Tonalite 41	43.54	56.46	0.00
Tonalite 42	43.20	56.51	0.29
Tonalite 43	44.80	55.20	0.00
Tonalite 44	45.06	54.42	0.52
Tonalite 45	49.21	50.79	0.00

Appendix VI – Amphibole mineral analysis results (Oxides as wt% and elements as mole)

Sample name	SiO_2	TiO_2	Al_2O_3	Fe_2O_3	FeO	MnO	MgO	CaO	Na_2O	K2O	Si	Al iv	Al vi	Ti	Fe^{3+}	Fe^{2+}	Mn	Mg	Ca	Na	K
Paleosome 1	47.49	0.65	11.57	9.84	5.74	0.31	11.64	9.96	1.00	0.30	6.75	1.25	0.69	0.07	1.05	0.68	0.04	2.47	1.52	0.28	0.05
Paleosome 2	46.62	0.77	12.17	13.22	2.77	0.24	12.07	9.45	1.04	0.48	6.59	1.41	0.61	0.08	1.41	0.33	0.03	2.54	1.43	0.28	0.09
Paleosome 3	47.71	0.80	11.55	11.14	3.69	0.00	12.63	9.69	1.04	0.38	6.73	1.27	0.64	0.08	1.18	0.43	0.00	2.65	1.46	0.28	0.07
Paleosome 4	46.94	0.68	11.15	12.31	4.16	0.19	12.11	10.00	0.88	0.31	6.67	1.33	0.53	0.07	1.32	0.49	0.02	2.56	1.52	0.24	0.06
Paleosome 5	46.78	0.46	12.01	13.42	2.52	0.48	12.17	9.57	1.10	0.34	6.61	1.39	0.61	0.05	1.43	0.30	0.06	2.56	1.45	0.30	0.06
Paleosome 6	47.91	0.61	11.27	10.35	4.55	0.00	12.57	9.89	1.09	0.31	6.77	1.23	0.65	0.06	1.10	0.54	0.00	2.65	1.50	0.30	0.06
Paleosome 7	46.66	0.97	11.50	13.46	3.33	0.26	11.86	10.10	0.26	0.44	6.61	1.39	0.53	0.10	1.44	0.39	0.03	2.50	1.53	0.07	0.08
Paleosome 8	46.63	0.63	11.81	13.27	3.32	0.10	12.05	9.84	0.88	0.29	6.60	1.40	0.57	0.07	1.41	0.39	0.01	2.54	1.49	0.24	0.05
Paleosome 9	47.32	0.42	11.56	15.01	1.54	0.55	12.14	9.25	0.93	0.28	6.66	1.34	0.57	0.04	1.59	0.18	0.07	2.55	1.39	0.25	0.05
Paleosome 10	47.17	0.69	11.48	10.70	5.16	0.21	11.86	10.13	0.78	0.41	6.71	1.29	0.63	0.07	1.14	0.61	0.03	2.51	1.54	0.21	0.07
Paleosome 11	47.00	0.70	10.65	15.02	2.31	0.28	12.31	9.35	1.01	0.37	6.65	1.35	0.42	0.07	1.60	0.27	0.03	2.60	1.42	0.28	0.07
Paleosome 12	46.76	0.74	11.54	10.36	5.39	0.39	11.81	10.20	0.93	0.43	6.67	1.33	0.61	0.08	1.11	0.64	0.05	2.51	1.56	0.26	0.08
Paleosome 13	47.40	0.61	11.49	10.21	5.67	0.10	11.78	10.30	0.68	0.30	6.74	1.26	0.66	0.07	1.09	0.67	0.01	2.50	1.57	0.19	0.05
Paleosome 14	46.02	0.82	12.47	13.34	3.46	0.35	11.44	9.65	0.93	0.36	6.53	1.47	0.62	0.09	1.42	0.41	0.04	2.42	1.47	0.26	0.06
Paleosome 15	45.88	0.91	12.29	13.83	3.00	0.50	11.53	9.54	0.98	0.43	6.51	1.49	0.57	0.10	1.48	0.36	0.06	2.44	1.45	0.27	0.08
Paleosome 16	48.01	0.70	10.36	13.94	2.21	0.27	12.80	9.65	0.71	0.25	6.76	1.24	0.47	0.07	1.48	0.26	0.03	2.69	1.45	0.19	0.05
Paleosome 17	47.52	0.36	10.34	15.92	0.80	0.76	12.79	9.53	0.82	0.23	6.69	1.31	0.41	0.04	1.69	0.09	0.09	2.68	1.44	0.23	0.04
Paleosome 18	47.64	0.66	11.16	13.30	2.46	0.33	12.53	9.44	1.03	0.28	6.71	1.29	0.56	0.07	1.41	0.29	0.04	2.63	1.42	0.28	0.05
Paleosome 19	47.35	0.61	10.61	15.50	1.32	0.62	12.55	9.59	0.81	0.10	6.67	1.33	0.43	0.06	1.64	0.16	0.07	2.64	1.45	0.22	0.02
Paleosome 20	47.60	0.96	11.47	12.02	3.05	0.00	12.70	9.51	1.14	0.25	6.70	1.30	0.60	0.10	1.27	0.36	0.00	2.67	1.43	0.31	0.05
Paleosome 21	47.09	0.85	12.14	13.36	2.22	0.34	12.17	9.32	0.96	0.37	6.63	1.37	0.64	0.09	1.41	0.26	0.04	2.55	1.40	0.26	0.07
Paleosome 22	47.53	0.60	11.03	11.75	3.83	0.11	12.63	10.39	0.57	0.24	6.72	1.28	0.56	0.06	1.25	0.45	0.01	2.66	1.57	0.16	0.04
Paleosome 23	46.78	0.81	11.76	11.44	5.14	0.10	11.50	9.87	0.88	0.38	6.66	1.34	0.63	0.09	1.23	0.61	0.01	2.44	1.50	0.24	0.07
Paleosome 24	47.83	0.45	11.18	10.51	4.61	0.10	12.48	10.08	0.84	0.46	6.77	1.23	0.64	0.05	1.12	0.55	0.01	2.63	1.53	0.23	0.08
Paleosome 25	47.20	0.52	11.47	13.32	3.21	0.29	12.00	9.56	0.96	0.30	6.67	1.33	0.58	0.06	1.42	0.38	0.04	2.53	1.45	0.26	0.05
Paleosome 26	47.74	0.55	11.40	10.25	4.86	0.23	12.19	9.85	1.07	0.37	6.77	1.23	0.67	0.06	1.09	0.58	0.03	2.57	1.50	0.30	0.07
Paleosome 27	46.99	0.85	12.26	12.00	3.30	0.42	11.98	9.58	1.05	0.28	6.63	1.37	0.67	0.09	1.27	0.39	0.05	2.52	1.45	0.29	0.05
Paleosome 28	46.94	0.63	11.26	13.81	2.72	0.24	12.37	9.92	0.76	0.24	6.63	1.37	0.51	0.07	1.47	0.32	0.03	2.61	1.50	0.21	0.04
Paleosome 31	47.54	0.78	12.16	12.24	3.45	0.34	11.68	9.22	1.06	0.26	6.70	1.30	0.72	0.08	1.30	0.41	0.04	2.45	1.39	0.29	0.05
Paleosome 32	47.00	0.43	12.41	12.66	3.09	0.29	11.98	9.64	1.08	0.20	6.63	1.37	0.69	0.05	1.34	0.36	0.03	2.52	1.46	0.29	0.04
Paleosome 33	47.89	0.39	11.01	10.76	4.43	0.11	12.61	10.04	0.98	0.36	6.78	1.22	0.61	0.04	1.15	0.52	0.01	2.66	1.52	0.27	0.06
Paleosome 35	47.25	0.77	11.48	13.83	1.82	0.43	12.55	9.20	1.18	0.37	6.65	1.35	0.55	0.08	1.47	0.21	0.05	2.63	1.39	0.32	0.07
Paleosome 36	46.98	0.56	11.56	13.59	2.71	0.38	12.19	9.60	1.01	0.29	6.64	1.36	0.56	0.06	1.45	0.32	0.05	2.57	1.45	0.28	0.05
Paleosome 37	46.61	0.46	11.68	12.71	4.57	0.33	11.35	9.77	0.99	0.28	6.64	1.36	0.60	0.05	1.36	0.54	0.04	2.41	1.49	0.27	0.05
Paleosome 38	46.20	0.68	12.40	11.08	5.70	0.11	11.08	9.66	1.24	0.46	6.60	1.40	0.68	0.07	1.19	0.68	0.01	2.36	1.48	0.34	0.08
Paleosome 39	48.98	0.40	9.60	12.63	3.18	0.13	13.09	9.81	0.80	0.13	6.89	1.11	0.48	0.04	1.34	0.37	0.02	2.75	1.48	0.22	0.02
Paleosome 40	45.44	0.76	12.66	11.92	5.21	0.22	11.02	9.74	1.24	0.48	6.50	1.50	0.63	0.08	1.28	0.62	0.03	2.35	1.49	0.34	0.09
Paleosome 41	38.55	1.05	20.06	0.00	16.08	0.10	12.95	0.00	0.00	8.71	5.81	2.19	1.38	0.12	0.00	2.03	0.01	2.91	0.00	0.00	1.68
Paleosome 42	46.50	0.72	12.74	12.01	4.72	0.35	10.84	9.39	1.00	0.44	6.61	1.39	0.74	0.08	1.28	0.56	0.04	2.30	1.43	0.28	0.08
Paleosome 43	46.64	0.77	12.82	11.55	4.80	0.52	10.76	9.35	0.97	0.49	6.63	1.37	0.77	0.08	1.23	0.57	0.06	2.28	1.42	0.27	0.09

Paleosome 44	47.33	0.56	11.01	7.01	9.16	0.28	10.93	10.51	1.04	0.37	6.82	1.18	0.69	0.06	0.76	1.10	0.03	2.35	1.62	0.29	0.07
Paleosome 45	45.99	0.74	11.98	12.35	4.92	0.11	11.34	9.80	1.06	0.45	6.56	1.44	0.58	0.08	1.33	0.59	0.01	2.41	1.50	0.29	0.08
Paleosome 46	46.71	0.47	11.74	11.39	4.91	0.18	11.77	9.79	1.16	0.51	6.65	1.35	0.62	0.05	1.22	0.58	0.02	2.50	1.49	0.32	0.09
Melanosome 1	56.87	0.00	13.47	0.00	0.00	0.29	22.00	5.78	1.36	0.23	7.34	0.66	1.39	0.00	0.00	0.00	0.03	4.23	0.80	0.34	0.04
Melanosome 2	56.27	0.00	12.00	0.00	1.97	0.27	21.67	6.35	1.28	0.18	7.35	0.65	1.20	0.00	0.00	0.22	0.03	4.22	0.89	0.33	0.03
Melanosome 3	56.79	0.43	12.32	0.00	1.57	0.00	21.01	6.14	1.73	0.00	7.38	0.62	1.27	0.04	0.00	0.17	0.00	4.07	0.86	0.44	0.00
Melanosome 4	54.82	0.18	13.16	0.00	2.34	0.55	20.48	6.61	1.45	0.42	7.21	0.79	1.25	0.02	0.00	0.26	0.06	4.01	0.93	0.37	0.07
Melanosome 5	55.59	0.16	13.65	0.00	0.00	0.00	21.55	6.53	2.05	0.47	7.23	0.77	1.32	0.02	0.00	0.00	0.00	4.17	0.91	0.52	0.08
Melanosome 6	56.33	0.59	13.18	0.00	0.00	0.00	20.57	6.66	2.30	0.37	7.31	0.69	1.33	0.06	0.00	0.00	0.00	3.98	0.93	0.58	0.06
Melanosome 7	57.20	0.48	11.68	0.00	1.12	0.50	21.75	5.77	1.06	0.44	7.43	0.57	1.22	0.05	0.00	0.12	0.05	4.21	0.80	0.27	0.07
Melanosome 8	56.48	0.00	13.24	0.00	0.67	0.00	22.65	5.49	1.47	0.00	7.30	0.70	1.31	0.00	0.00	0.07	0.00	4.36	0.76	0.37	0.00
Melanosome 9	56.22	0.31	13.21	0.00	1.09	0.00	21.39	6.14	1.19	0.44	7.30	0.70	1.32	0.03	0.00	0.12	0.00	4.14	0.85	0.30	0.07
Melanosome 10	57.66	0.00	11.12	0.00	1.24	0.00	21.84	6.53	1.30	0.31	7.49	0.51	1.19	0.00	0.00	0.13	0.00	4.23	0.91	0.33	0.05
Melanosome 11	56.45	0.37	12.10	0.00	0.80	0.00	22.86	5.64	1.37	0.41	7.33	0.67	1.18	0.04	0.00	0.09	0.00	4.42	0.78	0.34	0.07
Melanosome 12	56.16	0.45	12.91	0.00	1.16	0.24	21.87	5.98	1.10	0.14	7.29	0.71	1.27	0.04	0.00	0.13	0.03	4.23	0.83	0.28	0.02
Melanosome 13	56.76	0.35	13.22	0.00	0.00	0.58	21.17	6.63	0.96	0.33	7.35	0.65	1.36	0.03	0.00	0.00	0.06	4.08	0.92	0.24	0.05
Melanosome 14	55.57	0.50	13.18	0.00	1.71	0.00	21.22	6.47	1.26	0.10	7.24	0.76	1.27	0.05	0.00	0.19	0.00	4.12	0.90	0.32	0.02
Melanosome 15	54.99	0.00	11.67	4.21	0.00	0.00	20.69	6.76	1.77	0.33	7.21	0.79	1.02	0.00	0.42	0.00	0.00	4.04	0.95	0.45	0.05
Melanosome 16	56.22	0.00	11.82	0.00	2.59	0.40	21.35	5.83	1.60	0.19	7.36	0.64	1.19	0.00	0.00	0.28	0.04	4.17	0.82	0.41	0.03
Melanosome 17	56.12	0.45	11.90	0.00	0.91	0.15	23.03	5.66	1.49	0.28	7.30	0.70	1.12	0.04	0.00	0.10	0.02	4.46	0.79	0.38	0.05
Melanosome 18	57.08	0.27	11.37	0.00	2.04	0.00	21.39	6.38	1.15	0.33	7.44	0.56	1.19	0.03	0.00	0.22	0.00	4.16	0.89	0.29	0.05
Melanosome 19	58.15	0.24	11.75	0.00	1.52	0.00	21.81	6.21	0.00	0.31	7.51	0.49	1.30	0.02	0.00	0.16	0.00	4.20	0.86	0.00	0.05
Melanosome 20	54.54	0.49	13.27	0.00	2.13	0.56	21.25	5.88	1.54	0.34	7.16	0.84	1.21	0.05	0.00	0.23	0.06	4.16	0.83	0.39	0.06
Melanosome 21	55.58	0.31	13.14	0.00	2.56	0.20	20.07	6.70	1.04	0.39	7.28	0.72	1.31	0.03	0.00	0.28	0.02	3.92	0.94	0.26	0.07
Melanosome 22	55.01	0.32	13.44	0.00	2.29	0.16	20.53	6.53	1.33	0.40	7.21	0.79	1.29	0.03	0.00	0.25	0.02	4.01	0.92	0.34	0.07
Melanosome 23	54.87	0.28	12.42	3.73	0.00	0.00	19.72	7.27	1.59	0.49	7.20	0.80	1.12	0.03	0.37	0.00	0.00	3.86	1.02	0.41	0.08
Melanosome 24	53.97	0.12	12.67	5.09	0.00	0.15	19.08	7.21	1.72	0.49	7.11	0.89	1.08	0.01	0.50	0.00	0.02	3.75	1.02	0.44	0.08
Melanosome 25	54.06	0.44	11.83	4.60	0.00	0.15	19.97	7.35	1.76	0.30	7.12	0.88	0.96	0.04	0.46	0.00	0.02	3.92	1.04	0.45	0.05
Melanosome 26	55.65	0.13	12.23	0.00	2.53	0.20	20.83	6.70	1.30	0.44	7.31	0.69	1.20	0.01	0.00	0.28	0.02	4.08	0.94	0.33	0.07
Melanosome 27	55.02	0.55	10.32	0.00	5.00	0.39	19.56	8.04	0.79	0.34	7.34	0.66	0.97	0.05	0.00	0.56	0.04	3.89	1.15	0.20	0.06
Melanosome 28	55.12	0.29	11.39	0.00	4.30	0.23	20.13	6.98	1.23	0.34	7.31	0.69	1.09	0.03	0.00	0.48	0.03	3.98	0.99	0.32	0.06
Melanosome 29	56.89	0.30	10.55	0.00	2.10	0.00	22.38	6.35	1.24	0.19	7.43	0.57	1.05	0.03	0.00	0.23	0.00	4.36	0.89	0.31	0.03
Melanosome 30	55.36	0.18	11.38	0.00	3.79	0.48	20.22	7.25	0.95	0.40	7.33	0.67	1.10	0.02	0.00	0.42	0.05	3.99	1.03	0.24	0.07
Melanosome 31	53.52	0.22	12.92	4.85	0.00	0.21	19.74	7.04	1.54	0.45	7.05	0.95	1.06	0.02	0.48	0.00	0.02	3.88	0.99	0.39	0.07
Melanosome 32	57.24	0.49	12.09	0.00	0.00	0.42	22.04	5.78	1.78	0.16	7.40	0.60	1.25	0.05	0.00	0.00	0.05	4.25	0.80	0.45	0.03
Melanosome 33	55.77	0.13	11.65	0.00	2.74	0.18	21.35	6.34	1.48	0.37	7.33	0.67	1.13	0.01	0.00	0.30	0.02	4.18	0.89	0.38	0.06
Melanosome 34	55.26	0.00	11.72	4.68	0.00	0.00	19.62	7.57	1.19	0.43	7.25	0.75	1.06	0.00	0.46	0.00	0.00	3.84	1.06	0.30	0.07
Melanosome 35	56.57	0.00	12.61	0.00	1.39	0.46	21.84	5.78	1.19	0.16	7.35	0.65	1.28	0.00	0.00	0.15	0.05	4.23	0.80	0.30	0.03
Melanosome 36	56.85	0.16	12.21	0.00	2.05	0.00	21.29	7.05	0.00	0.40	7.40	0.60	1.27	0.02	0.00	0.22	0.00	4.13	0.98	0.00	0.07
Melanosome 37	56.35	0.29	11.37	0.00	3.12	0.35	21.60	6.42	0.28	0.23	7.38	0.62	1.13	0.03	0.00	0.34	0.04	4.22	0.90	0.07	0.04
Melanosome 38	56.40	0.00	12.95	0.00	1.40	0.00	21.22	6.16	1.32	0.54	7.34	0.66	1.33	0.00	0.00	0.15	0.00	4.12	0.86	0.33	0.09
Melanosome 39	56.52	0.00	11.63	0.00	1.81	0.61	21.97	6.08	1.13	0.25	7.38	0.62	1.17	0.00	0.00	0.20	0.07	4.28	0.85	0.29	0.04
Leucosome 1	47.20	0.32	11.83	10.07	6.71	0.27	10.82	9.65	1.12	0.51	6.75	1.25	0.74	0.03	1.08	0.80	0.03	2.31	1.48	0.31	0.09
Leucosome 2	46.66	0.49	12.16	13.94	4.28	0.46	10.48	9.97	0.00	0.33	6.63	1.37	0.67	0.05	1.49	0.51	0.06	2.22	1.52	0.00	0.06
Leucosome 3	45.79	0.58	12.13	11.46	7.16	0.47	9.83	9.60	1.08	0.55	6.60	1.40	0.66	0.06	1.24	0.86	0.06	2.11	1.48	0.30	0.10

Leucosome 4	47.37	0.29	11.02	11.55	5.91	0.47	10.99	9.72	0.89	0.45	6.77	1.23	0.62	0.03	1.24	0.71	0.06	2.34	1.49	0.25	0.08
Leucosome 5	46.95	0.47	12.00	11.65	5.68	0.41	10.61	9.41	0.95	0.54	6.70	1.30	0.72	0.05	1.25	0.68	0.05	2.26	1.44	0.26	0.10
Leucosome 6	46.67	0.54	11.96	10.30	7.16	0.41	10.28	9.86	0.74	0.62	6.70	1.30	0.72	0.06	1.11	0.86	0.05	2.20	1.52	0.21	0.11
Leucosome 7	46.89	0.51	11.75	11.08	6.11	0.35	10.80	9.44	1.26	0.44	6.70	1.30	0.68	0.05	1.19	0.73	0.04	2.30	1.45	0.35	0.08
Leucosome 8	46.95	0.62	12.35	9.44	6.90	0.37	10.58	9.61	1.13	0.48	6.71	1.29	0.79	0.07	1.02	0.82	0.04	2.25	1.47	0.31	0.09
Leucosome 9	46.01	0.39	11.78	11.17	7.08	0.58	10.20	9.95	1.04	0.41	6.63	1.37	0.63	0.04	1.21	0.85	0.07	2.19	1.54	0.29	0.08
Leucosome 10	45.47	0.72	12.10	11.97	6.62	0.39	10.11	9.56	1.17	0.58	6.55	1.45	0.61	0.08	1.30	0.80	0.05	2.17	1.48	0.33	0.11
Leucosome 11	45.60	0.81	11.53	12.53	6.49	0.53	10.10	9.73	0.90	0.54	6.57	1.43	0.53	0.09	1.36	0.78	0.06	2.17	1.50	0.25	0.10
Leucosome 12	46.11	0.51	11.40	13.78	5.44	0.71	10.15	9.62	0.72	0.43	6.62	1.38	0.55	0.05	1.49	0.65	0.09	2.17	1.48	0.20	0.08
Leucosome 13	46.02	0.27	12.54	9.95	7.89	0.45	9.88	10.12	0.92	0.46	6.63	1.37	0.76	0.03	1.08	0.95	0.05	2.12	1.56	0.26	0.08
Leucosome 14	46.17	0.46	12.08	10.60	7.95	0.24	9.78	9.71	0.97	0.61	6.66	1.34	0.71	0.05	1.15	0.96	0.03	2.10	1.50	0.27	0.11
Leucosome 15	46.05	0.54	11.56	10.96	7.46	0.49	10.11	9.67	1.23	0.52	6.65	1.35	0.61	0.06	1.19	0.90	0.06	2.18	1.50	0.34	0.10
Leucosome 16	46.24	0.23	11.39	14.50	4.60	0.67	10.49	9.17	1.16	0.49	6.62	1.38	0.54	0.03	1.56	0.55	0.08	2.24	1.41	0.32	0.09
Leucosome 17	44.44	0.29	15.18	9.19	9.10	0.39	8.33	9.90	1.22	0.38	6.43	1.57	1.02	0.03	1.00	1.10	0.05	1.80	1.53	0.34	0.07
Leucosome 18	45.66	0.66	12.12	13.75	4.90	0.62	10.30	9.43	0.97	0.48	6.54	1.46	0.59	0.07	1.48	0.59	0.08	2.20	1.45	0.27	0.09
Leucosome 19	45.35	0.83	12.12	10.73	7.83	0.41	9.80	9.75	1.16	0.59	6.56	1.44	0.63	0.09	1.17	0.95	0.05	2.11	1.51	0.33	0.11
Leucosome 20	45.32	0.65	12.46	12.18	6.74	0.59	9.62	9.63	0.95	0.58	6.54	1.46	0.65	0.07	1.32	0.81	0.07	2.07	1.49	0.26	0.11
Leucosome 21	46.22	0.62	11.53	10.78	7.60	0.36	10.14	9.95	0.90	0.47	6.66	1.34	0.62	0.07	1.17	0.92	0.04	2.18	1.54	0.25	0.09
Leucosome 22	45.75	0.57	11.89	10.71	8.42	0.27	9.56	9.74	1.05	0.61	6.62	1.38	0.65	0.06	1.17	1.02	0.03	2.06	1.51	0.30	0.11
Leucosome 23	46.61	0.52	11.41	11.78	6.44	0.22	10.60	9.80	0.83	0.48	6.68	1.32	0.61	0.06	1.27	0.77	0.03	2.27	1.51	0.23	0.09
Leucosome 24	45.61	0.28	12.13	9.98	8.68	0.18	9.80	9.86	1.24	0.74	6.61	1.39	0.69	0.03	1.09	1.05	0.02	2.12	1.53	0.35	0.14
Leucosome 25	46.68	0.30	11.12	11.38	6.72	0.45	10.65	9.96	0.88	0.49	6.71	1.29	0.59	0.03	1.23	0.81	0.05	2.28	1.53	0.24	0.09
Leucosome 26	47.80	0.13	10.01	11.30	6.64	0.47	11.11	10.00	0.77	0.41	6.85	1.15	0.54	0.01	1.22	0.80	0.06	2.37	1.54	0.21	0.07
Leucosome 27	51.02	0.43	6.28	12.02	3.61	0.58	14.02	9.99	0.50	0.25	7.19	0.81	0.24	0.05	1.28	0.43	0.07	2.95	1.51	0.14	0.05
Leucosome 28	46.90	0.50	10.92	13.38	5.28	0.55	10.63	9.41	0.95	0.33	6.70	1.30	0.54	0.05	1.44	0.63	0.07	2.26	1.44	0.26	0.06
Leucosome 29	45.93	0.35	11.60	13.02	6.28	0.46	10.09	9.75	0.88	0.43	6.61	1.39	0.58	0.04	1.41	0.76	0.06	2.16	1.50	0.24	0.08
Leucosome 30	46.40	0.59	10.97	11.15	7.00	0.46	10.62	9.85	1.06	0.51	6.68	1.32	0.55	0.06	1.21	0.84	0.06	2.28	1.52	0.30	0.09
Leucosome 31	45.83	0.64	11.83	11.68	7.06	0.47	9.95	9.86	0.79	0.58	6.61	1.39	0.62	0.07	1.27	0.85	0.06	2.14	1.52	0.22	0.11
Leucosome 32	46.39	0.58	11.34	12.56	5.80	0.65	10.45	9.47	1.10	0.42	6.65	1.35	0.57	0.06	1.36	0.70	0.08	2.24	1.46	0.31	0.08
Leucosome 33	46.18	0.52	11.30	11.96	6.61	0.39	10.49	10.08	0.73	0.45	6.64	1.36	0.56	0.06	1.29	0.79	0.05	2.25	1.55	0.20	0.08
Leucosome 34	46.27	0.51	11.53	11.31	6.72	0.70	10.30	9.92	0.82	0.56	6.66	1.34	0.62	0.05	1.22	0.81	0.09	2.21	1.53	0.23	0.10
Leucosome 35	46.48	0.71	10.85	11.98	6.77	0.20	10.58	9.70	1.04	0.37	6.68	1.32	0.52	0.08	1.30	0.81	0.02	2.27	1.49	0.29	0.07
Leucosome 36	45.85	0.58	11.50	11.20	7.68	0.46	9.97	9.97	1.00	0.40	6.63	1.37	0.59	0.06	1.22	0.93	0.06	2.15	1.54	0.28	0.07
Leucosome 37	46.71	0.54	11.33	11.38	6.40	0.61	10.51	9.45	1.14	0.58	6.71	1.29	0.62	0.06	1.23	0.77	0.07	2.25	1.45	0.32	0.11
Leucosome 38	46.23	0.51	11.72	10.22	8.04	0.36	10.02	9.81	1.15	0.48	6.67	1.33	0.67	0.06	1.11	0.97	0.04	2.16	1.52	0.32	0.09
Leucosome 39	45.90	0.60	12.52	10.34	7.59	0.54	9.75	9.74	1.06	0.50	6.61	1.39	0.74	0.07	1.12	0.91	0.07	2.09	1.50	0.30	0.09
Leucosome 40	45.58	0.48	12.02	11.93	6.92	0.47	9.94	9.60	1.10	0.66	6.58	1.42	0.62	0.05	1.30	0.84	0.06	2.14	1.48	0.31	0.12
Leucosome 41	45.96	0.51	11.29	11.28	7.04	0.83	10.24	9.87	1.14	0.48	6.64	1.36	0.56	0.06	1.23	0.85	0.10	2.20	1.53	0.32	0.09
Tonalite 1	45.52	0.71	11.14	14.47	4.51	0.86	10.94	9.35	1.46	0.41	6.54	1.46	0.42	0.08	1.52	0.53	0.10	2.34	1.44	0.41	0.08
Tonalite 2	45.36	0.86	11.74	15.64	3.55	0.52	10.99	9.10	1.47	0.29	6.48	1.52	0.45	0.09	1.64	0.41	0.06	2.34	1.39	0.41	0.05
Tonalite 3	45.49	0.98	11.55	10.55	7.28	0.32	10.93	9.95	1.50	0.42	6.56	1.44	0.53	0.11	1.12	0.86	0.04	2.35	1.54	0.42	0.08
Tonalite 4	46.05	0.73	11.19	14.77	3.78	0.55	11.39	9.17	1.61	0.18	6.57	1.43	0.45	0.08	1.55	0.44	0.07	2.42	1.40	0.44	0.03
Tonalite 5	46.72	0.51	11.61	10.19	7.25	0.17	10.98	9.59	1.72	0.20	6.70	1.30	0.66	0.05	1.07	0.85	0.02	2.35	1.47	0.48	0.04
Tonalite 6	45.41	0.71	12.57	12.93	5.15	0.19	10.92	9.17	1.79	0.38	6.50	1.50	0.61	0.08	1.36	0.60	0.02	2.33	1.41	0.50	0.07
Tonalite 7	45.79	0.65	11.48	15.52	3.62	0.43	11.14	9.11	1.42	0.34	6.53	1.47	0.46	0.07	1.62	0.42	0.05	2.37	1.39	0.39	0.06

Tonalite 8	45.30	0.83	11.98	16.90	3.03	0.57	10.57	8.64	1.53	0.30	6.46	1.54	0.47	0.09	1.77	0.35	0.07	2.25	1.32	0.42	0.05
Tonalite 9	45.64	0.63	11.00	16.03	3.80	0.50	11.04	8.89	1.68	0.35	6.53	1.47	0.39	0.07	1.68	0.44	0.06	2.36	1.36	0.47	0.06
Tonalite 10	46.71	0.50	10.65	11.59	5.97	0.00	11.97	9.91	1.58	0.20	6.68	1.32	0.48	0.05	1.22	0.70	0.00	2.55	1.52	0.44	0.04
Tonalite 11	46.28	0.61	11.14	13.66	4.96	0.32	11.21	9.44	1.37	0.28	6.62	1.38	0.49	0.07	1.43	0.58	0.04	2.39	1.45	0.38	0.05
Tonalite 12	46.27	0.57	11.15	16.15	2.23	0.58	11.83	9.04	1.50	0.23	6.57	1.43	0.43	0.06	1.68	0.26	0.07	2.50	1.37	0.41	0.04
Tonalite 13	44.39	1.04	12.49	13.96	5.26	0.50	10.38	9.50	1.45	0.38	6.39	1.61	0.51	0.11	1.47	0.62	0.06	2.23	1.46	0.41	0.07
Tonalite 14	44.93	0.97	13.09	10.99	6.72	0.00	10.63	9.29	2.12	0.29	6.46	1.54	0.67	0.10	1.16	0.79	0.00	2.28	1.43	0.59	0.05
Tonalite 15	45.85	0.93	11.70	12.54	5.40	0.20	11.24	9.52	1.52	0.28	6.56	1.44	0.53	0.10	1.32	0.63	0.02	2.40	1.46	0.42	0.05
Tonalite 16	45.53	0.84	12.63	11.33	6.76	0.28	10.32	9.36	1.64	0.36	6.54	1.46	0.68	0.09	1.19	0.79	0.03	2.21	1.44	0.46	0.07
Tonalite 17	46.04	0.62	10.75	19.21	1.46	0.37	11.27	8.36	1.39	0.40	6.53	1.47	0.33	0.07	2.00	0.17	0.04	2.38	1.27	0.38	0.07
Tonalite 18	45.80	0.59	11.14	14.31	4.50	0.41	11.35	9.49	1.49	0.29	6.56	1.44	0.44	0.06	1.50	0.53	0.05	2.42	1.46	0.41	0.05
Tonalite 19	44.85	0.93	12.42	16.05	3.54	0.20	10.69	8.95	1.54	0.19	6.41	1.59	0.50	0.10	1.68	0.41	0.02	2.28	1.37	0.43	0.03
Tonalite 20	44.90	0.77	12.91	12.88	5.39	0.44	10.64	9.40	1.79	0.31	6.43	1.57	0.61	0.08	1.35	0.63	0.05	2.27	1.44	0.50	0.06
Tonalite 21	45.91	0.48	12.24	12.17	5.76	0.10	11.04	9.39	1.72	0.34	6.57	1.43	0.63	0.05	1.28	0.67	0.01	2.35	1.44	0.48	0.06
Tonalite 22	45.91	0.59	10.65	21.26	0.00	0.77	11.63	7.59	1.35	0.36	6.49	1.51	0.27	0.06	2.21	0.00	0.09	2.45	1.15	0.37	0.07
Tonalite 23	46.01	0.86	12.13	12.68	5.03	0.43	10.94	9.05	1.69	0.37	6.57	1.43	0.61	0.09	1.33	0.59	0.05	2.33	1.38	0.47	0.07
Tonalite 24	46.74	0.50	11.81	13.57	3.93	0.40	11.44	9.00	1.65	0.24	6.64	1.36	0.61	0.05	1.41	0.45	0.05	2.42	1.37	0.45	0.04
Tonalite 25	45.44	0.71	12.10	11.57	6.48	0.14	10.94	9.63	1.73	0.34	6.53	1.47	0.58	0.08	1.22	0.76	0.02	2.34	1.48	0.48	0.06
Tonalite 26	46.11	0.57	12.42	12.51	5.01	0.19	11.12	8.90	1.96	0.38	6.58	1.42	0.66	0.06	1.31	0.58	0.02	2.36	1.36	0.54	0.07
Tonalite 27	45.83	0.85	12.33	12.80	4.96	0.42	10.92	9.33	1.52	0.23	6.54	1.46	0.62	0.09	1.34	0.58	0.05	2.32	1.43	0.42	0.04
Tonalite 28	45.09	0.71	12.33	13.54	5.24	0.43	10.62	9.24	1.69	0.41	6.47	1.53	0.56	0.08	1.43	0.61	0.05	2.27	1.42	0.47	0.07
Tonalite 29	46.12	0.63	12.46	11.38	5.96	0.24	10.91	9.40	1.64	0.31	6.59	1.41	0.69	0.07	1.19	0.69	0.03	2.32	1.44	0.45	0.06
Tonalite 30	45.90	0.38	11.89	15.89	3.15	0.54	11.03	8.75	1.73	0.28	6.53	1.47	0.53	0.04	1.66	0.37	0.06	2.34	1.33	0.48	0.05
Tonalite 31	45.89	0.59	12.09	12.40	5.25	0.71	10.90	9.39	1.71	0.21	6.57	1.43	0.61	0.06	1.30	0.61	0.09	2.33	1.44	0.47	0.04
Tonalite 32	45.87	0.61	11.73	13.09	5.02	0.41	11.15	9.29	1.71	0.33	6.57	1.43	0.54	0.07	1.37	0.59	0.05	2.38	1.42	0.47	0.06
Tonalite 33	46.39	0.58	11.71	13.92	4.20	0.00	11.52	9.02	1.78	0.19	6.59	1.41	0.56	0.06	1.45	0.49	0.00	2.44	1.37	0.49	0.03
Tonalite 34	46.31	0.63	11.67	13.92	3.74	0.53	11.49	9.10	1.65	0.27	6.59	1.41	0.55	0.07	1.45	0.43	0.06	2.44	1.39	0.45	0.05
Tonalite 35	45.09	0.76	13.18	12.85	5.39	0.27	10.41	9.12	1.72	0.40	6.46	1.54	0.68	0.08	1.35	0.63	0.03	2.22	1.40	0.48	0.07
Tonalite 36	46.04	0.79	11.87	9.89	7.78	0.23	10.60	9.42	1.78	0.51	6.63	1.37	0.65	0.09	1.05	0.91	0.03	2.28	1.45	0.50	0.09
Tonalite 37	45.62	0.70	12.66	12.87	5.08	0.29	10.81	9.30	1.60	0.26	6.52	1.48	0.65	0.08	1.35	0.59	0.04	2.30	1.42	0.44	0.05
Tonalite 38	46.33	0.58	12.17	11.27	5.84	0.41	11.05	9.28	1.84	0.25	6.62	1.38	0.67	0.06	1.18	0.68	0.05	2.35	1.42	0.51	0.05
Tonalite 39	45.82	0.50	12.75	12.83	4.97	0.20	10.92	9.17	1.75	0.29	6.53	1.47	0.68	0.05	1.34	0.58	0.02	2.32	1.40	0.48	0.05

Appendix VII – Biotite mineral analysis results (Oxides as wt% and elements as mole)

Sample name	SiO_2	TiO_2	Al_2O_3	FeO	MnO	MgO	CaO	Na_2O	K_2O	Si	Al iv	Al vi	Ti	Fe	Mn	Mg	Ca	Na	K
Paleosome 1	37.52	0.93	19.32	15.24	0.20	12.82	0.06	0.09	8.82	5.56	2.44	0.94	0.10	1.89	0.03	2.83	0.01	0.02	1.67
Paleosome 2	38.22	0.76	19.16	15.51	0.11	12.99	0.24	0.00	8.00	5.63	2.37	0.96	0.08	1.91	0.01	2.85	0.04	0.00	1.50
Paleosome 3	37.28	1.14	19.24	16.23	0.22	13.69	0.00	0.06	7.13	5.50	2.50	0.85	0.13	2.00	0.03	3.01	0.00	0.02	1.34
Paleosome 4	37.36	0.70	18.91	16.97	0.23	12.41	0.00	0.06	8.38	5.57	2.43	0.90	0.08	2.12	0.03	2.76	0.00	0.02	1.59
Paleosome 5	37.16	0.53	19.26	17.15	0.23	12.84	0.12	0.00	7.70	5.53	2.47	0.90	0.06	2.13	0.03	2.85	0.02	0.00	1.46
Paleosome 6	37.53	0.69	18.85	16.64	0.31	12.67	0.12	0.06	8.14	5.58	2.42	0.89	0.08	2.07	0.04	2.81	0.02	0.02	1.54
Paleosome 7	37.18	0.97	19.16	16.39	0.22	12.48	0.21	0.09	8.32	5.53	2.47	0.90	0.11	2.04	0.03	2.77	0.03	0.02	1.58
Paleosome 8	35.82	0.71	19.70	18.70	0.00	13.57	0.10	0.00	6.40	5.34	2.66	0.80	0.08	2.33	0.00	3.01	0.02	0.00	1.22
Paleosome 9	37.54	0.94	18.72	16.59	0.23	12.45	0.00	0.20	8.33	5.59	2.41	0.88	0.11	2.07	0.03	2.76	0.00	0.06	1.58
Paleosome 10	37.45	0.96	19.05	16.85	0.00	13.33	0.14	0.00	7.24	5.54	2.46	0.86	0.11	2.08	0.00	2.94	0.02	0.00	1.37
Paleosome 11	37.08	0.71	19.77	16.40	0.00	13.71	0.12	0.09	7.12	5.47	2.53	0.91	0.08	2.02	0.00	3.02	0.02	0.03	1.34
Paleosome 12	37.43	1.01	18.80	16.14	0.14	12.52	0.25	0.14	8.56	5.57	2.43	0.87	0.11	2.01	0.02	2.78	0.04	0.04	1.63
Paleosome 13	37.54	1.08	18.76	16.03	0.12	13.07	0.12	0.13	8.15	5.57	2.43	0.85	0.12	1.99	0.02	2.89	0.02	0.04	1.54
Paleosome 14	37.79	0.76	18.69	15.97	0.14	13.16	0.23	0.17	8.10	5.60	2.40	0.87	0.08	1.98	0.02	2.91	0.04	0.05	1.53
Paleosome 15	37.20	0.88	19.04	15.77	0.28	13.01	0.28	0.18	8.35	5.53	2.47	0.86	0.10	1.96	0.04	2.88	0.04	0.05	1.58
Paleosome 16	37.19	0.78	19.24	16.66	0.11	12.69	0.09	0.06	8.19	5.53	2.47	0.91	0.09	2.07	0.01	2.81	0.01	0.02	1.55
Paleosome 17	35.93	1.00	19.35	18.21	0.25	13.67	0.29	0.00	6.30	5.35	2.65	0.75	0.11	2.27	0.03	3.03	0.05	0.00	1.20
Paleosome 18	37.88	0.73	19.48	15.30	0.00	12.72	0.17	0.29	8.43	5.60	2.40	0.99	0.08	1.89	0.00	2.80	0.03	0.08	1.59
Paleosome 19	38.34	0.69	19.07	15.08	0.24	13.36	0.06	0.00	8.16	5.64	2.36	0.95	0.08	1.86	0.03	2.93	0.01	0.00	1.53
Paleosome 20	38.07	0.54	19.01	15.72	0.00	13.24	0.10	0.08	8.23	5.62	2.38	0.94	0.06	1.94	0.00	2.92	0.02	0.02	1.55
Paleosome 21	37.82	0.89	19.35	15.74	0.00	12.64	0.18	0.13	8.25	5.59	2.41	0.97	0.10	1.95	0.00	2.79	0.03	0.04	1.56
Paleosome 22	37.65	0.71	19.35	15.56	0.19	13.18	0.00	0.12	8.23	5.57	2.43	0.94	0.08	1.92	0.02	2.91	0.00	0.03	1.55
Paleosome 23	37.58	0.63	19.44	16.11	0.26	12.63	0.10	0.00	8.25	5.57	2.43	0.97	0.07	2.00	0.03	2.79	0.02	0.00	1.56
Paleosome 24	36.39	2.05	18.39	17.26	0.00	12.44	0.21	0.14	8.12	5.45	2.55	0.70	0.23	2.16	0.00	2.78	0.03	0.04	1.55
Paleosome 25	37.58	0.93	19.26	15.95	0.22	13.06	0.07	0.10	7.81	5.56	2.44	0.91	0.10	1.97	0.03	2.88	0.01	0.03	1.47
Paleosome 26	37.23	0.74	19.62	15.59	0.13	12.98	0.30	0.26	8.14	5.51	2.49	0.94	0.08	1.93	0.02	2.87	0.05	0.08	1.54
Paleosome 27	37.50	1.04	19.25	15.74	0.00	13.30	0.14	0.07	7.96	5.54	2.46	0.89	0.12	1.94	0.00	2.93	0.02	0.02	1.50
Paleosome 28	37.66	0.99	19.45	15.61	0.11	12.94	0.05	0.09	8.11	5.56	2.44	0.95	0.11	1.93	0.01	2.85	0.01	0.02	1.53
Paleosome 29	38.08	0.63	19.36	15.04	0.00	13.37	0.12	0.00	8.39	5.61	2.39	0.97	0.07	1.85	0.00	2.94	0.02	0.00	1.58
Paleosome 30	37.56	1.27	19.48	15.40	0.00	13.13	0.00	0.00	8.17	5.54	2.46	0.93	0.14	1.90	0.00	2.89	0.00	0.00	1.54
Paleosome 31	37.83	1.24	19.02	15.24	0.00	13.13	0.11	0.19	8.26	5.58	2.42	0.89	0.14	1.88	0.00	2.89	0.02	0.05	1.55
Paleosome 32	37.40	1.07	19.24	16.32	0.00	12.64	0.15	0.00	8.19	5.55	2.45	0.91	0.12	2.03	0.00	2.79	0.02	0.00	1.55
Paleosome 33	38.09	0.46	19.68	15.30	0.17	13.05	0.06	0.19	8.00	5.61	2.39	1.02	0.05	1.88	0.02	2.86	0.01	0.05	1.50
Paleosome 34	37.75	0.47	19.23	16.51	0.26	12.72	0.05	0.17	7.83	5.60	2.40	0.96	0.05	2.05	0.03	2.81	0.01	0.05	1.48
Paleosome 35	37.28	0.92	19.00	16.63	0.34	12.40	0.12	0.09	8.23	5.55	2.45	0.89	0.10	2.07	0.04	2.75	0.02	0.03	1.56
Paleosome 36	37.67	0.81	19.41	15.80	0.27	12.73	0.14	0.09	8.08	5.57	2.43	0.96	0.09	1.96	0.03	2.81	0.02	0.03	1.53
Paleosome 37	37.54	0.43	19.10	16.21	0.13	12.91	0.21	0.00	8.47	5.58	2.42	0.92	0.05	2.02	0.02	2.86	0.03	0.00	1.61
Paleosome 38	37.62	0.98	19.43	15.15	0.11	12.92	0.22	0.14	8.43	5.56	2.44	0.95	0.11	1.87	0.01	2.85	0.04	0.04	1.59
Paleosome 39	38.02	0.89	19.20	15.23	0.26	12.76	0.27	0.17	8.20	5.61	2.39	0.96	0.10	1.88	0.03	2.81	0.04	0.05	1.54
Paleosome 40	37.19	1.32	19.17	16.33	0.29	12.49	0.18	0.10	7.94	5.52	2.48	0.88	0.15	2.03	0.04	2.76	0.03	0.03	1.50

Paleosome 41	37.29	0.74	19.46	16.05	0.18	12.56	0.23	0.13	8.37	5.54	2.46	0.95	0.08	1.99	0.02	2.78	0.04	0.04	1.59
Paleosome 42	36.98	0.96	18.51	17.47	0.30	12.30	0.17	0.00	8.32	5.54	2.46	0.81	0.11	2.19	0.04	2.75	0.03	0.00	1.59
Paleosome 43	37.45	0.77	19.51	16.12	0.00	12.63	0.08	0.17	8.27	5.55	2.45	0.96	0.09	2.00	0.00	2.79	0.01	0.05	1.56
Paleosome 44	37.77	0.43	19.21	15.94	0.21	12.62	0.19	0.22	8.41	5.60	2.40	0.96	0.05	1.98	0.03	2.79	0.03	0.06	1.59
Paleosome 45	36.29	1.06	18.84	17.59	0.39	12.75	0.00	0.10	7.97	5.44	2.56	0.77	0.12	2.21	0.05	2.85	0.00	0.03	1.52
Paleosome 46	37.48	0.00	19.04	17.00	0.40	12.68	0.00	0.00	8.39	5.59	2.41	0.94	0.00	2.12	0.05	2.82	0.00	0.00	1.60
Paleosome 47	37.32	0.00	19.33	16.81	0.10	12.60	0.09	0.00	8.75	5.57	2.43	0.97	0.00	2.10	0.01	2.80	0.01	0.00	1.67
Paleosome 48	37.22	1.10	19.15	15.80	0.15	13.03	0.07	0.13	8.34	5.52	2.48	0.87	0.12	1.96	0.02	2.88	0.01	0.04	1.58
Paleosome 49	36.93	0.71	19.05	17.42	0.23	13.20	0.17	0.00	7.30	5.49	2.51	0.83	0.08	2.17	0.03	2.93	0.03	0.00	1.39
Paleosome 50	37.74	0.64	19.10	16.84	0.00	12.45	0.00	0.10	8.13	5.60	2.40	0.95	0.07	2.09	0.00	2.76	0.00	0.03	1.54
Leucosome 1	39.41	0.50	21.88	12.83	0.00	14.01	0.42	0.00	5.96	5.63	2.37	1.31	0.05	1.53	0.00	2.98	0.06	0.00	1.08
Leucosome 2	39.59	0.64	20.30	13.06	0.29	12.91	0.15	0.21	7.85	5.74	2.26	1.21	0.07	1.58	0.04	2.79	0.02	0.06	1.45
Leucosome 3	40.14	0.78	20.87	12.74	0.00	12.68	0.00	0.19	7.61	5.77	2.23	1.31	0.08	1.53	0.00	2.72	0.00	0.05	1.40
Leucosome 4	40.49	1.24	21.80	11.37	0.30	12.48	0.00	0.00	7.32	5.77	2.23	1.43	0.13	1.35	0.04	2.65	0.00	0.00	1.33
Leucosome 5	40.42	0.44	22.86	10.72	0.12	14.12	0.16	0.00	6.17	5.70	2.30	1.49	0.05	1.26	0.01	2.97	0.02	0.00	1.11
Leucosome 6	40.59	1.08	22.17	9.62	0.00	14.33	0.00	0.00	7.21	5.72	2.28	1.41	0.11	1.13	0.00	3.01	0.00	0.00	1.30
Leucosome 7	40.49	0.37	22.11	10.53	0.38	13.87	0.00	0.00	7.25	5.74	2.26	1.44	0.04	1.25	0.05	2.93	0.00	0.00	1.31
Leucosome 8	40.06	0.69	22.43	11.24	0.28	12.89	0.00	0.12	7.30	5.71	2.29	1.47	0.07	1.34	0.03	2.74	0.00	0.03	1.33
Leucosome 9	41.06	1.35	21.50	9.95	0.00	13.79	0.00	0.16	7.19	5.80	2.20	1.38	0.14	1.18	0.00	2.90	0.00	0.04	1.29
Leucosome 10	40.03	1.27	21.60	11.33	0.21	12.89	0.00	0.00	7.67	5.72	2.28	1.36	0.14	1.35	0.03	2.75	0.00	0.00	1.40
Leucosome 11	39.15	1.00	21.50	13.16	0.33	11.85	0.21	0.17	7.62	5.67	2.33	1.33	0.11	1.59	0.04	2.56	0.03	0.05	1.41
Leucosome 12	39.85	0.89	20.90	13.27	0.00	12.33	0.53	0.43	6.81	5.74	2.26	1.28	0.10	1.60	0.00	2.65	0.08	0.12	1.25
Leucosome 13	39.02	0.74	20.05	14.25	0.54	12.32	0.15	0.14	7.80	5.70	2.30	1.15	0.08	1.74	0.07	2.68	0.02	0.04	1.45
Leucosome 14	39.40	0.61	20.78	13.83	0.00	12.60	0.10	0.00	7.69	5.71	2.29	1.26	0.07	1.68	0.00	2.72	0.02	0.00	1.42
Leucosome 15	40.64	0.39	22.08	10.91	0.00	13.57	0.00	0.15	7.26	5.77	2.23	1.46	0.04	1.29	0.00	2.87	0.00	0.04	1.31
Leucosome 16	40.23	1.31	22.63	9.95	0.32	13.70	0.00	0.00	6.86	5.68	2.32	1.45	0.14	1.18	0.04	2.88	0.00	0.00	1.24
Leucosome 17	40.56	0.55	21.35	10.23	0.15	14.34	0.21	0.22	7.38	5.76	2.24	1.33	0.06	1.22	0.02	3.04	0.03	0.06	1.34
Leucosome 18	40.30	0.41	22.20	10.86	0.00	13.65	0.00	0.08	7.49	5.73	2.27	1.45	0.04	1.29	0.00	2.89	0.00	0.02	1.36
Leucosome 19	40.72	1.24	22.64	8.74	0.00	14.21	0.22	0.23	7.00	5.72	2.28	1.46	0.13	1.03	0.00	2.97	0.03	0.06	1.25
Leucosome 20	40.54	0.00	21.53	11.62	0.00	13.48	0.25	0.29	7.29	5.79	2.21	1.41	0.00	1.39	0.00	2.87	0.04	0.08	1.33
Leucosome 21	40.89	0.49	21.55	10.92	0.00	13.21	0.00	0.23	7.72	5.82	2.18	1.44	0.05	1.30	0.00	2.80	0.00	0.06	1.40
Leucosome 22	39.40	0.47	21.96	11.95	0.28	13.47	0.00	0.54	6.93	5.64	2.36	1.35	0.05	1.43	0.03	2.88	0.00	0.15	1.27
Leucosome 23	40.65	0.37	21.63	11.12	0.14	13.42	0.10	0.20	7.38	5.79	2.21	1.42	0.04	1.32	0.02	2.85	0.02	0.05	1.34
Leucosome 24	40.55	0.49	21.81	10.43	0.29	13.24	0.19	0.13	7.86	5.78	2.22	1.44	0.05	1.24	0.03	2.81	0.03	0.04	1.43
Leucosome 25	40.90	1.49	22.16	10.07	0.22	13.03	0.00	0.09	7.04	0.00	0.00	0.00	0.00	0.00	0.00	0.00	0.00	0.00	0.00
Leucosome 26	39.57	0.45	21.84	11.54	0.24	13.62	0.00	0.13	7.60	5.67	2.33	1.36	0.05	1.38	0.03	2.91	0.00	0.04	1.39
Leucosome 27	40.81	1.02	23.24	9.72	0.20	13.01	0.00	0.00	7.00	5.74	2.26	1.59	0.11	1.14	0.02	2.73	0.00	0.00	1.26
Leucosome 28	40.77	1.28	22.75	10.17	0.00	12.80	0.00	0.00	7.22	5.75	2.25	1.54	0.14	1.20	0.00	2.69	0.00	0.00	1.30
Leucosome 29	39.21	1.14	22.35	11.28	0.20	13.49	0.00	0.10	7.24	5.60	2.40	1.36	0.12	1.35	0.02	2.87	0.00	0.03	1.32
Leucosome 30	39.11	1.25	21.92	12.14	0.14	12.93	0.00	0.18	7.33	5.61	2.39	1.32	0.14	1.46	0.02	2.77	0.00	0.05	1.34
Leucosome 31	39.88	1.24	22.13	11.27	0.47	12.65	0.00	0.00	7.37	5.69	2.31	1.42	0.13	1.34	0.06	2.69	0.00	0.00	1.34
Leucosome 32	39.61	1.55	21.07	11.66	0.13	13.36	0.00	0.00	7.63	5.68	2.32	1.24	0.17	1.40	0.02	2.85	0.00	0.00	1.39
Leucosome 33	40.26	1.30	23.00	9.81	0.00	13.15	0.00	0.20	7.28	5.69	2.31	1.51	0.14	1.16	0.00	2.77	0.00	0.06	1.31
Tonalite 1	36.56	1.54	17.67	18.29	0.00	12.65	0.00	0.58	7.71	5.50	2.50	0.63	0.17	2.30	0.00	2.84	0.00	0.17	1.48
Tonalite 2	36.67	1.75	17.47	18.98	0.13	11.25	0.10	0.20	8.45	5.55	2.45	0.67	0.20	2.40	0.02	2.54	0.02	0.06	1.63

Tonalite 3	35.91	1.55	18.22	18.91	0.10	11.89	0.12	0.54	7.75	5.43	2.57	0.67	0.18	2.39	0.01	2.68	0.02	0.16	1.49
Tonalite 4	36.02	1.75	18.17	18.72	0.00	11.43	0.00	0.50	8.40	5.45	2.55	0.70	0.20	2.37	0.00	2.58	0.00	0.15	1.62
Tonalite 5	36.66	1.81	17.38	18.69	0.22	11.69	0.00	0.59	7.97	5.54	2.46	0.63	0.21	2.36	0.03	2.63	0.00	0.17	1.54
Tonalite 6	35.77	1.91	17.56	19.30	0.29	11.68	0.16	0.45	7.89	5.43	2.57	0.57	0.22	2.45	0.04	2.64	0.03	0.13	1.53
Tonalite 7	36.47	1.65	17.19	18.88	0.35	11.93	0.17	0.61	7.76	5.52	2.48	0.58	0.19	2.39	0.05	2.69	0.03	0.18	1.50
Tonalite 8	36.37	1.79	17.75	18.90	0.00	11.57	0.00	0.77	7.87	5.49	2.51	0.65	0.20	2.39	0.00	2.61	0.00	0.23	1.52
Tonalite 9	36.34	2.11	16.71	19.01	0.18	11.88	0.19	0.54	8.06	5.51	2.49	0.50	0.24	2.41	0.02	2.69	0.03	0.16	1.56
Tonalite 10	36.58	1.87	17.21	18.94	0.08	11.81	0.00	0.41	8.09	5.53	2.47	0.60	0.21	2.40	0.01	2.66	0.00	0.12	1.56
Tonalite 11	36.87	1.42	17.96	17.97	0.00	12.36	0.24	0.62	7.56	5.53	2.47	0.70	0.16	2.25	0.00	2.76	0.04	0.18	1.45
Tonalite 12	36.20	1.95	17.48	18.53	0.29	11.73	0.14	0.54	8.13	5.48	2.52	0.60	0.22	2.35	0.04	2.65	0.02	0.16	1.57
Tonalite 13	36.89	1.54	17.54	18.20	0.08	12.16	0.10	0.67	7.81	5.55	2.45	0.66	0.17	2.29	0.01	2.73	0.02	0.20	1.50
Tonalite 14	36.63	1.67	17.19	19.13	0.00	11.91	0.14	0.63	7.70	5.54	2.46	0.60	0.19	2.42	0.00	2.68	0.02	0.18	1.48
Tonalite 15	36.92	1.51	17.49	18.31	0.22	11.99	0.21	0.70	7.66	5.56	2.44	0.66	0.17	2.30	0.03	2.69	0.03	0.21	1.47
Tonalite 16	36.41	1.43	17.26	19.26	0.00	12.09	0.14	0.61	7.79	5.51	2.49	0.59	0.16	2.44	0.00	2.73	0.02	0.18	1.50
Tonalite 17	36.41	1.62	17.11	18.64	0.13	12.36	0.18	0.62	7.92	5.51	2.49	0.56	0.18	2.36	0.02	2.79	0.03	0.18	1.53
Tonalite 18	37.26	1.61	18.85	16.18	0.00	12.04	0.25	0.70	8.13	5.54	2.46	0.85	0.18	2.01	0.00	2.67	0.04	0.20	1.54
Tonalite 19	36.51	1.82	17.69	17.97	0.10	11.67	0.14	0.72	8.38	5.51	2.49	0.66	0.21	2.27	0.01	2.63	0.02	0.21	1.61
Tonalite 20	36.70	1.83	17.21	18.57	0.12	11.84	0.05	0.47	8.22	5.54	2.46	0.61	0.21	2.35	0.02	2.67	0.01	0.14	1.58
Tonalite 21	36.40	1.94	19.50	16.93	0.22	11.31	0.00	0.64	8.06	5.44	2.56	0.88	0.22	2.12	0.03	2.52	0.00	0.18	1.54
Tonalite 22	37.05	1.64	17.83	17.54	0.00	12.18	0.04	0.73	8.00	5.55	2.45	0.70	0.19	2.20	0.00	2.72	0.01	0.21	1.53
Tonalite 23	37.98	2.04	19.43	16.32	0.00	10.30	0.15	0.65	8.13	5.63	2.37	1.03	0.23	2.02	0.00	2.28	0.02	0.19	1.54
Tonalite 24	36.18	1.70	17.98	18.51	0.00	12.19	0.00	0.58	7.87	5.45	2.55	0.65	0.19	2.33	0.00	2.74	0.00	0.17	1.51
Tonalite 25	36.77	1.50	18.54	17.94	0.00	11.57	0.07	0.49	8.11	5.52	2.48	0.80	0.17	2.25	0.00	2.59	0.01	0.14	1.55
Tonalite 26	36.62	2.09	18.38	16.81	0.13	12.07	0.20	0.56	8.13	5.48	2.52	0.72	0.24	2.10	0.02	2.69	0.03	0.16	1.55
Tonalite 27	36.19	1.84	17.35	19.12	0.00	11.87	0.07	0.48	8.09	5.48	2.52	0.58	0.21	2.42	0.00	2.68	0.01	0.14	1.56
Tonalite 28	36.28	2.28	17.79	18.77	0.00	11.36	0.00	0.54	7.97	5.48	2.52	0.65	0.26	2.37	0.00	2.56	0.00	0.16	1.54
Tonalite 29	36.04	1.62	17.57	18.05	0.24	12.56	0.13	0.80	7.99	5.45	2.55	0.57	0.18	2.28	0.03	2.83	0.02	0.23	1.54
Tonalite 30	36.47	1.53	17.66	18.05	0.11	12.23	0.12	0.72	8.10	5.50	2.50	0.64	0.17	2.28	0.01	2.75	0.02	0.21	1.56
Tonalite 31	36.76	1.81	17.67	18.51	0.26	11.56	0.00	0.65	7.79	5.54	2.46	0.68	0.21	2.33	0.03	2.60	0.00	0.19	1.50
Tonalite 32	36.45	1.83	17.23	18.53	0.00	12.19	0.15	0.66	7.94	5.51	2.49	0.57	0.21	2.34	0.00	2.74	0.02	0.19	1.53
Tonalite 33	36.54	1.58	17.35	18.58	0.27	12.28	0.00	0.62	7.79	5.51	2.49	0.60	0.18	2.35	0.03	2.76	0.00	0.18	1.50
Tonalite 34	36.72	1.70	17.19	18.51	0.12	12.18	0.00	0.73	7.85	5.54	2.46	0.60	0.19	2.33	0.02	2.74	0.00	0.21	1.51
Tonalite 35	36.34	1.62	16.93	19.36	0.17	12.02	0.17	0.72	7.66	5.51	2.49	0.54	0.19	2.46	0.02	2.72	0.03	0.21	1.48

Appendix VIII – SEM-EDX analysis for plagioclase-amphibole geothermobarometry

Sample	Al iv	Al vi	Al tot	Ca	Si	Ab	P (kbar)	T (°C)	P (-0.6 kbar)	P (+0.6 kbar)	T (-40 °C)	T (+40 °C)
Leucosome 1	1.53	1.06	2.60	0.26	6.47	73.88	9.36	**516.17**	8.76	9.96	**476.17**	**556.17**
Leucosome 2	1.35	0.69	2.04	0.44	6.65	51.74	6.68	546.68	6.08	7.28	506.68	586.68
Leucosome 3	1.39	0.63	2.01	0.48	6.61	48.79	6.58	553.31	5.98	7.18	513.31	593.31
Leucosome 4	0.81	1.14	1.95	0.40	7.19	42.85	**6.28**	522.91	**5.68**	**6.88**	482.91	562.91
Leucosome 5	1.79	1.21	3.00	0.37	6.21	53.07	11.25	532.32	10.65	11.85	492.32	572.32
Leucosome 6	1.95	1.15	3.10	0.36	6.05	61.77	**11.77**	528.60	**11.17**	**12.37**	488.60	568.60
Leucosome 7	1.78	1.12	2.90	0.47	6.22	50.17	10.78	539.14	10.18	11.38	499.14	579.14
Leucosome 8	1.86	1.21	3.07	0.48	6.14	48.78	11.60	538.48	11.00	12.20	498.48	578.48
Leucosome 9	1.66	1.00	2.66	0.53	6.34	44.17	9.66	549.56	9.06	10.26	509.56	589.56
Leucosome 10	1.33	0.64	1.97	0.52	6.67	44.35	6.36	**557.05**	5.76	6.96	**517.05**	**597.05**
Leucosome 11	1.58	1.00	2.57	0.41	6.42	50.48	9.23	540.37	8.63	9.83	500.37	580.37
Leucosome 12	1.36	0.67	2.03	0.47	6.64	50.08	6.67	549.31	6.07	7.27	509.31	589.31
Leucosome 13	1.42	0.58	2.00	0.48	6.58	49.23	6.51	555.52	5.91	7.11	515.52	595.52
Leucosome 14	1.32	0.68	2.00	0.49	6.68	47.48	6.51	551.25	5.91	7.11	511.25	591.25
Leucosome 15	1.34	0.63	1.97	0.49	6.66	47.97	6.35	552.90	5.75	6.95	512.90	592.90
Leucosome 16	1.31	0.74	2.04	0.49	6.69	47.79	6.72	548.04	6.12	7.32	508.04	588.04
Leucosome average	1.49	0.88	2.37	0.45	6.51	50.79	**8.27**	**542.78**	**7.67**	**8.87**	**502.78**	**582.78**
Tonalite 1	1.41	0.41	1.82	0.49	6.59	48.53	5.65	**562.94**	5.05	6.25	522.94	602.94
Tonalite 2	1.37	0.56	1.92	0.52	6.63	44.76	6.14	560.55	5.54	6.74	520.55	600.55
Tonalite 3	1.44	0.57	2.01	0.30	6.56	69.44	6.54	**536.95**	5.94	7.14	496.95	576.95
Tonalite 4	1.33	0.61	1.94	0.46	6.67	50.78	6.23	550.50	5.63	6.83	510.50	590.50
Tonalite 5	1.47	0.51	1.98	0.50	6.53	48.50	6.41	560.30	5.81	7.01	520.30	600.30
Tonalite 6	1.50	0.59	2.10	0.47	6.50	50.51	6.97	555.26	6.37	7.57	515.26	595.26
Tonalite 7	1.33	0.59	1.92	0.48	6.67	48.48	6.12	553.81	5.52	6.72	513.81	593.81
Tonalite 8	1.35	0.57	1.92	0.52	6.65	44.23	6.12	560.33	5.52	6.72	520.33	600.33
Tonalite 9	1.51	0.60	2.11	0.50	6.49	46.94	7.05	559.40	6.45	7.65	519.40	599.40
Tonalite 10	1.49	0.69	2.17	0.51	6.51	46.77	7.34	555.57	6.74	7.94	515.57	595.57
Tonalite 11	2.08	1.26	3.33	0.54	5.92	41.27	**12.86**	550.25	**12.26**	**13.46**	**510.25**	**590.25**
Tonalite 12	1.27	0.57	1.84	0.53	6.73	44.13	5.76	558.34	5.16	6.36	518.34	598.34
Tonalite 13	1.14	0.55	1.69	0.51	6.86	44.21	**5.01**	555.43	**4.41**	**5.61**	**515.43**	**595.43**
Tonalite 14	1.30	0.59	1.90	0.32	6.70	60.82	6.02	540.43	5.42	6.62	500.43	580.43
Tonalite 15	1.20	0.59	1.79	0.43	6.80	54.94	5.50	543.61	4.90	6.10	503.61	583.61
Tonalite average	1.41	0.62	2.03	0.47	6.59	49.62	**6.65**	**553.30**	**6.05**	**7.25**	**513.30**	**593.30**